Technische Universität München
Physik-Department
Lehrstuhl für Biophysik E22

Vesicle Adhesion via Interaction of Integrin $a_{IIb}b_3$ and Cyclic-RGD-Lipopeptide: A Model of Cell Adhesion Processes.

Bin Hu

Vollständiger Abdruck der von der Fakultät für Physik
der Technischen Universität München
zur Erlangung des akademischen Grades eines
Doktors der Naturwissenschaften
genehmigten Dissertation

Vorsitzender: Univ.-Prof. Dr. M. Kleber

Prüfer der Dissertation: 1. Univ.-Prof. Dr. E. Sackmann
2. Univ.-Prof. Dr. H. Kessler

Die Dissertation wurde am 13.02.2001 bei der Technischen Universität München eingereicht und durch die Fakultät für Physik am 19.04.2001 angenommen.

CONTENTS

1 Summary

Adhesive interaction of cells with the extracellular matrix or with other cells are important determinants in regulating many physiological processes, including cell growth, differentiation, development, migration, wound healing, inflammation, and tumorigenesis. The major class of cell surface receptors which mediate formation of focal adhesion and other modes of association with the extracellular matrix is the integrins. These receptors recognize the RGD sequence commonly existing in their major ligands. In this thesis, vesicle adhesion mediated by the interaction of human platelet integrin $\alpha_{IIb}\beta_3$ and a synthetic cyclic RGD peptide was studied. The work provides a simple and well-established model system for the biophysical studies of cell adhesion processes mediated by the lock-and-key interaction.

The binding ability of the biotinylated cyclic RGD-containing hexapeptide [cyclo(-Arg-Gly-Asp-D-Phe-Lys-Gly-)] to $\alpha_{IIb}\beta_3$ was tested with the surface detection methods of ELISA and surface plasmon resonance on the streptavidin/ExtrAvidin surfaces. Results showed that a spacer of 2.2 nm between the peptide and the biotin residue was required to enable penetration of the RGD sequence into the binding center of $\alpha_{IIb}\beta_3$. The equilibrium dissociation constant was determined to be 1.1 μM. The RGD lipid was composed of the cyclic RGD peptide, a 2.2 nm spacer and the residue of (1,2-dimyristoyl-3-thioglyceryl)succinimido-propanoyl. Film balance and DSC results showed that the synthetic lipid could be mixed with DMPC homogeneously within normal concentration and temperature range, either in monolayers or in bilayers. When immobilized on glass surfaces by the lipid bilayer spreading method, the RGD lipid could initiate specific platelet adhesion processes.

Giant vesicles with reconsituted RGD lipid (diameters larger than 20μm) were produced with the electroswelling method, and were used as phantom cells to study their adhesion on the solubilized $\alpha_{IIb}\beta_3$ immobilized on glass surfaces, by means of RICM. By analysis of the surface profiles of the vesicles, it was shown that the adhesion process was the result of the interplay of the lock-and-key interaction of $\alpha_{IIb}\beta_3$-RGD, the vesicle surface undulations, and the repulsion forces produced by the lipopolymer, dimyristoyl-phosphatidyl- ethanolamine-N-[poly(ethyleneglycol)2000] (PEG 2000 PE), reconstituted in the vesicle membranes. When the vesicles contained 1% of PEG 2000 PE and 2% of the RGD lipid, the adhesion appeared as an obviously cooperative process. Vesicle contours were reconstructed close to the vesicle surface contact line, with help of the related theories. The adhesion energy values were in the range of 10^{-9} – 10^{-7} J/m^2, which were comparable to those obtained from the studies of other model systems.

$\alpha_{IIb}\beta_3$ was reconstituted into the lipid vesicles by using Bio-beads SM2 to remove Trition X-100 in the protein/lipid mixture. The reconstituted $\alpha_{IIb}\beta_3$ was observed with cryo electron microscopy. The images showed that, $\alpha_{IIb}\beta_3$ was clearly recognizable as small protrusions extending from both sides of the vesicle membranes, and exhibited a regular size with a diameter of 8 – 10 nm and a length of 19 – 23 nm. The adhesion between the RGD lipid-containing giant vesicles mediated by the reconstituted $\alpha_{IIb}\beta_3$ vesicles was studied with the methods of fluorescence microscopy and confocal fluorescence microscopy. The adhesion energy was found to be 10^{-9} – 10^{-8} J/m^2 by the same method as used in the RICM experiments. Between two adhering giant vesicles, the $\alpha_{IIb}\beta_3$ vesicles mainly distributed along the edge of adhesion disk. Besides, adhesion between the vesicles with reconstituted $\alpha_{IIb}\beta_3$ and the RGD lipid-containing small vesicles produced by the extruder method was observed by means of cryo electron microscopy. The $\alpha_{IIb}\beta_3$ ´bridges´ between adhering $\alpha_{IIb}\beta_3$ vesicles and the RGD vesicles were clearly shown, and the minimum distance between the adhering vesicles was in the range of 9 – 12 nm.

2 Introduction

Cell adhesion, integrin family, and the RGD sequence

The cells of the body adhere to one another and to the extracellular matrix (ECM) surrounding them. This adhesion holds tissues together and is therefore essential to maintenance of body structure. In addition it helps to direct both embryonic development and important processes in the fully formed organism, including blood clotting, wound healing and infection. The formation of attachments either between cells or between cells and ECM can affect the cells in many ways; the response of the cells depends on the type of cells involved, their state at the moment and the specific makeup of the matrix. Sometimes cells respond by shape changes. On other occasions, they migrate, proliferate, differentiate or revise their activities in a more subtle way.
Cellular adhesion often proceeds through formation of small adhesion domains (focal adhesions or adhesion plaques) of aggregated receptor-ligand complexes (Alberts et al., 1983). The formation of these domains provides both stability and directionality to the cell motility process. Focal adhesions constitute a site of dynamic membrane-microfilament interactions involved in regulating cell shape and cell motility (Luna and Hitt, 1992).
The major receptor which mediates formation of focal adhesions and other modes of association with the extracellular matrix is the integrins. Integrins are heterodimeric transmembrane glycoprotein complexes composed of α and β subunits. Both of the subunits contain a large extracellular domain, a transmembrane domain and a small cytoplasmic domain (except for β_4). Integrin clusters provide anchoring sites for the self-assembly of focal adhesion complexes and for the formation of actin cables. They mediate the transfer of signals between the actin-based cytoskeleton and extracellular contacts both in the outside-in and inside-out directions (Yamada and Miyamoto, 1995; Howe et al. 1998; Clark and Brugge, 1995; Giancotti and Ruoslahti, 1999).
The most common feature of the major integrin ligands is short peptide sequences, exemplified by the RGD sequence (Arg-Gly-Asp) in the multifunctional matrix proteins such as fibronectin, fibrinogen and vitronectin. Functional activity of synthetic RGD peptides provided new tools for identifying and characterizing the surface receptors for matrix proteins, and stimulated the search for and the design of new therapeutic agents to treat diseases associated with aberrations in cell adhesion such as thrombosis and neoplasia (Ginsberg and Plow, 1991).

Platelet adhesion and integrin $\alpha_{IIb}\beta_3$

The platelet is among the most thoroughly studied and best understood examples of a cell which undergoes adhesion, spreading and contractile functions which provide the mechanisms for motility (though strictly speaking, the platelet is not a motile cell). Platelets play a critical role in hemostasis and thrombosis by their involvement in the maintenance of blood vessel integrity (Frojmovic and Milton, 1982). Tissue injury releases agents which activate platelets to undergo shape changes. The disc-shaped inactivated platelet is first converted to a sphere which then forms two types of protrusions, flat lamellae and filopodia. Lamellae adhere to extracellular matrix components of injury sites of the endothelial lining. Filopodia bind fibrin strands and other platelets to form a clot. Adhesion initiates a complex set of phenomena, including platelet activation, release of further activating substances, spreading, aggregation and eventual clot retraction to seal the site of the injury.

A number of platelet adhesive receptors have been implicated in these events (Shattil et al., 1994; Williams et al., 1995): GP Ib-IX complex, P-selectin, immunoglobulin-like PECAM-1, CD9, CD36, and integrin $\alpha_{IIb}\beta_3$. When platelets stick (without the help of integrins) to areas of extracellular matrix that have become exposed by disruption of the endothelial cells, the attachment, or subsequent binding to a protein called thrombin, sends a signal into the cytoplasm that ultimately leads to inside-out activation of the $\alpha_{IIb}\beta_3$ integrin on the platelet surface. Integrin $\alpha_{IIb}\beta_3$ then becomes more adhesive and attaches circulating molecules like fibrinogen or von Willebrand factor, which in turn form molecular bridges to more platelets and to the matrix. The resulting aggregate of platelets and proteins culminates in a dense meshwork of cells and fibers.
Integrin $\alpha_{IIb}\beta_3$ is the major integral plasma membrane protein of platelets, which occupies 3% of the total platelet proteins and 17% of the platelet membrane protein mass (Phillips et al., 1988). It consists of an α subunit (136 kDa) which is made up of a heavy chain (GPIIbH, 114 kDa) and a light chain (GPIIbL, 23 kDa) linked by a single disulphide bond, and a β subunit (92 kDa) which is a single polypeptide chain (*Figure 2.1*) (Phillips and Agin, 1977; Calvete et al., 1989; Calvete et al., 1991). The two subunits form a 1 : 1 stoichiometric Ca^{2+}-dependent, noncovalently associated complex (Phillips et al., 1977; Fujimura and Phillips, 1983). A normal platelet contains about 100,000 copies of $\alpha_{IIb}\beta_3$, 80% of which are randomly distributed and exposed on the platelet surface. The remaining fraction is located on the surface-connected canalicular system, which are invaginations the plasma membrane, and in the inner membrane of the cytoplasmic alpha-granules (Calvete, 1994). This cryptic population of $\alpha_{IIb}\beta_3$ becomes surface-expressed and function-capable upon platelet activation, change in platelet shape from a disc to an irregular sphere with many filopodia, and fusion of the alpha-granule membrane with the platelet surface (Niiya et al., 1987).

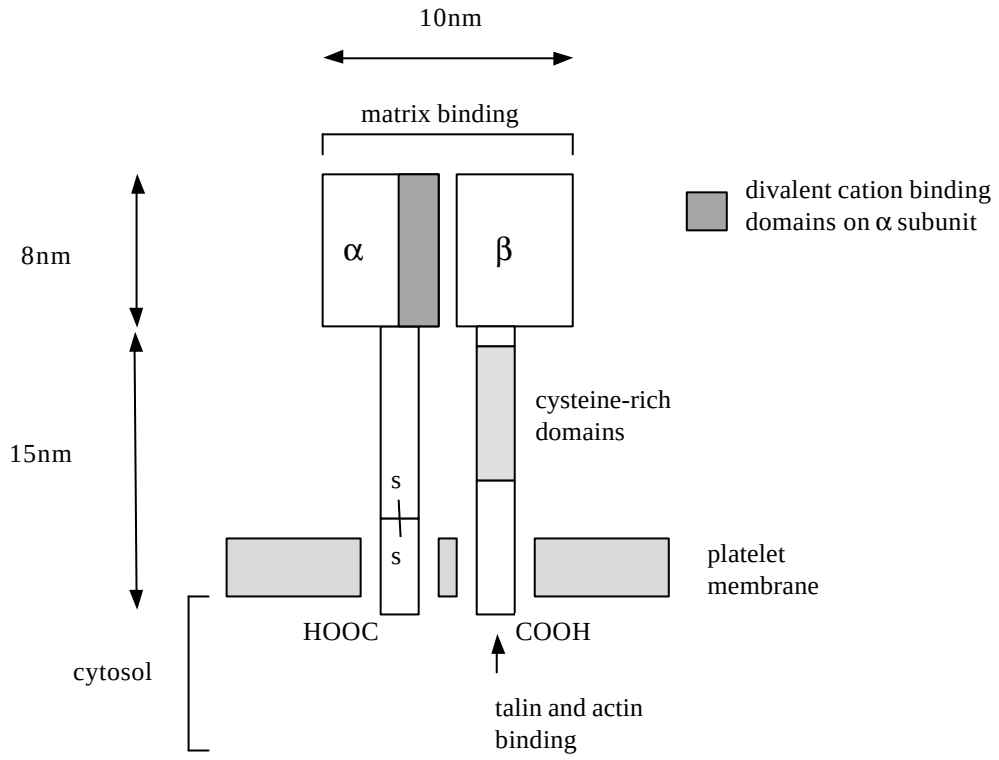

Figure 2.1: Schematic drawing of the molecular structure of $\alpha_{IIb}\beta_3$.

Besides its main role as fibrinogen receptor, $\alpha_{IIb}\beta_3$ also has binding capability for other adhesive proteins found in plasma or in the subendothelium, like fibronectin, vintronectin, and von Willebrand factor. $\alpha_{IIb}\beta_3$ recognizes two basic linear motifs in these ligands, the H12 sequence (HHLGGAKQAGDV) at the carboxyl terminus of the fibrinogen γ-chain (Kloczcwiak et al., 1984), and the RGD motif. The conversion of $\alpha_{IIb}\beta_3$ to a ligand-binding competent conformation is tightly regulated, and activated by cytoplasmic, inside-out signaling. This signaling can be triggered by activation of platelet G-proteins and involves changes in intracellular pH, Ca^{2+}, phosphatidylinositides and protein (including integrin) phosphorylation (Dehar and Hannigan, 1996). Once ligands bind to $\alpha_{IIb}\beta_3$, additional conformational changes within the integrin provides sites of interaction for additional plasma or cytoplasmic proteins (such as talin), and facilitates outside-in signaling leading to physiologic events like clot retraction (Naik and Parise, 1997).

Biophysics of cell adhesion

The physical characterization of cell adhesion is attracting growing interests for many reasons. For instance, as a cell spreads, it arranges its cytoskeleton to exert force towards the adhesive contacts (focal adhesions) that they form ECM and to structurally support the cell interior (Sims et al., 1992). The intracellular stress field thus established (Galbraith and Sheetz, 1998) influences a number of functions such as apoptosis, migration, signal transduction, and ECM remodeling. Another example is that, the complex series of events, which determine the occurrence of a normal hemostatic response, is influenced by the shear fields produced by the blood flow in the vessels. The fluid dynamic conditions modulate all aspects of platelet response to vascular injury (Ruggeri, 1997).
From a physist point of view, cell adhesion is controlled by a complex interplay of specific lock-and-key forces between receptors and ligands; universal forces such as hydration and van der Waals interactions, electrostatic forces, and various polymer-induced forces; and most importantly, the plasma membrane elasticity and the shape of the soft shell. The physical principles that regulate adhesion of soft elastic shells have been elucidated in the so-called continuum theory (Seifert and Lipowsky, 1990; Bruinsma, 1995). In this theory, the adhesion free energy and the tension of a cell adhering to a substrate is related with the shape of the cell (Section 4.2.2). Thus adhesion energy can be calculated from the results of the experiments in which adhesion processes are observed by different microscopic methods including reflection interference contrast microscopy (RICM) and fluorescence microscopy.

Aim of this thesis

Cell adhesion can be mimicked by the designed model systems, composed either only of model membranes (vesicles with reconstituted receptors and ligands), or of the model membranes and functionalized solid supports. A good example is the work of Albersdoerfer and co-workers (Albersdoerfer et al., 1997). Here the biotinylated lipids were incorporated into the DOPC vesicles which also included the lipopolymer DOPE-PEO_{2000} as artificial glycocalix. Attractive lock-and-key forces were mimicked by mediating strong vesicle coupling through streptavidin. RICM combined with the above-mentioned continuum theory was used in this study. The results demonstrated the close correlation between adhesion and lateral phase separation, leading to the formation of adhesion plaques.
The aim of this Ph. D. thesis is to establish a simple model system of adheion for further biophysical research. The model system makes use of the lock-and-key interaction between integrin $\alpha_{IIb}\beta_3$ and the RGD sequence. Through incorporation of the integrin and the lipid-coupled cyclic RGD containing hexapeptide (cyclo(-Arg-Gly-Asp-D-Phe-Lys-Gly-)) into lipid

membranes, the model system is more realistic for studies of fundamental problems of cell adhesion than the biotin-streptavidin system. Due to the universal existence of integrin/RGD interaction in natural cell adhesion processes, the model system is of greater biological relevance.

3 The RGD lipid: molecular design and properties

3.1 Introduction

Based on the assumption that in the ligand/receptor complex, RGD-containing peptide chains have to comply with the specific geometry of the RGD-binding site, extensive studies have been performed in the past on such RGD-containing peptides to mimic the steric requirements for the selective recognition by individual species of the integrin family. In fact, the synthetic RGD peptides and related peptidomimetics constitute potential drugs for the treatment of thrombosis and for other therapeutic applications (Coller, 1994; Kouns et al., 1993; Haubner et al., 1997; Samanen et al., 1997). By varying the RGD-sequence environment, agonists have been obtained that are selective for distinct integrins (Aumailley et al., 1991; Gurrath et al., 1992; Pfaff et al., 1994). Among these agonists cyclic RGD peptides with well-defined structural preferences were found to be highly potent and selective for either $\alpha_{IIb}\beta_3$ or $\alpha_V\beta_3$ integrins (Pfaff et al., 1994; Finsinger, 1997; Kantlehner et al., 1999).
In this thesis a new integrin $\alpha_{IIb}\beta_3$-specific, cyclic RGD-containing hexapeptide, cyclo(-Arg-Gly-Asp-D-Phe-Lys-Gly-), was used. It was coupled either to biotin or to a dimyristoylthioglyceryl anchor through special spacers. Basic properties of the obtained derivatives were studied in the present chapter. Part one of the chapter describes the molecular design of these derivatives. Part two deals with the determination of a proper spacer length and the binding constant between $\alpha_{IIb}\beta_3$ and the hexapeptide through ELISA and SPR measurements. Part three and four present results of DSC and film balance techniques, showing that the lipidated hexapeptide with the proper spacer length (**the RGD lipid**) can be incorporated into both DMPC monolayers and DMPC vesicles. Part five shows that the lipid bílayer anchored hexapeptide initiated specific platelet adhesion behaviors on solid supports. From the studies of this chapter, one can conclude that the RGD lipid with the determined spacer length is well suitable for adhesion studies using model membranes.

3.2 Molecular design

Initially two kinds of cyclic RGD hexapeptides were obtained from Prof. H. Kessler´s lab in the Institut für Organische Chemie and Biochemie of TUM: cyclo(-Arg-Gly-Asp-D-Phe-Val-Lys-) and cyclo(-Arg-Gly-Asp-D-Phe-Lys-Gly-). It had been shown that the latter one has a higher affinity to $\alpha_{IIb}\beta_3$ (Finsinger, 1997). To graft this peptide to different surfaces, biotin and the [(2-RS)-1,2-dimyristoyl-3-thioglyceryl]succinimido-propanoyl lipid anchor were chosen to be linked to it. With biotin, the peptide can be easily immobilized on solid surfaces through the strong interaction between biotin and streptavidin or ExtrAvidin. With the lipid anchor, the lipidated peptide may be reconstituted into lipid vesicles either for surface functionalization (through lipid spreading or vesicle fusion methods) or for direct vesicle adhesion experiments.

It has been suggested that the ligand binding site of $\alpha_{IIb}\beta_3$ is 1 – 2 nm deep in its extracellular part (Calvete, 1994). Two kinds of spacers, ε−aminohexanoic acid (εAhx) and εAhx–Gly-Gly, were introduced between cyclo(-Arg-Gly-Asp-D-Phe-Lys-Gly-) and biotin or the lipid anchor (*Figure 3.1*), to make sure that the surface anchored cyclic RGD peptide can effectively bind to $\alpha_{IIb}\beta_3$. Both spacers were linked to the side chain amino group of Lys of the peptide. This part of synthesis work was done by Achim Escherich of Prof. L. Moroder´s lab in the Max Planck Institut für Biochemie (Martinsried) (Hu et al., 2000).

The spacer length is defined as the maximum length of an extended spacer between the lysine β-carbon and the biotin carbonyl and was calculated from known bond lengths and bond angles. It is 1.48nm for the εAhx spacer (Figure 3.1, **compound 1**) and 2.2nm for the εAhx–Gly-Gly spacer (**compound 2**). The latter one is about 49% longer. To examine the effectiveness of the two spacers, they were introduced between biotin and the cyclic RGD peptide at first, in order to apply ELISA and SPR to measure the binding of $\alpha_{IIb}\beta_3$ to the biotinylated peptide which is immobilized on solid surfaces through biotin/Streptavidin or biotin/ExtrAvidin interaction. The spacer found to have the proper length can then be introduced between the RGD peptide and the above mentioned lipid anchor.

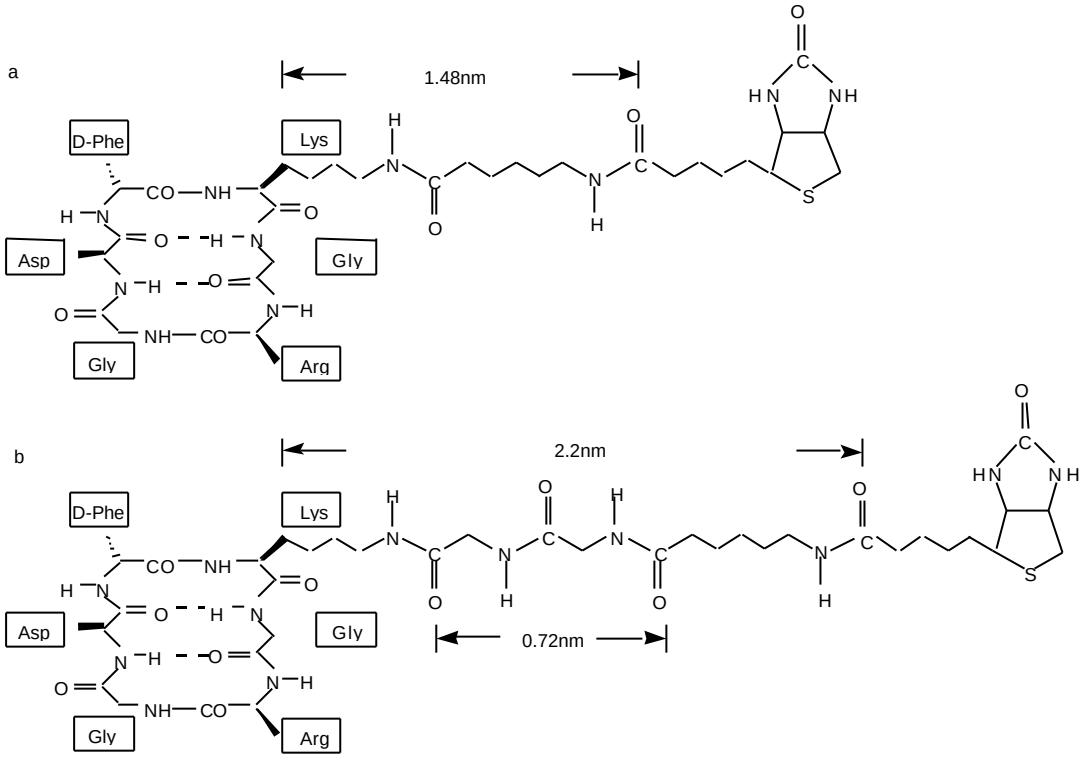

Figure 3.1: Chemical structure of the biotinylated cyclic RGD-containing hexapeptide with different spacer lengths: **a**) compound 1; **b**) compound 2.

3.3 Determination of the proper spacer length and the dissociation constant

3.3.1 Materials

Proteins and antibodies

Fibrinogen was purchased from Calbiochem (Bad Soden, Germany), BSA and ExtrAvidin (recombinant, non-glycosylated avidin) from Sigma (Deisenhofen, Germany). The primary rabbit against human platelet integrin β_3 polyclonal antibody was purchased from Chemicon International Inc. (Temecula, CA, USA) and the secondary goat against rabbit IgG (whole molecule) conjugated to alkaline phosphatase was from Sigma (Deisenhofen, Germany).

Columns

ConA-Sepharose, Heparin-Sepharose, Sephacryl S-300, and Sepharose G-25 PD-10 columns were from Pharmacia (Freiburg, Germany).

Chemicals

Biotin XX SE (biotinoylaminohexanoylaminohexanoic acid succinimidyl ester) and Carboxytetramethylrhodamine succinimidylester were obtained from Molecular Probes (Eugene, OR, USA), and p-nitrophenylphosphate, phenylmethylsulfonyl fluoride (PMSF), diphenylcarbamyl-Cl (DPC-Cl), detergents, α-methyl-D-mannose, dimethylformamide (DMF) from Sigma. Leupeptin hemisulfate was purchased from Fluka (Deisenhofen, Germany). All other chemicals, electrophoresis reagents, buffer substances, and salts were of the highest available purity and were purchased from Sigma or Merck (Darmstadt, Germany).

3.3.2 Methods

Preparation of $\alpha_{IIb}\beta_3$

$\alpha_{IIb}\beta_3$ was purified from human platelets following essentially the method of Fitzgerald et al. (Fitzgerald et al., 1985). Up to 40 outdated platelet concentrates from a local blood bank were cleared from red blood cell contaminants by centrifugation at 215 × g for 20 min at room temperature, and then washed three times in washing buffer (20 mM Tris-HCl pH 7.4, 150 mM NaCl, 1 mM EDTA, and 0.55 mM acetylsalicic acid) for 30 min at 1,750 × g. Cells were broken by 2 bursts of 20 s with a homogenator (Ultra-Turrax, IKA, Staufen, Germany) on ice in washing buffer and in the presence of protease inhibitors (0.1 mM leupeptin, 1 mM PMSF, 0.1 mM DPC-Cl) and then centrifuged at 120,000 × g for 30 min at 4 °C. Membrane proteins were solubilized from the pellets in lysis buffer (1% Triton X-100 in 50 mM Tris-HCl pH 7.4, 1 mM $CaCl_2$, and 1 mM $MgCl_2$), and again homogenized in the presence of protease inhibitors. After centrifugation (30,000 × g, 15 min) the supernatant was applied to a concanavalin A-Sepharose column (20 ml bed volume, equilibrated against affinity column buffer: 20 mM Tris-HCl pH 7.4, 100 mM NaCl, 0.1 % Triton X-100, 1 mM $CaCl_2$, 1 mM $MgCl_2$, and 0.05 % NaN_3), and the column was washed with several bed volumes of affinity column buffer. The concanavalin A-retained glycoproteins were eluted from the column with the same buffer containing 100 mM α-methyl-D-mannoside. The integrin-containing peak from the ConA column was applied to a heparin affinity column (20 ml bed volume) in affinity column buffer. The flow-through collected from the heparin column was concentrated

to 10 mL or less, and applied to a Sephacryl S-300 gel filtration column (2.5 × 100 cm) in gel filtration buffer - **buffer A** (20 mM Tris-HCl pH 7.4, 150 mM NaCl, 0.1 % Triton X-100, 1 mM $CaCl_2$, 1 mM $MgCl_2$, and 0.05 % NaN_3). All chromatographic steps were carried out at room temperature and the whole isolation procedure was performed within three days. The integrin content and purity of protein fractions were determined by SDS gel electrophoresis (LaemmLi, 1970). Protein concentration was determined according to Peterson (Peterson, 1977). The final product can be kept on ice for several weeks without significant loss of binding activity.

Biotinylation of fibrinogen

Fibrinogen was dissolved in (150 mM $NaHCO_3$, pH 8.5), at a concentration of 10 mg/ml**.** To 9 volumes of this solution, 1 volume of 10 mg/ml Biotin XX SE in DMF were slowly added and mixed. After being incubated for 1 hour at room temperature, the mixture was applied to a Sepharose G-25 PD-10 column to separate unbound biotin (*Figure 3.2*).

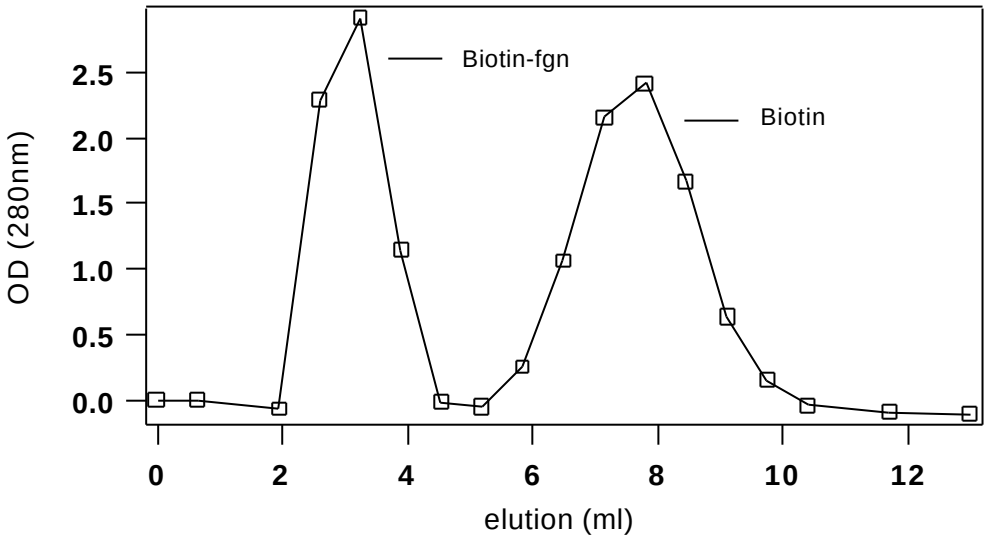

Figure 3.2 Separation of biotinylated fibrinogen from free biotin molecules by the Pharmacia PD-10 Sephadex G-25 portable column.

Enzyme-linked immunosorbant assay (ELISA)

General steps include: 1) Protein immobilization and subsequent BSA blocking (to prevent unspecific binding) on the surface of a microtiter plate; 2) Ligand binding; 3) Primary (anti-ligand) antibody binding; 4) Secondary antibody binding; 5) Color reaction is catalyzed by the enzyme coupled to the secondary antibody and is measured on an ELISA reader. Final values were obtained by averaging results of eight parallel measurments. When the same preparation of proteins and the same lot of antibodies were used, there are good linear relationships between OD_{405nm} and protein concentration or antibody dilution level (*Figure 3.3*).

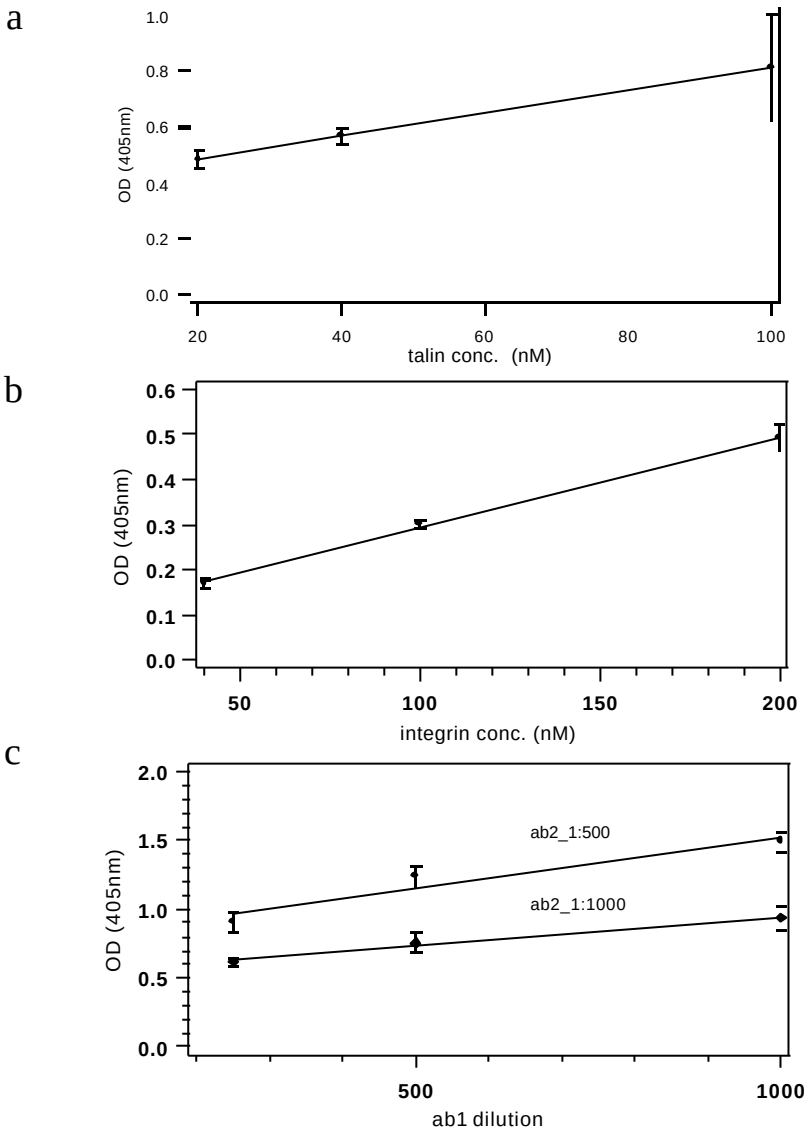

Figure 3.3: ELISA. Dependence of final color reaction on: **a**) coating protein concentration; **b**) ligand protein concentration; **c**) antibody dilution. For (a), the coating protein was talin, the ligand protein was 300 nM $\alpha_{IIb}\beta_3$, and ab1 and ab2 were diluted by 1:1000. For (b), the coating protein was 20 nM fibrinogen, the ligand protein was $\alpha_{IIb}\beta_3$, and ab1 and ab2 were diluted by 1:1000. For (c), the coating protein was 20nM talin and the ligand protein was 300 nM $\alpha_{IIb}\beta_3$.

All steps were performed at room temperature except when stated otherwise. In a typical integrin binding assay, 50 nM ExtrAvidin in buffer A without detergent were immobilized on microtiter plates (100 µl/well) at 4 °C overnight. The plates were washed twice with the same buffer, and then blocked with 3 % BSA for 2 hours. 50 nM fibrinogen (as control), 50 nM biotinylated fibrinogen, and different concentrations of biotinylated peptides in blocking buffer (buffer A with 0.04 % Tween 20 instead of Triton X-100) were added and allowed to react with immobilized ExtrAvidin for 1 hour. After unbound ligands were removed by washing the wells 4 times with blocking buffer, integrin $\alpha_{IIb}\beta_3$ in buffer A was added, and incubated with immobilized ligands for 2 hours. Primary rabbit against human platelet

integrin β_3 polyclonal antibodies, and secondary goat against rabbit antibodies coupled to alkaline phosphatase were then applied for one hour each. After removal of unbound antibodies by an additional washing step, 1 mg/mL p-nitrophenylphosphate in 10 mM diethanolamine, 0.5 mM $MgCl_2$, pH 9.5, was added and after 30 min the enzymatic reaction was stopped by 100 mM EDTA (pH 8.5). Substrate hydrolysis was determined by an ELISA reader at 405 nm. Detailed conditions of other ELISA reactions are described in the related texts and figure legends.
Maxisorp™ type of Nunc-Immuno™ plates (8×12 wells, Nalge Nunc International, Wiesbaden-Biebrich, Germany) were used in the experiments. The plates are made of polystyrene and have high affinity to molecules with mixed hydrophilic / hydrophobic domains. The ELISA reader was Microplate Reader MRX from Dynatech Deutschland GmbH, Germany.

Surface plasma resonance (SPR)

Theory

A BIACORE X (Biacore AB, Uppsala, Sweden) was used in SPR measurements. It is based on the Pharmacia real-time BIA (Biomolecular Interaction Analysis) system. This system uses the optical phenomenon, surface plasmon resonance (SPR), to monitor biomolecular interactions.
At an interface between two transparent media of different refractive index (e.g. glass and water), light coming from the side of higher refractive index is partly reflected and partly refracted. Above a certain critical angle of incidence no light is refracted across the interface and total internal reflection is observed. Although the incident light is totally reflected, an electromagnetic field component called the evanescent wave penetrates a short distance (of the order of one wavelength) into the medium of lower refractive index (*Figure 3.4*). If the interface between the media is coated with a thin layer of metal, and the light is monochromatic and p-polarized (i.e. the electric vector component is parallel to the plane of incidence), the intensity of the reflected light is markedly reduced at a specific incident angle. This phenomenon is called surface plasmon resonance or SPR, and the angle is called the SPR angle. This angle depends on several factors, one of which is the refractive index of the medium into which the evanescent wave propagates, on the non-illuminated side of the surface. In real-time BIA, the refractive index of the medium is affected by the surface concentration of solutes, so that monitoring the SPR angle provides a real-time measure of changes in the surface concentration (other factors being equal).
In BIA instruments, light coming from a high-efficiency light emitting diode with a wavelength in the near infra-red region is focused on the glass-gold interface of the sensor chip in a wedge-shaped beam, giving a fixed range of incident angles. Reflected light is monitored by a two-dimensional diode array, and interpolation algorithms in the instruments software determine the resonance angle to a resolution corresponding to 0.1 RU (resonance unit). Measurements are made under conditions of continuous flow. The sensor chip surface is made biospecific by immobilizing one component of the interaction on the sensor chip. The other component(s) flow(s) over the surface in solution. The dextran matrix on the sensor chip surface facilitates immobilization of biomolecules under non-denaturing conditions, increasing the surface capacity and minimizing the denaturing effects of direct adsorption to a gold film.

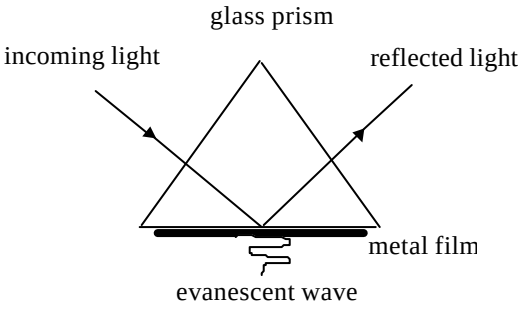

Figure 3.4: Principle of SPR: Under conditions of total internal reflection at a metal-coated interface, an evanescent wave propagates into the medium of lower refractive index on the non-illuminated side.

1) Association kinetics: The reaction between immobilized biotinylated cyclic RGD-peptide (with longer spacer) and integrin $\alpha_{IIb}\beta_3$ in the bulk solution may be described by the equation

$$A + B \underset{k_d}{\overset{k_a}{\Leftrightarrow}} AB$$

The rate is given by

$$\frac{d[AB]}{dt} = k_a[A][B] - k_d[AB]$$

which may be expressed in terms of the SPR signal as

$$\frac{dR}{dt} = k_a C R_{max} - (k_a C + k_d)R$$

where $\frac{dR}{dt}$ is the rate of change of the SPR signal, C is the concentration of $\alpha_{IIb}\beta_3$, R_{max} is the maximum $\alpha_{IIb}\beta_3$ binding capacity in RU, and R is the SPR signal in RU at time t. A plot of $\frac{dR}{dt}$ against R will be a straight line with slope $-(k_a C + k_d)$. Define S = $k_a C + k_d$. Plotting the S values obtained at different concentrations will give a line with slope k_a and intercept on the ordinate k_d. The final equillibrium dissociation constant K_D is given by $K_D = k_d / k_a$.

2) Dissociation kinetics: The dissociation phase is described by

$$\frac{dR}{dt} = -k_d R$$

Separating variables and integrating gives

$$R_t = R_0 \cdot e^{-k_d(t-t_0)}$$

k_d can then be directly obtained from the exponential fit of the dissociation curves.

Experimental

Sensor Chip SA from Biacore AB was used in the experiments. On the chip surface streptavidin had been covalently immobilized on a carboxymethylated dextran matrix (*Figure 3.5*).

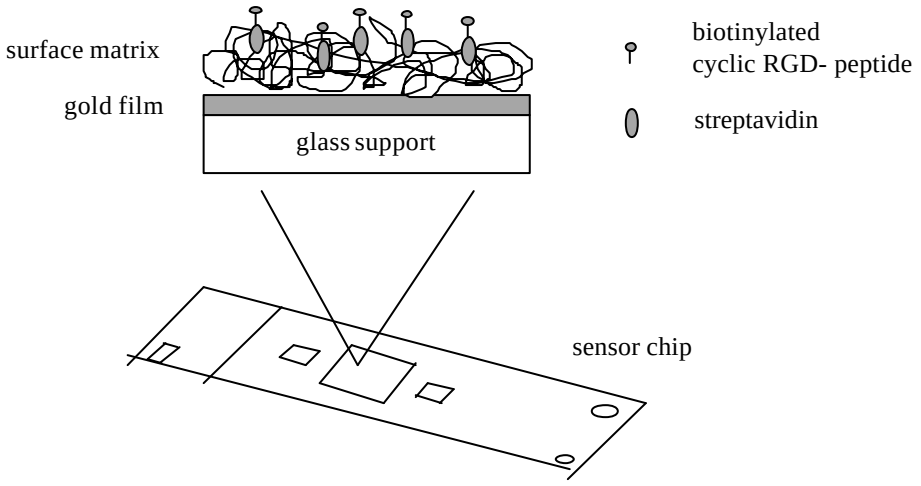

Figure 3.5: Schematic drawing of Sensor Chip SA.

The buffer A served as solvent for all experiments, and a flow rate of 10 µl/min was applied. Both the sample and the reference cell of the sensor chip were conditioned with three consecutive 1-minute injections of 1 M NaCl in 50 mM NaOH. In the sample cell the chip was then coated by a 30 µl injection of 1 µM biotinylated cyclic RGD-peptide. Different concentrations of $\alpha_{IIb}\beta_3$ were injected into the sample cell, and the differential signals between the sample cell and the reference cell were observed during 6 min. Between two subsequent integrin injections, 2 mg/mL of a linear RGD peptide (Ac-GRGDFSK) were added (6-min injection) to displace the bound integrin from the surface until the baseline returned to the original level. The binding kinetics was usually preceded by a sharp signal increase of a few seconds (around 1 µl of flow) which derived from the difference of refraction indices between the sample and the reference solution. This part of the signal was ignored in the final data processing.

3.3.3 Results

In Peter´s ELISA experiment (Peter, 1999), fibrinogen was coated on a miocrotiter plate and $\alpha_{IIb}\beta_3$ binding was examed in the presence of compound **1**. The experiment proved that compound **1** is a competitive agonist for integrin $\alpha_{IIb}\beta_3$. But in the present work, *Figure 3.6* shows (columns i and j) compound **1** was ineffective in mediating the binding of $\alpha_{IIb}\beta_3$ to ExtrAvidin-coated microtiter wells. These results suggested that compound **1** acts as a specific agonist in bulk solutions, but is incapable of penetrating into the RGD binding pocket of integrin if it is bound to surfaces. Most likely, the ε-aminohexanoyl spacer is too short. The spacer length was increased by roughly 50% via addition of two glycine residues to the spacer of compound **1** leading to compound **2**. Glycine was chosen since an additional εAhx residue was expected to enhance the hydrophobic character of the spacer. As shown in Figure 3.6 (g, h) the elongation of the spacer completely restores the integrin-binding capacity of the cyclic RGD-peptide.

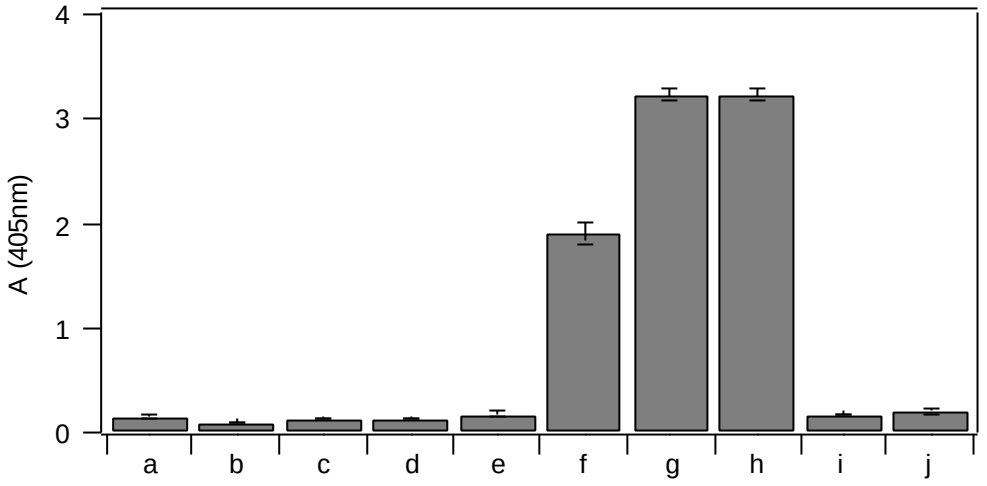

Figure 3.6: Integrin binding to ExtrAvidin-bound cyclic RGD peptides with different spacer length (ELISA). In all experiments the microtiter plate was coated with 50 nM ExtrAvidin, as described in Materials and Methods. **a** - **d**, controls without integrin; **a**: without fibrinogen and cyclic RGD-peptides; **b**: 50 nM biotinylated fibrinogen; **c**: 10 µM of compound **2**; **d**: 10 µM of compound **1**. **e** - **j**, after binding of ligands to ExtrAvidin, incubation with 200 nM integrin; **e**: 50 nM fibrinogen; **f**: 50 nM biotinylated fibrinogen; **g**: 1 µM of compound **2**; **h**: same as in g but 10 µM; **i**: 1 µM of compound **1**; **j**: same as in i but 10 µM. Note that fibrinogen (column *e* and *f*) can only be considered as a qualitative control in this experiment.

From *Figure 3.7A* it can be seen that a concentration of 1 µM of compound **2** was already saturating the binding sites of the ExtrAvidin-coated microtiter wells. For the determination of the dissociation constant between compound **2** and $\alpha_{IIb}\beta_3$, the wells were preincubated with 10 µM of compound **2**, washed, and incubated with varying $\alpha_{IIb}\beta_3$ concentrations. The result is shown in *Figure 3.7B*. Since the color reaction of the ELISA did no longer increase linearly at higher integrin concentrations, we determined the maximal binding concentration by a double-reciprocal plot which is less sensitive towards non-linear behavior at higher concentrations (evaluation procedure not shown). With this method the half-maximum binding concentration was found to be 158 nM. This value can be taken as an approximate measure for the equilibrium dissociation constant, K_D. Since the K_D of biotin (10^{-15} M and 10^{-14} M for avidin and streptavidin, respectively (Green, 1990)) is 7 to 8 orders of magnitude lower, the dissociation of biotin from ExtrAvidin can be neglected. The amount of bound biotinylated fibrinogen (column *b* in Figure 3.7A) can be taken as a qualitative but not quantitative control. It cannot be compared quantitatively because of different binding characteristics: fibrinogen has two integrin binding sites per molecule, and dissociation constants differ from that of RGD peptides alone (see below). Moreover, the single fibrinogen molecule occupies a much larger area on the surface than the peptide and may be functionally impaired by the chemical modification.

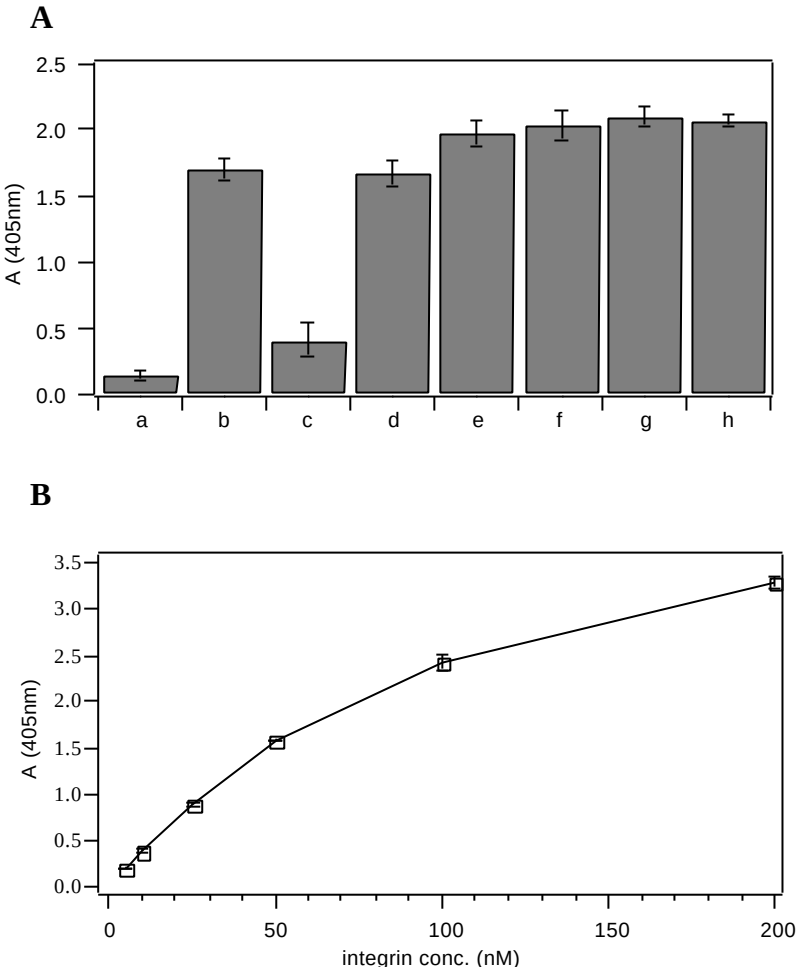

Figure 3.7: Integrin binding to compound **2** (Figure 3.1b) immobilized on surface-bound ExtrAvidin (ELISA). **A**: Variation of integrin binding with the concentration of compound **2**. The concentration of integrin added was always 200 nM, ExtrAvidin coating occured as in figure 3. **a**: 50 nM Fibrinogen, absence of compound **2**; **b**: 50 nM biotinylated Fibrinogen, absence of compound **2**; **c - h**: compound **2**; **c**: 10 nM; **d**: 50 nM; **e**: 100 nM; **f**: 500 nM; **g**: 1 μM; **h**: 10 μM. Note that, as in Figure 3.6, fibrinogen binding was introduced as a qualitative control and cannot be directly compared to cRGD-binding of integrin. **B**: Variation of integrin binding to compound **2** with the concentration of integrin. The microtiter plate was coated with 50 nM ExtrAvidin and then treated with 10 μM of compound **2**.

In order to obtain more detailed information on the binding kinetics of integrin to the surface-grafted peptide, the on/off kinetics of integrin binding to the surface anchored cyclic peptide was directly measured by the surface plasmon resonance method. Original kinetic curves are shown in *Figure 3.8*. Association and dissociation curves obtained from Figure 3.8 are shown in *Figure 3.9A* and *Figure 3.9C*, respectively. From Figure 3.9A the exponential rates S were extracted by exponential fits and displayed against the protein concentrations in *Figure 3.9B*. With a linear fit according to the relation, $S = k_a C + k_d$, an association rate of k_a = 5400 ± 600 M^{-1} s^{-1} and a dissociation rate of k_d = (6 ± 0.3) × 10^{-3} s^{-1} were determined. From these data an equilibrium dissociation constant, $K_D = k_d / k_a$, of 1.1 ± 0.1 µM was derived. Taking k_d directly from the exponential fit of the dissociation curves of Figure 3.9C, an average value of (8 ± 4) × 10^{-3} s^{-1} was obtained which is in acceptable agreement with the value extracted from the plot in Figure 3.9A. Using this value a K_D of 1.5 ± 0.8 µM is obtained. Thus, the K_D values derived from the ELISA experiments, and the K_D value determined by SPR differ by a factor of 7 – 9.5, a discrepancy that will be discussed below.

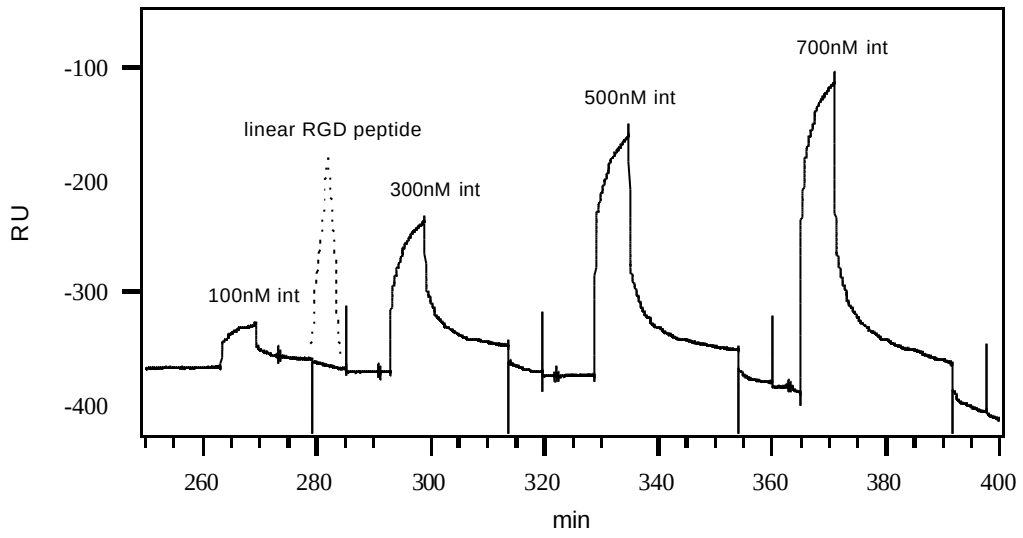

Figure 3.8: SPR. Kinetics of adsorption/desorption of $\alpha_{IIb}\beta_3$ to / from the immobilized biontinylated cyclic RGD-peptide with longer spacer. Response points of four $\alpha_{IIb}\beta_3$ concentrations (100 nM, 300 nM, 500 nM and 700 nM) were recorded. After each adsorption/desorption measurement, both the sample and reference cells were washed with 2 mg/ml of the linear RGD peptide Ac-GRGDFSK.

A

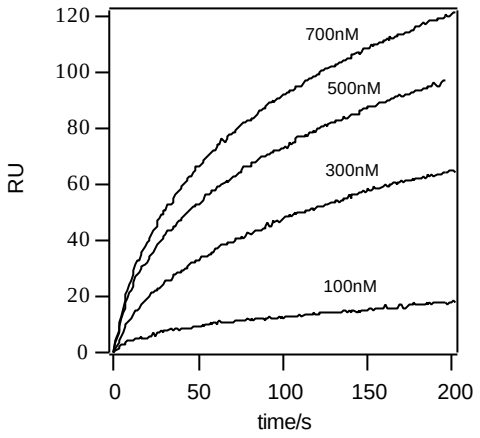

B

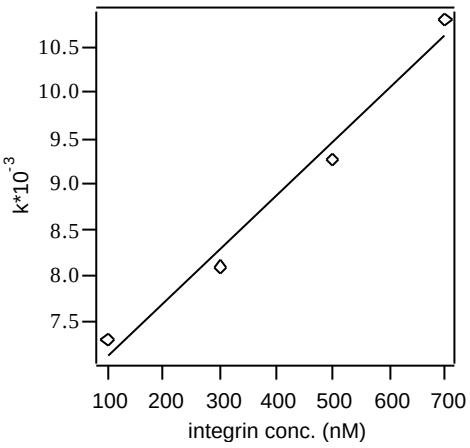

C

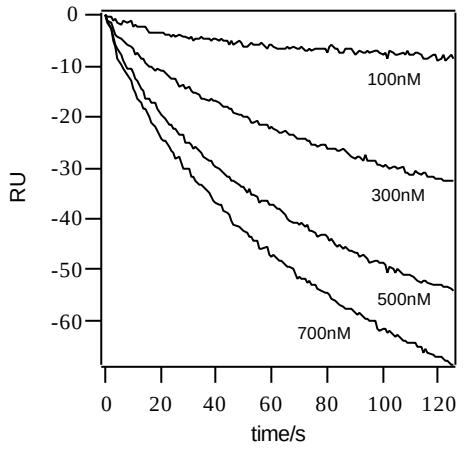

Figure 3.9: Kinetics of the binding of integrin to compound **2** immobilized on streptavidin (SPR). **A**: Adsorption of integrin to the sensor chip surface (traces representing 100 nM, 300 nM, 500 nM, 700 nM from bottom upwards, respectively); **B**: observed exponential rates from (A) displayed against the protein concentration. Superimposed is a linear fit for the evaluation of k_a and k_d; **C**: desorption of integrin from the chip surface with washes of excess Ac-GRGDFSK (traces for increasing integrin concentrations follow from top downwards).

3.3.4 Discussion

Since the RGD motif is an important component in the interaction of cells with extracellular matrix proteins, peptides containing this motif are of particular interest. RGD-containing lipopeptides have been used to study conformational changes of surface-bound peptides (Marguerie et al., 1980) and to investigate the influence of forming a RGD-containing loop by conjugating lipid anchors to both the amino and the carboxy terminal of the peptide (Pakalns et al., 1999). In the latter study it was shown that such a loop was most effective in influencing cellular responses like adhesion, spreading, and cytoskeletal reorganization of cells. In the present study, a conformationally restricted cyclic peptide instead of a flexible RGD-containing loop was employed. The results confirm that the cyclic hexapeptide moiety of compound **2** can be used as competitive agonist for $\alpha_{IIb}\beta_3$. However, the length of the spacer arm connecting such a peptide to the surface represents a key parameter and must be larger than 15 Å if the integrin is to be grafted effectively upon the surface. This agrees with recent findings on the adhesion of $\alpha_V\beta_3$ and/or $\alpha_V\beta_3$ expressing osteoblasts to cyclic RGD-pentapeptides which were covalently coupled to PMMA-coated surfaces. Kantlehner et al. (Kantlehner et al., 1999) showed that a distance of about 35 Å between the RGD pharmacophoric group and the surface was needed for efficient cell adhesion. This distance was determined by beginning with the α-carbon of the lysine residue of the cyclic peptide which must be added to the calculated length of our spacer. The remaining difference may be due to the fact that cells are covered by a glycocalix, varying in thickness depending on the cell type (Alberts et al., 1994). Other factors like thermal undulation of the plasma membrane and domain formation may play an additional role (Albersdoefer et al., 1997). Since the present studies were performed with purified integrin inserted into artificial bilayers, a spacer of suitable length is most probably required to allow the cyclic peptide to penetrate deep enough into the RGD binding pocket of the receptor. This binding pocket is assumed to play a crucial role for the control of activation (Naik and Parise, 1997). Information on the binding pocket is available from models of integrins (Plow et al., 1992; Calvete, 1994). The evidence for such a deep location of the binding site is still indirect and mainly based on antibody-epitope analysis (Calvete, 1993), since the 3-dimensional structure of the extracellular domain is only roughly known from electron microscopic studies (Weisel et al., 1992). However, structural data are available on several disintegrins, a group of small RGD-containing proteins isolated from various snake venoms, which act as strong integrin agonists interfering with integrin-mediated adhesion. The 3D NMR structure analysis of some of these polypeptides revealed that the RGD motive is exposed on a highly flexible loop protruding 14-17 Å from the protein surface (Saudek et al., 1991; Adler, 1991). In the case of echistatin, it was shown that this RGD-containing loop reacts selectively with both $\alpha_V\beta_3$ and or $\alpha_V\beta_3$ but that the binding is dependent on cooperation between the (N-terminal) RGD loop and the C-terminal domain which is necessary for optimal presentation of the binding site (Marcinkiewisz, 1997). With cyclic peptides, it was possible even to discriminate between these two closely related integrins (Aumailley et al., 1991; Pfaff et al., 1994).

Regarding the different K_D values determined in two different assays the question may be raised whether solid surface-bound binding tests of integrin are reliable. For fibrinogen/integrin $\alpha_{IIb}\beta_3$, several studies have been done with different results. With a solid-phase binding assay on the immobilized intergrin, a K_D of 12nM was found (Charo et al., 1991), seemingly coinciding with exactly the same value found for fibrinogen binding to purified platelet membranes before (Phillips and Baughan, 1983). Using different techniques, however, higher K_D values were measured: 50nM with total internal reflection fluorescence (TIRF) microscopy (Müller et al., 1993) and 20-70nM with SPR (Huber et al., 1995). In an

attempt to clarify the reasons for diverging results, Tangemann and Engel (Tangemann and Engel, 1995) demonstrated variations of the dissociation constants up to a factor of 1000 depending on the technique applied (RIA, ELISA, or biotin/streptavidin). In addition to these divergent results, the binding reaction was found to be a two-step process comprising a fast and a slow component (Müller et al., 1993; Huber et al., 1995). However, the two different K_D values, which were determined in the present study for compound **2**, do not indicate a two-step mechanism. The two-step mechanism in the case of fibrinogen/integrin interaction may derive from conformational changes in the process. Thus, Erb (Erb et al., 1997) showed that a two-step mechanism of the activated integrin was dependent on the more complex interaction with fibrinogen. For RGD-containing peptides, such a two-step mechanism has not been reported. For linear RGD-peptides, K_Ds of 1.0 µM by equilibrium dialysis (Steiner et al., 1989) and 1.7 µM by the TIRF method (Pfaff et al., 1994) were found. In the latter study, several cyclic RGD-peptides were also characterized with K_D values between 1.3 and 5 µM, one closely resembling the cyclic hexapeptide of compound 2 had a K_D of 1.43 µM. To our knowledge there is only one report on a cyclic RGD-peptide with a much lower K_D (10 nM) (Suehiro et al., 1996) but that compound has a quite different chemistry and may not be comparable with our results. In our case basically the same type of biotin-mediated anchorage was used with both methods, neither of the techniques applied is a simple equilibrium method. The precautions based on the work of Tangemann and Engel (Tangemann and Engel, 1995) apply mainly to the ELISA technique since it is based on a color reaction which occurs after three consecutive binding steps (integrin, primary, and secondary antibody). Thus, in the light of the above discussion of the results from other groups using various different techniques, and realizing that the SPR technique provides the possibility of calculating an equilibrium dissociation constant from direct measurements of on and off reaction rates, we consider the higher K_D of 1.1 - 1.5 µM derived from SPR measurements as the more probable value.

3.4 The RGD lipid: DSC measurements

3.4.1 Materials and methods

Materials

The RGD lipid (*Figure 3.10*) was made by linking the cyclic RGD hexapeptide (cyclo(-Arg-Gly-Asp-D-Phe-Lys-Gly-)) and the [(2-RS)-1,2-dimyristoyl-3-thioglyceryl] succinimido-propanoyl lipid anchor via the 2.2 nm spacer (εAhx–Gly-Gly) (Hu et al., 2000). It was found to have the highest solubility in the solution of Chloroform : Methanol : Millipore water = 65 : 25 : 4 (volume ratio) (data not shown). Residual filament-like aggregations in the solution were removed by filtering with Millex-GV_4 filters (organic solvent resistant, Millipore Products Division, Bedford, USA) with 0.22 μm film.

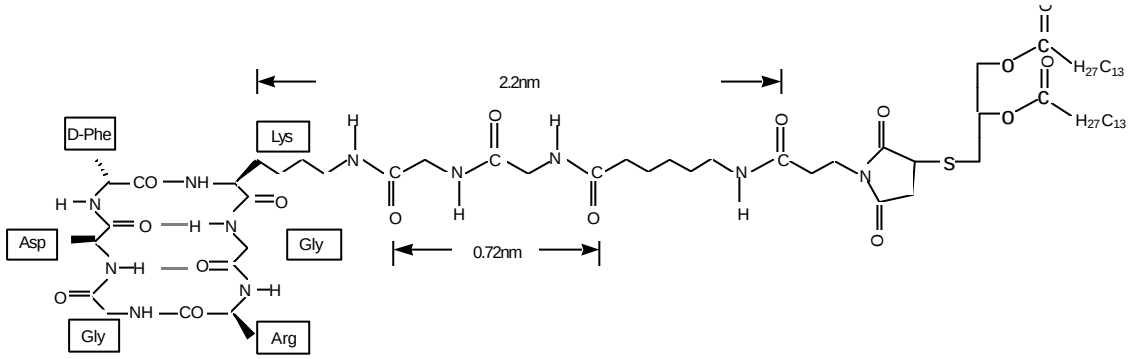

Figure 3.10: Chemical structure of the RGD lipid.

Chloroform and methanol were bought from Fluka (Neu-Ulm, Germany) and were reagent p.a. grade. Dimyristoylphosphatidylcholine (DMPC) was bought from Avanti Polar Lipids (Alabaster, AL, USA). All other chemicals were of the highest available purity and were purchased from Sigma (Deisenhofen, Germany) or Merck (Darmstadt, Germany).

Vesicle preparation by sonication

Dissolved DMPC and the RGD lipid were mixed at the required amounts in a small glass container, dried briefly by nitrogen gas, and put under vacuum overnight to completely remove organic solvents. 1 - 2 ml of buffer A was added into the container. The solution was then sonicated for 2 minutes with 50% power, 30% cycle, and 20 second intervals between each 30 seconds. The vesicle solution was degased in vacuum for 5 minutes before use.

Differential scanning calerimetry

The VP-DSC MiroCalorimeter (MicroCal™ Incorporated, Northampton, U. S. A.) uses a cell feedback network (CFB) to differentially measure heat produced or absorbed between a sample and a reference cells. The twin coin-shaped cells are mounted in a cylindrical adiabatic environment, and communicate with the outside through narrow access tubes. The cells (effective volumes: 0.5149 ml) are made from Tantaloy 61™, which has corrosion properties similar to glass. A thermoelectric device measures the temperature difference between the two cells and a second device measures the temperature difference between the

cells and the jacket. As chemical reactions occur in the sample cell, heat is generated or absorbed. The temperature difference between the sample and reference cells (ΔT_1) is kept at zero by the addition of heat to the sample or reference cell, as appropriate, using the CFB system. The integral of the heat required to maintain $\Delta T_1 = 0$ over time is a measure of the total heat resulting from the process being studied.
The VP-DSC system is connected with a Gateway2000 PC and controlled by a software named VPViewer (MicroCal™ Incorporated). Data are processed with Origin for DSC (MicroCal™ Incorporated). The scan rate in the present work was 30 °C per hour, and the scan range was 5 – 45 °C. Prescan and postscan thermalstable time was 15 minutes each. No feedback mode was used. Filtering period was 16 seconds.

3.4.2 Results and discussion

With differential scanning calorimetry (DSC), the insertion of the RGD lipid into the lipid bilayer of vesicles was analyzed by the effect exerted on the phase transition thermograms (*Figure 3.11*). With DMPC, the main transition of the pure lipid was found at 24.14 °C as a sharp peak and a pre-transition peak at 14.61 °C (Figure 3.11, trace a) in good agreement with known data (Cevc, 1993). With increasing molar fraction of the lipopeptide, the pre-transition peak became smaller, and the shape of the main transition peak was broadened and slightly shifted to a higher temperature. It also became more asymmetrical with a slight shoulder at 25 °C (Figure 3.11, traces b-d). *Figure 3.12* shows detailed relationships between the RGD lipid concentration and some parameters of the DSC traces shown in Figure 3.11. Note that in Figure 3.12d, $\Delta T_{1/2}$ is the temperature width at half-height of the heat absorption peak, which is often used to represent the sharpness of a phase transition.
Since DSC traces are extremely sensitive towards small changes of the intermolecular order of lipid molecules within the bilayer but is unaffected by molecules free in solution, it can be concluded from the present experiments, that the lipidated cyclic RGD-peptide was well inserted into DMPC vesicle membranes (Marbrey-Gaud, 1981; McElhaney, 1986). Broadening of the main phase transition peak can be interpreted as being caused by statistical insertion of the lipid anchor whereas the shoulder suggests the forming of domains of the lipidated peptide. Disappearance of the pretransition peak is to be expected, since usually very small quantities of ´impurities´ in the phosphatidylcholine bilayer reduces and abolishes the pretransition (McElhaney, 1986). In the fluid lipid phase at higher temperatures, the lipid-anchored cRGD can thus be expected to be highly mobile in the level of the membrane.

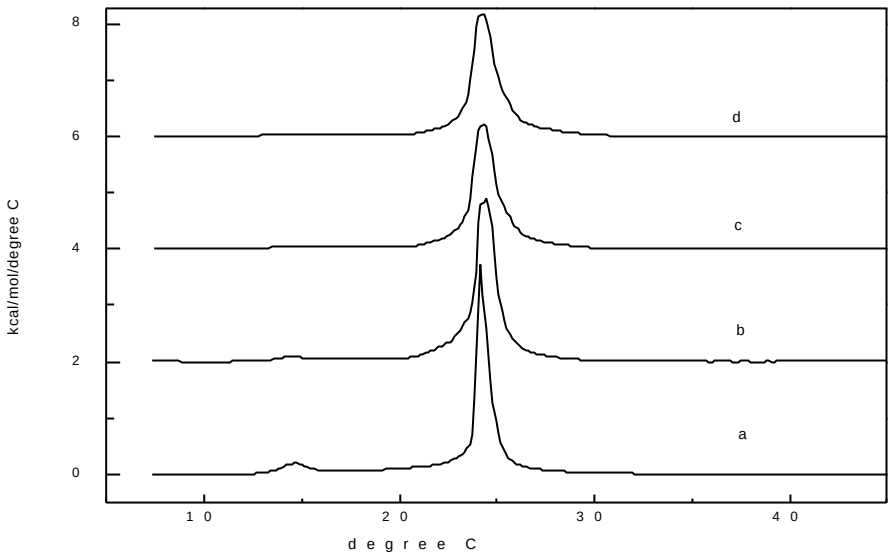

Figure 3.11: DSC traces of sonicated DMPC vesicles in the presence of different concentrations of the RGD lipid: **a**) 0; **b**) 2.4 %; **c**) 5 %; **d**) 7 %.

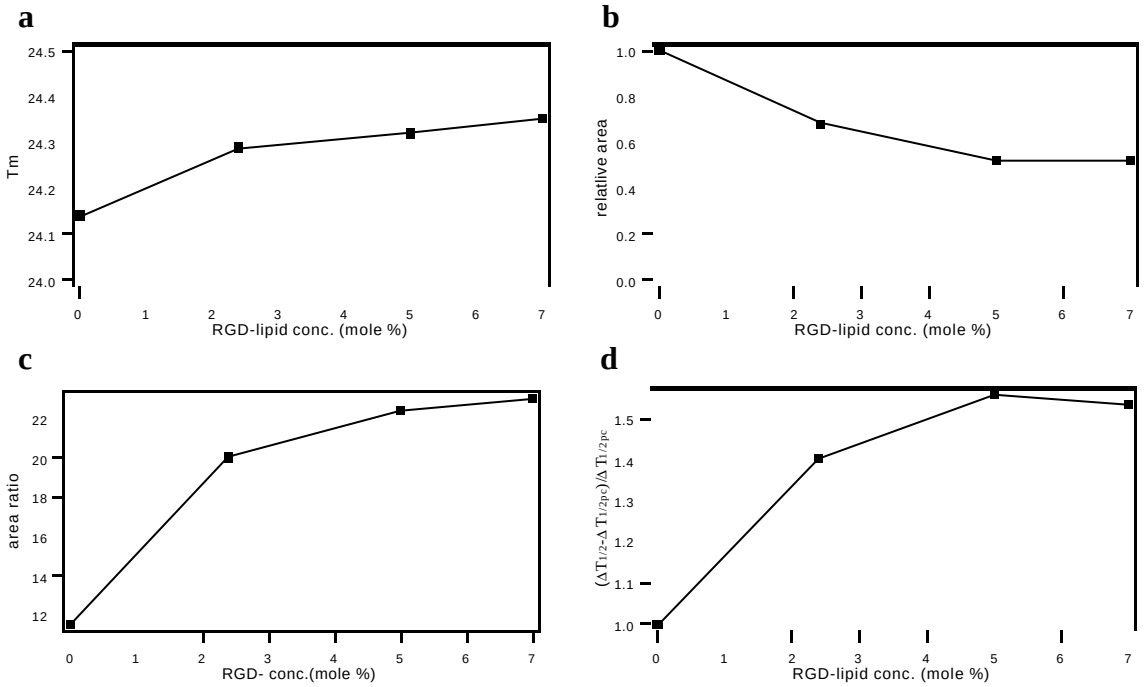

Figure 3.12: The RGD lipid concentration dependence of: **a**) main phase transition temperature; **b**) relative area value of the pretransition peak (area of the pure DMPC vesicle as 1); **c**) area ratio of the main phase transition and the pretransition peaks; **d**) relative broadening of the main phase transition peak ($\Delta T_{1/2}$ of the pure DMPC main phase transition peak as 1).

3.5 The RGD lipid: Film balance experiments

3.5.1 Materials and methods

Materials

Texas red®-DHPE (N-(Texas RED® sulfonyl)-1,2-dihexadecanoyl-sn-glycero-3-phosphoethanol-amine, triethylammonium salt) was bought from Molecular Probes (Eugene, U. S. A.). Chloroform and methanol were bought from Fluka (Neu-Ulm, Germany) and were reagent p.a. grade. DMPC was bought from Avanti Polar Lipids (Alabaster, AL, USA).

Film balance

Film balance troughs of two sizes were used in the experiments. The larger one ($450 \times 90 \times 5$ mm^3, subphase volume: 250 ml) was used for pressure – area isotherm measurements on a normal film balance. Temperature was controlled by a water bath (± 0.2 °C). The smaller one ($230 \times 30 \times 3.5$ mm^3, subphase volume: 25 ml) was used on a microfluorescence film balance (*Figure 3.13*) (Heyn et al., 1990): The Wilhelmy system was fixed on a movable barrier, and a piece of filter paper was used as a Wilhelmy plate. Peltier elements were fixed at the bottom of the trough for temperature regulation (± 0.2 °C). The fluorescence microscope was placed above the trough and mounted on a motorized x-y translation stage which allowed the observation of most of the monolayer surface. The microscope was interfaced either to a SIT camera (Hamamatsu, Hamamatsu, Japan) or to a photomultiplier.

3.5.2 Results and discussion

The RGD lipid was mixed with DMPC at different concentrations. For the experiments, each time 60 µl of a lipid solution (0.85 mg/ml) was added drop by drop to the Millipore water surface in the $450 \times 90 \times 5$ mm^3 trough. After waiting 15 min for complete evaporation of the organic solvents and spreading of the lipid mixture, the lipid film formed was compressed at 20 °C by moving the barrier at 100 µm/s. Monolayer isotherms are shown in *Figure 3.14*. There was no phase transition for pure DMPC. For the lipid mixtures, there appeared a phase transition which was dependent on the RGD lipid concentration: When the RGD lipid molar fraction was 10%, a small phase transition plateau appeared between 26 – 28 mN/m. When the molar fraction was 15%, the plateau (24 – 27 mN/m) became clearer. These results strongly suggest that the RGD lipid can be well incorporated into DMPC monolayers, and that the monolayer exhibits phase separation within certain range of surface presure.
The phase transition was visualized by flourescence microscopy as shown in *Figure 3.15*. The monolayer of 15% RGD lipid / 85% DMPC was homogeneous if the surface pressure was low (0 and 22 mN/m). Dark domains appeared and became more condensed when the surface pressure increased to (26 mN/m) and beyond (34 mN/m) the phase transition plateau, respectively. According to Moehwald (Moehwald, 1990), dark domains within monolayers are more ordered local areas resulting from exclusion of fluorescence-labeled lipids and condensation of special monolayer lipid components (the RGD lipid, most possibly in the present case). This also accords with the idea that in the DSC results (Figure 3.11), the shoulder appeared in the main transition peaks is indictive of domain formation of the RGD lipid.

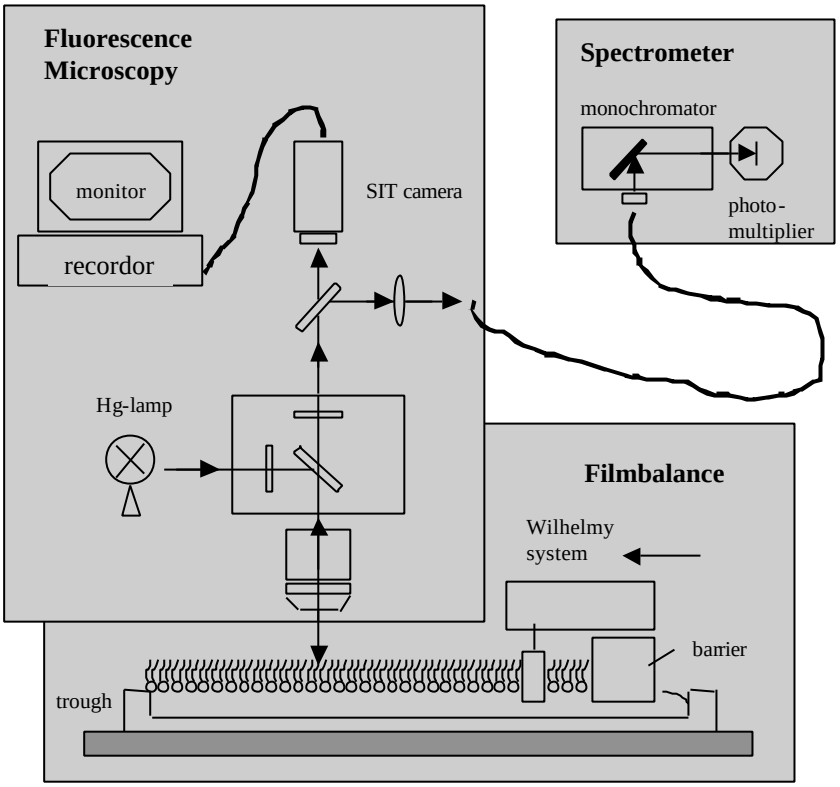

Figure 3.13: Schematic drawing of fluorescence microscopic film balance.

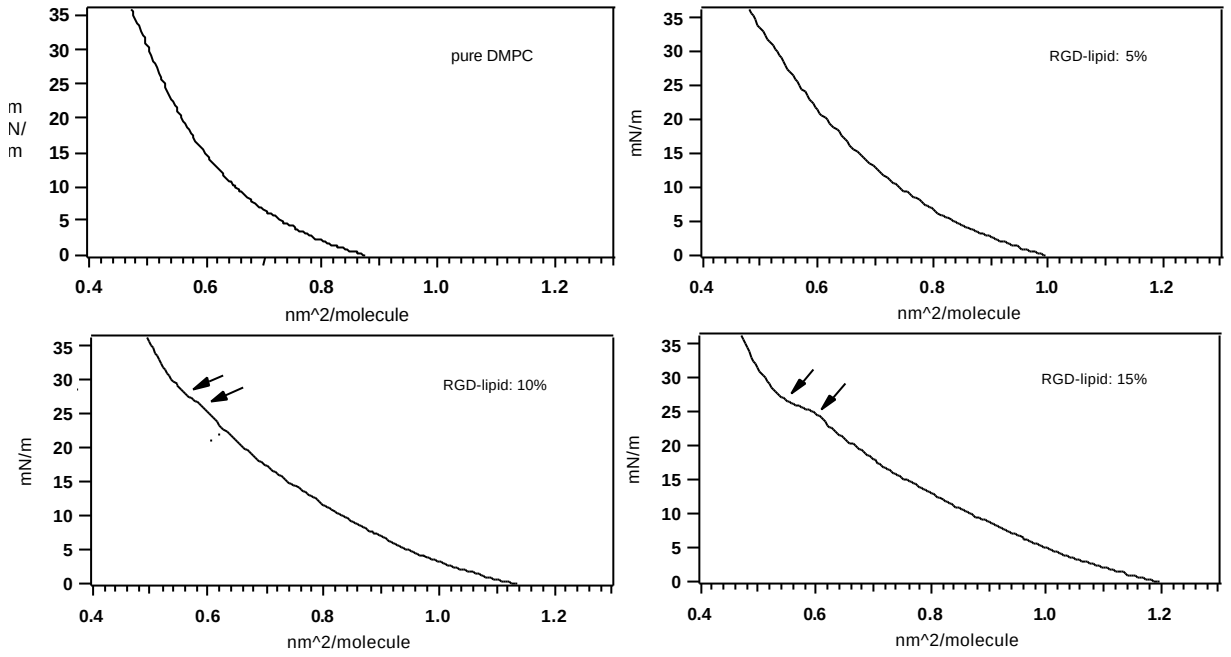

Figure 3.14: Monolayer isotherms of the RGD lipid / DMPC monolayers at 20 °C. Trough: 450 × 90 × 5 mm. Subphase: Millipore water. Molar fraction of the RGD lipid: 0, 5%, 10% and 15%.

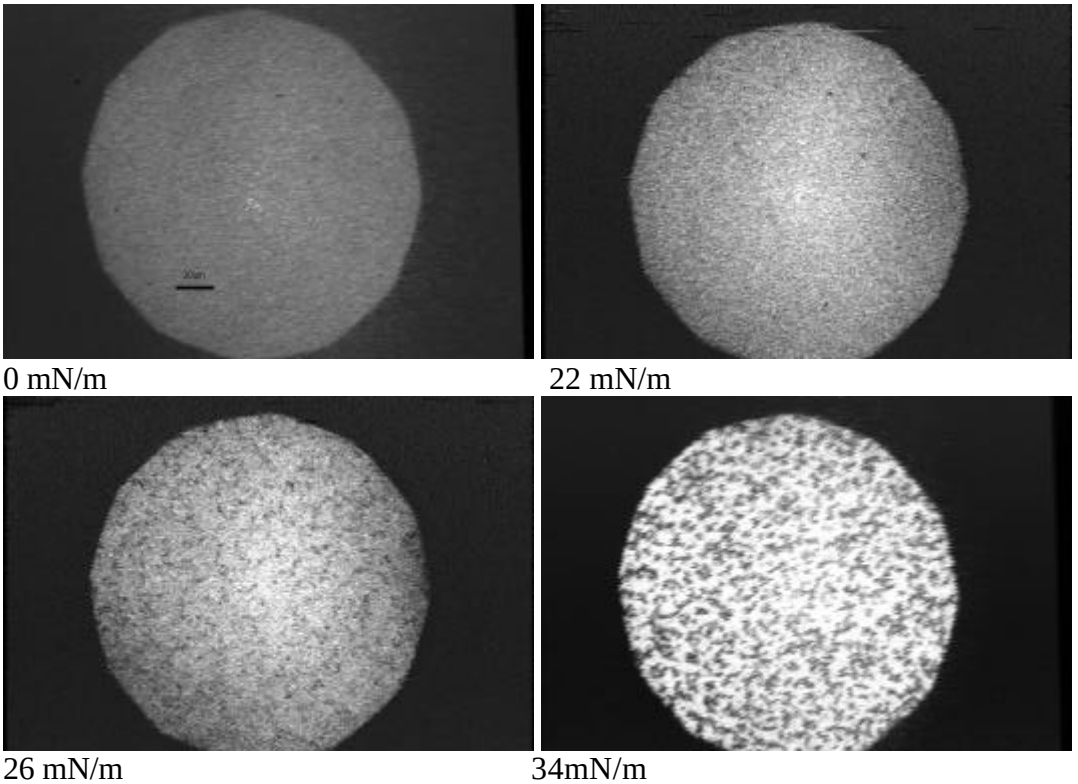

Figure 3.15: Pattern formation: Fluorescence microscope images of 15% of the RGD lipid / 85% DMPC / 0.1% Texas Red-DHPE monolayer at different surface pressures. Trough: 230 × 30 × 3 mm. Subphase: Millipore water. Temperature: 20 °C.

3.6 The RGD lipid: Adhesion of human blood platelets to the RGD lipid coated surfaces

3.6.1 Materials and methods

Materials

NBD-DPPE (N-(7-nitro-2-1,3-benzoxadiazol-4-yl) Dipalmitoyl Phosphatidyl-ethanolamine; Ex: 460 nm; Em: 534 nm) and DMPC were bought from Avanti Polar Lipids, Inc. (Alabaster, AL, USA). Chloroform and methanol were bought from Fluka (Neu-Ulm, Germany) and were reagent p.a. grade. Theophylline, Apyrase, and Prostagladin E1 (PGE1) were bought from Sigma (Deisenhofen, Germany). All other chemicals were of the highest available purity and were purchased from Sigma or Merck (Darmstadt, Germany).

Human platelet preparation

The method was kindly provided by Professor L. J. Wurzinger from Anatomisches Institut, Technische Universität Müvchen. All steps were taken at room temperature. 9 ml of fasting blood (first 10 ml discarded) was mixed immediately with 1 ml of the buffer ´acid ACD´. Platelet rich plasma (PRP, opaque supernatant) was obtained by centrifuging the blood at 2000 rpm on a Biofuge pico (Heraeus Instruments, Germany) for 3 minutes. PRP was then washed very quickly for two times with the washing buffer (1:1 volume ratio), by going up to 13,000 rpm and then spinning down at once. The pellet (platelets) was resuspended in 2 ml of the resuspension buffer and stored at 37 °X for use within several hours.

Buffers:
1) ´acid ACD´: (29 mM citric acid, 77 mM Tri-sodium citrate, 86 mM glucose, pH 6.5-7.0)
2) Washing buffer: (29 mM citric acid, 77 mM Tri-sodium citrate, 86 mM glucose, 1 mM Theophylline, 9 mM EDTA, 20 units of Apyrase, pH 6.5-7.0, 30 μM PGE1)
3) Resuspension buffer: (0.14 M NaCl, 2.7 mM KCl, 1.5 mM KH_2PO_4, 8.1 mM Na_2HPO_4, 2 units of Apyrase)

Spreading of lipids on glass surface to form bilayers (Nissen et al., 1999)

Dissolved lipids were mixed at appropriate molar fraction. The overall amount of lipid was around 0.8 mg. The mixture was deposited on the edge of a Teflon block (the thickness was around 1 cm) and dried in vacuum for 4 hours. Lipid was transferred from the block by imprinting (smearing) lipid onto a glass cover slide. Care was taken to obtain two lipid deposits with straight edges facing eaching other in parallel at a distance of about 0.5 cm. A lipid bilayer would form between the two edges. The cover slide was sealed onto a Teflon trough by silicon grease to form a sample chamber (Figure 4.2 in Section 4.2.2). The chamber was filled with Millipore water and another cover slide was used to seal its top. The sample was then mounted in a temperature controlling box (40 °C). After 2 days of spreading, the surface was intensively rinsed with Millipore water. Before the experiments, 3% BSA was used to block the surface for more than one hour.

Fluorescence recovery after photobleaching (FRAP) (Kuehner et al., 1994)

FRAP was performed on a Zeiss Axiomat microscope (Zeiss, Oberkochen, Germany). The microscope is equipped with a xenon high pressure lamp XBO75W-2 (Zeiss, Oberkochen, Germany) and a silicon intensified target (SIT) camera (C1000, Hamamatsu, Herrsching, Germany). For the FRAP measurements (bleaching and illumination) the microscope is equipped with a stabilized argon ion laser (Innova 70/4, Coherent). The fluorescence intensity is measured with a photomultiplier (R1527P, Hamamatsu, Herrsching, Germany) under illumination with the attenuated laser beam at a fixed and defined size of bleaching spot. In the present work, the spot diameter was 14.7 μm. The bleaching time was 1 second. The Gate-time was 100ms. The points recorded before bleaching were 5. Temperature was controlled at 37 °C by a water bath.

Phase contrast microscopy

The inverse microscope (Axiovert S100 TV, Carl Zeiss, Jena, Germany) was equipped with a LD ACHROPLAN 40×/0.60 Korr Ph2 air lens (Carl Zeiss). Images were recorded with a CCD camera (C2400, Hamamatsu Photonics, Herrsching, Germany) and stored on videotape using a SVHS recorder (Panasonic AG-7350, Panasonic, Matsushita Electric Industrial Corp., Osaka, Japan).

RICM (refer to Section 4.2.2)

Fluorescence microscopy (refer to Section 5.2.2)

3.6.2 Results and discussion

Lipid bilayers containing the RGD lipid were spread on the glass surface in the sample chamber. They were quite homogeneous when examed with the fluorescence microscope (*Figure 3.16, left*). FRAP experiments show that after photobleaching, fluorescence intensity could be recovered up to 45-50% of the original level, within 1 minute at 37 °C (*Figure 3.16, right*). So the RGD lipid was in a fluid environment and the dynamics of platelet adhesion would not be limited by two dimensional movement of the lipid molecules.

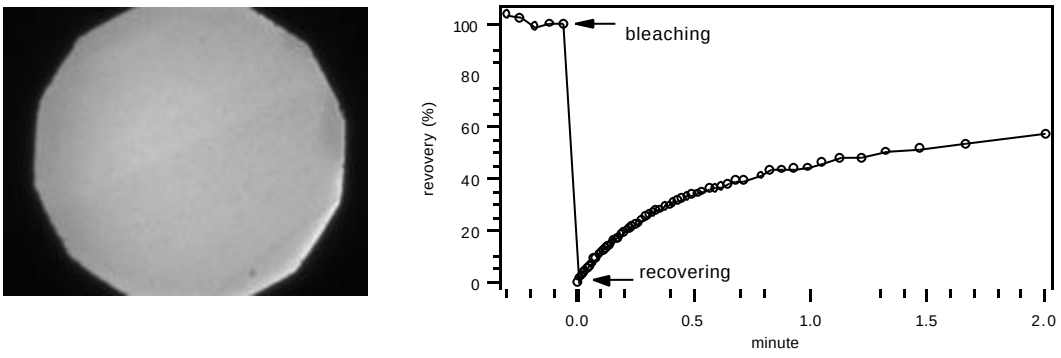

Figure 3.16: Left: fluorescence microscopic image of the lipid bilayer composed of 94.06% DMPC / 4.95% of the RGD lipid / 0.99% NBD-DPPE; **right**: fluorescence recovery of the bilayer after photobleaching. In both cases the sample chamber contained only Millipore water.

0.2 ml of resting platelets were mixed with 0.8 ml of resuspension buffer in the sample chamber. The sample was immediately used for the microscopic observations.

Resting platelets had a typical smooth discoid shape (*Figure 3.17*). The diameter was usually around 2.0 – 2.35 μm, which fits the former results quite well (Wurzinger, 1990).

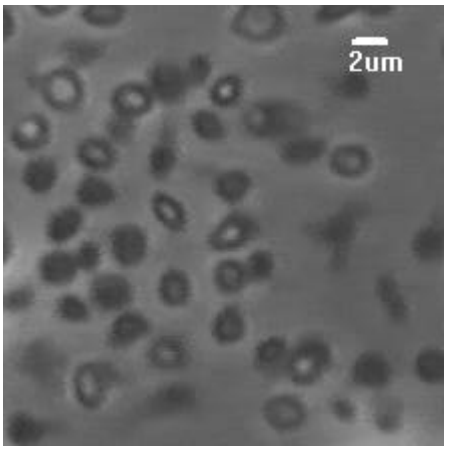

Figure 3.17: Phase contrast micrograph of resting platelets. Note that most of them have disc-like shapes.

When resting platelets were added to the bilayer containing the RGD lipid (5%), adhesion happened within minutes. Shape changes of adhered platelets were significant. Most of the platelets exhibited ´spiny sphere´ shapes (*Figure 3.18*) resulting from protrusion of multi-pseudopodia. In many cases the lengths of pseudopodia exceeded the diameters of the resting platelets. No significant centralization of the cell organelles was observed. Strong adhesion (indicated by elongation of pseudopodia and blackening of most parts of a cell body) could be seen within half an hour after addition of resting platelets, and adhesion seemed to be completed after more than one hour.
The adhesion process is well demonstrated in Figure 3.18 by the arrow-pointed platelets in the last three images which were taken from observation of the same area on the surface. The evolution over time of the number of the adhering platelets within this area is shown in *Figure 3.19a*. The diameter distribution of the adhering platelets in the image after 96 min is shown in *Figure 3.19b*.
As a control, adhesion of platelets on the pure DMPC bilayers blocked with 3% BSA was observed (*Figure 3.20*). Within 40 minutes platelets adhered only slightly on the surface. No strong adhesion occurred within this period.
Platelet adhesion on pure glass surfaces also differed significantly from that on the bilayer containing the RGD lipid. The results are shown in *Figure 3.21*. It is seen that most platelets only anchored on glass without intensive spreading within 75 minutes. Phase contrast microscopic images (*Figure 3.22*) show that as long as complete spreading happened, it was usually accompanied by obvious centralization of the cell organelles. Pseudopodia were only observed at the initial stage of the spreading, and were not as numerous as in the case of platelet adhesion on the RGD lipid containing bilayers.
The above experiments indicate that the RGD lipid containing bilayers can mediate platelet adhesion specifically: The platelet shape changes during adhesion were demonstrated by the formation of multiple pseudopodia. Moreover, with help of the interaction with the cyclic RGD head group, platelet adhered much faster than either on pure DMPC lipid bilayers or on glass surfaces.

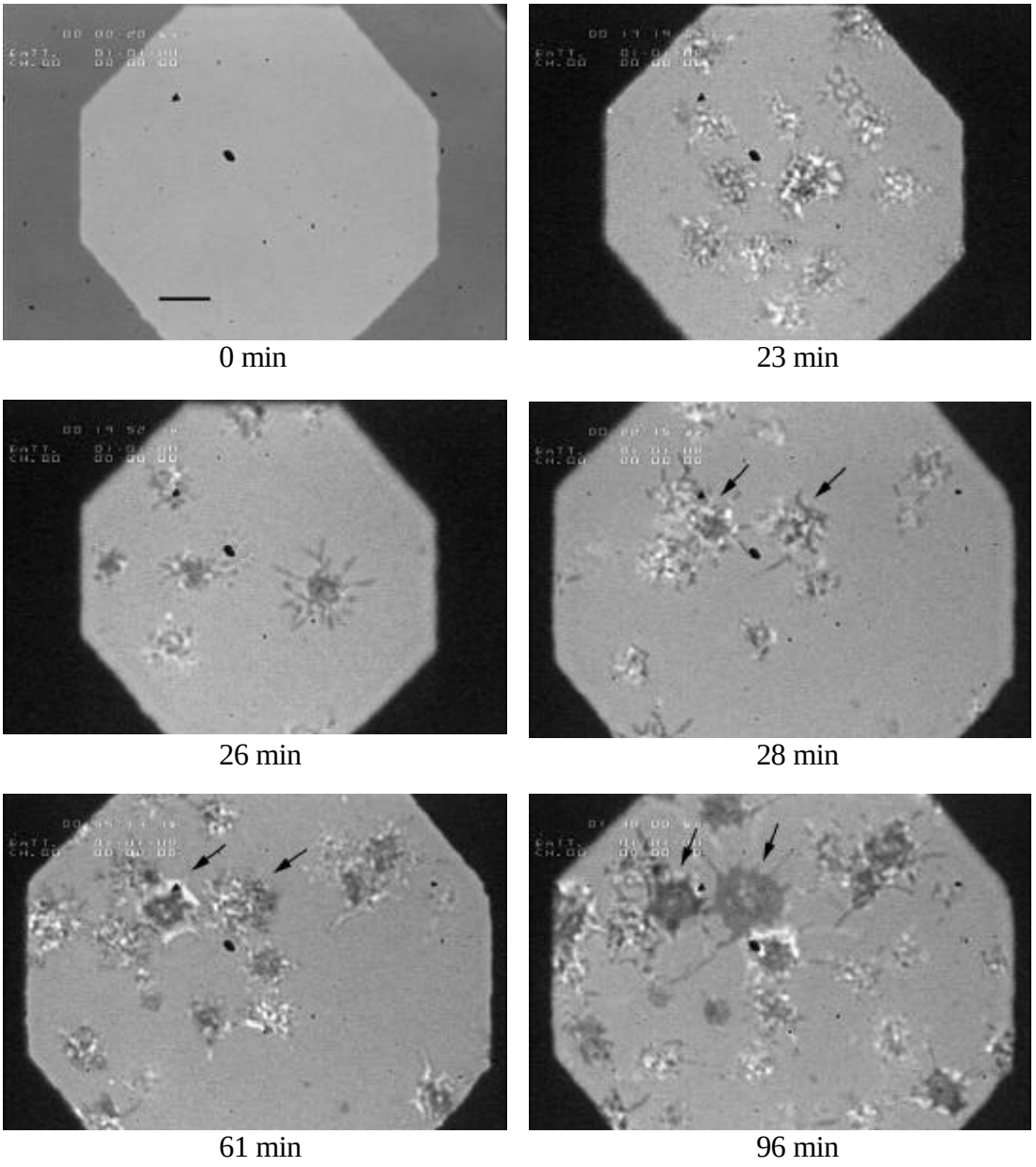

Figure 3.18: RICM: Platelets adhesion on a lipid bilayer composed of 94.06% DMPC / 4.95% of the RGD lipid / 0.99% NBD-DPPE. The bilayer surface had been blocked with 3% BSA before addition of the platelets. Note that only the last three images were taken from the same area on the surface. Arrows point to the same two platelets. Bar: 4µm.

a b

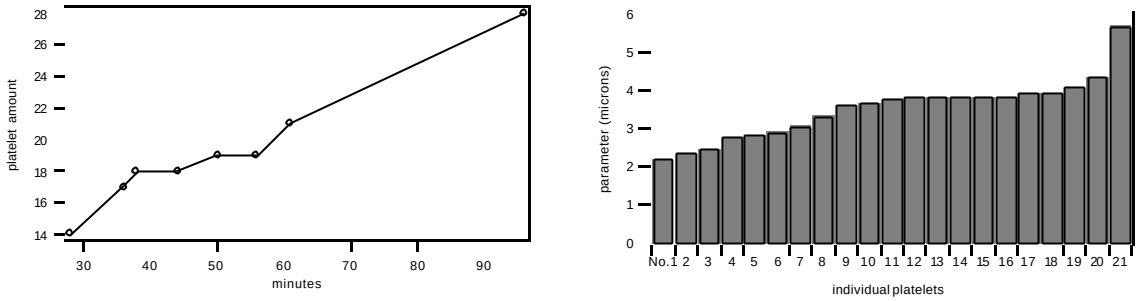

Figure 3.19: a) Time evolution of the number of adhering platelets within the area shown in the images after 28 min, 61 min, and 96 min in Figure 3.18. Note that those platelets were also included which only partly appeared in the images (along the edge of the aperture). **b**) The diameter distribution of the adhering platelets which completely appeared in the image frame after 96 min in Figure 3.18. Pseudopodia lengths were not included.

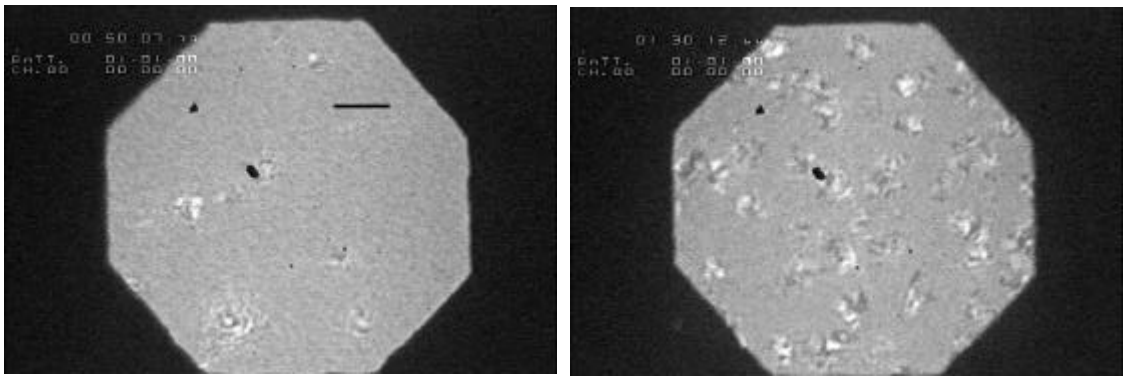

0 min 40 min

Figure 3.20: RICM. Platelet adhesion on the lipid bilayer composed of 99% DMPC, and 1% NBD-DPPE. The bilayer surface had been blocked with 3% BSA before addition of the platelets. Bar: 4 μm.

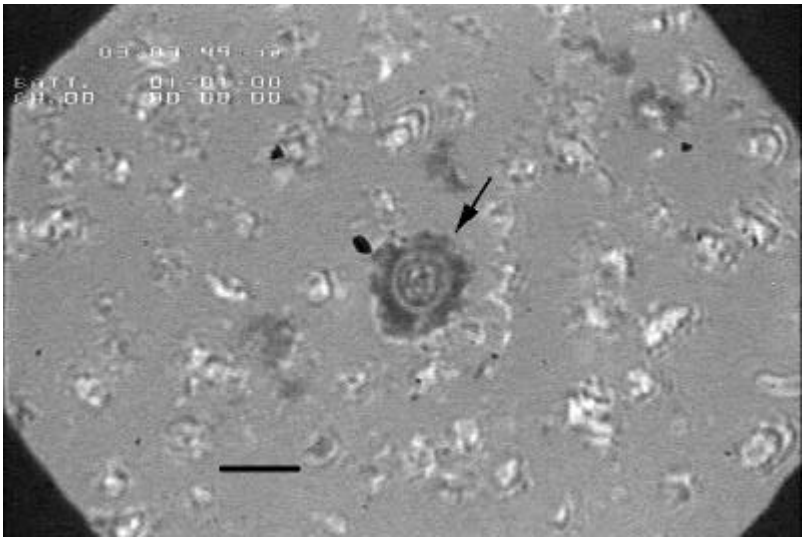

Figure 3.21: RICM. Platelet adhesion on glass surface. The arrow points to a possible fully adhering platelet with organell centralization. Bar: 4 μm.

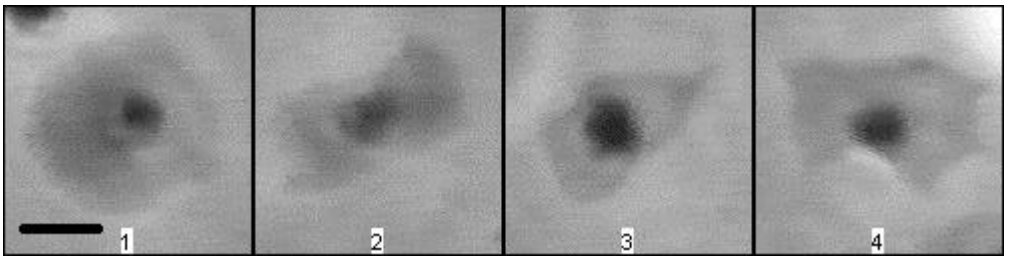

Figure 3.22: Phase contrast micrographs of spread platelets adhering on glass surface. Bar: 2 μm.

4 Adhesion of the giant RGD vesicles on the integrin $a_{IIb}b_3$ coated glass surface

4.1 Introduction

Reflection interference contrast microscopy (RICM) is widely used in cell science to study cell adhesion. A systematic and quantitative research on model membranes has been made to investigate the capability and limitation of the technique itself (Raedler and Sackmann, 1993). Based on this, several RICM studies (Nardi, 1998; Albersdoerfer, 1997; Behrisch, 1998) were performed to examine vesicle adhesion behaviors in shear fields quantitatively. These studies included the evaluation of the adhesion strength of adhering vesicles in terms of the work of adhesion, by application of the continuum theory of membranes (refer to Chapter 2, as well as the method description of the present chapter). The studies used model systems consisting of membranes with reconstituted non-biological receptor-ligand pairs such as biotin-streptavidin-biotin or oppositely charged lipids.
As mensioned in Chapter 2, the basic aim of this thesis is to establish a model system which makes use of the more biologically relevant lock-and-key interaction between integrin $\alpha_{IIb}\beta_3$ and the RGD sequence. To mimic natural cells most closely, efforts were made to produce giant $\alpha_{IIb}\beta_3$ containing vesicles that can be studied by light microscopy. Unfortunately these efforts failed. Thus in this chapter, the RGD lipid containg giant vesicles were used to study their adhesion behavior on the immobilized integrin $\alpha_{IIb}\beta_3$ on glass surface with the help of RICM.

4.2 Materials and methods

4.2.1 Materials

DMPC, dimyristoylphosphatidylglycerol (DMPG), cholesterol, and dimyristoyl-phosphatidylethanolamine-N-[poly(ethyleneglycol)2000] (PEG 2000 PE) were bought from Avanti Polar Lipids (Alabaster, AL, USA). Chloroform and methanol were bought from Fluka (Neu-Ulm, Germany) and were reagent p.a. grade. All other chemicals were of the highest available purity and were purchased from Sigma (Deisenhofen, Germany) or Merck (Darmstadt, Germany).

4.2.2 Methods

Cleaning

Glasses and teflon products were cleaned by sonification in 2% Hellmanex (Hellma, Germany) solution and in Millipore water (Millipore, U. S. A.), two times for 15 minutes each. After every sonification step they were rinsed in Millipore water ten times and finally dried at 75 °C.

Preparation of giant unilamelar lipid vesicles: electroswelling method

Giant unilamelar lipid vesicles were made by electroswelling method (Angelova and Dimitrov, 1986) (*Figure 4.1*). One drop of a lipid mixture was deposited on each of two indium-tin-oxide (ITO) covered glasses, which were then stored in vacuum for more than 2 hours for complete solvent evaporation. The glasses were put into a swelling chamber, with the ITO sides (lipid covered) facing to each other in parallel. After addition of 2 ml of swelling solution (170 mM sucrose, 1 mM NaN_3), the chamber was put in a temperature controlled box (40 °C), and the ITO glasses were connected with a frequency generator (Processor-Multi-Function-Generator, FG 9000, ELV GmbH, Germany). Vesicles were swollen for 2 hours at 1 V with 10 Hz.

Sample chamber

A home-made teflon chamber ($1.5 \times 1.5 \times 0.5$ cm^3, *Figure 4.2*) was used for vesicle adhesion observation. At the bottom of the chamber a cleaned glass cover slide was glued to the body of the chamber by silicone grease.

Instruments and image processing

RICM. An Axiomat inverted microscope (Zeiss, Oberkochen, Germany) was used together with a Zeiss Antiflex-Neofluar 63 × 1.25 oil immersion objective, supplemented by nonstandard optical devices for additional magnification. For illumination, the 546.1-nm line of a high-pressure mercury arc lamp (HBO 100/W2, Osram) was filtered out with a band-pass filter (line width 5nm, peak transmission 85%). The interference images of adhering vesicles were projected onto a CCD camera (HR-480; Aqua-TV, Kempten, Germany) and recorded with a ¼-inch S-VHS video recorder (AG7350; Panasonic). Recorded sequences were digitized with a Macintosh Quadra 950 (Apple Computer) equipped with Pixel Tools imaging boards (Perceptics, Knoxville, TN) and Image VDM software (Perceptics). A customized

version of the image analysis software National Institutes of Health-Image (W. Rasband, National Institutes of Health, Bethesda, MD) was used to analyze the interference images.
Bright field microscopy. The RICM microscope can also be used as a bright field microscope, with a 200W Halogen lamp used for illumination.

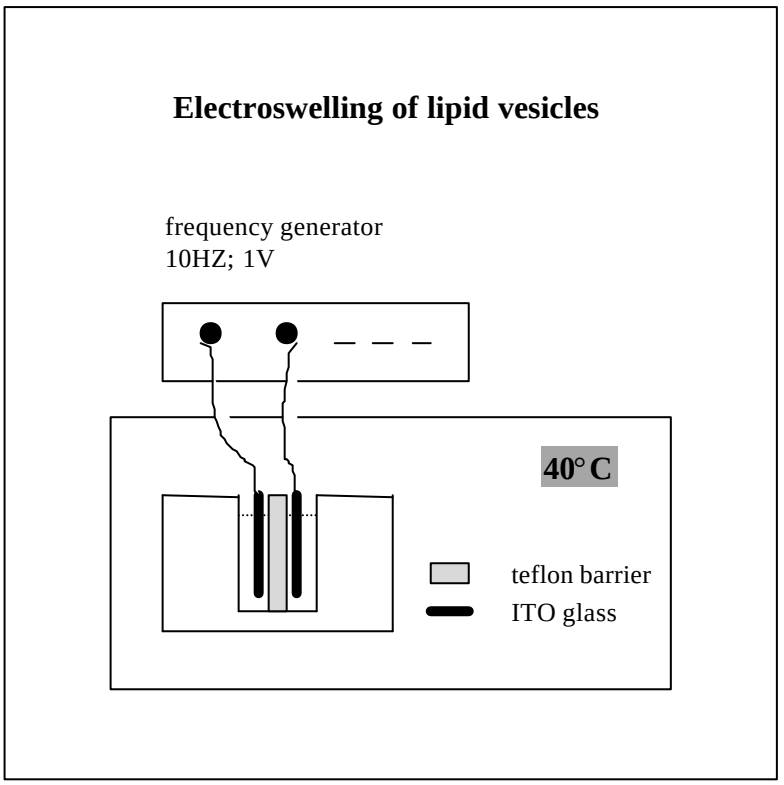

Figure 4.1: Schematic drawing of the electroswelling method for producing giant RGD vesicles.

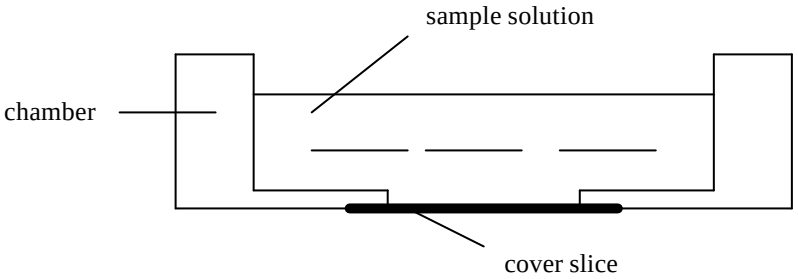

Figure 4.2: Schematic drawing of the sample chamber used for RICM, normal fluorescence microscopy and confocal fluorescence microscopy.

Reconstruction of the vesicle contour near the contact zone with RICM and digital image processing

The contour of adhering vesicles (or cells) was examined in terms of the spacing *h(x)* between vesicle membrane and substratum, in the proximity of their contact zone, using RICM. The principle of image formation (Gingell and Todd, 1979; Gingell et al., 1982; Raedler and Sackmann, 1992; Kuehner and Sackmann, 1996) is illustrated in *Figure 4.3*.

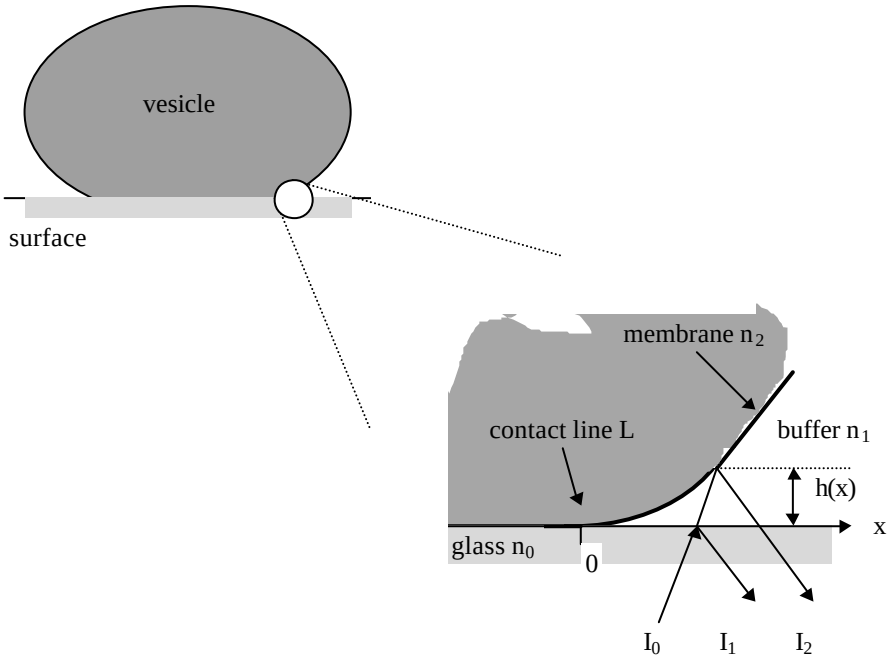

Figure 4.3: Schematic view of RICM principle on vesicle adhesion.

Light reflected from the substratum (I_1) interferes with light reflected from the ventral vesicle surface (I_2), giving rise to the following intensity distribution of the image:

$$I(x) = I_1 + I_2 + 2\sqrt{I_1 I_2} \cdot F[a, h(x)] \cdot \cos(2kh(x) \cdot (1 - G(a)) + d) \qquad (1)$$

Both F and G are functions of the angle α of the illumination aperture, and $k = 2pn / l$ denotes the wave vector of the illumination light in the buffer (n is the refractive index of the buffer).

Assuming that the refractive index of the vesicle membrane is higher than that of the surrounding buffer, light reflected on the buffer-vesicle interface experiences a phase shift of $d = p$. Thus, the contact area of an adhering vesicle appears dark in RICM. Around the adhesion area, interference produces a specific fringe pattern (*Figure 4.4*) that depends on the shape of the vesicle contour *h(x)* above the substrate. The vesicle contour was always reconstructed around the edge of the adhesion area, where the distance of the vesicle wall from the substrate rises continuously with increasing distance from the contact line L.

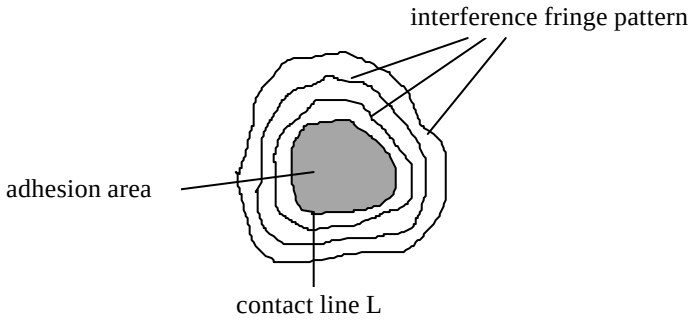

Figure 4.4: *Schematic drawing of a RICM fringe pattern.*

When one line is drawn across a fringe pattern, the light intensity distribution along this line can be obtained as shown in *Figure 4.5*, according to the equation (1). Note that the contact line is usually well defined by a sharp increase in the intensity of the RICM image at the edge of the adhesion area, as the 0 µm point in Figure 4.5. The light reflected from the vesicle surface (I_2 in Figure 4.3) has to pass the distance *h(x)* twice, so the phase difference between I_2 and the light reflected from the glass surface (I_1 in Figure 4.3) is $2n_1h(x)$. For the peak maximums in Figure 4.5, $2n_1h(x) = n\,l$, $n = 1, 2, 3, \ldots$; for the peak minimums, $2n_1h(x) = n\frac{l}{2}$, $n = 3, 5, 7, \ldots$. These represent the points on the vesicle contour whose distances from the glass surface are $\frac{n\,l}{2n_1}$, $n = 1, 2, 3, \ldots$ and $\frac{n\,l}{4n_1}$, $n = 3, 5, 7, \ldots$, respectively. Here l is 546.1 nm, and n_1 is 1.38.

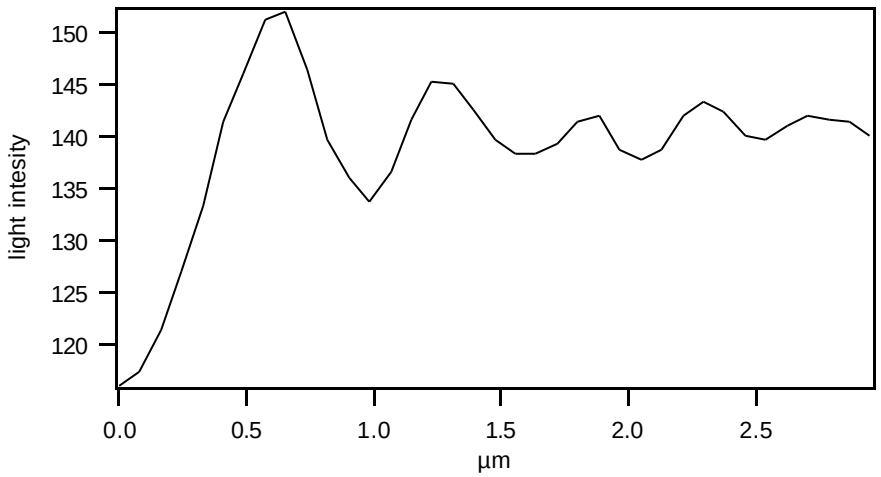

Figure 4.5: Light intensity distribution along one line across the interference fringe pattern.

Light reflected from cell organelles in close proximity to the substratum can strongly perturb the interference pattern. These disturbances are recognized by changing the illumination numerical aperture. The nonzero aperture angle of illumination is important for the measurement of the absolute height of an abject above the substratum (Kuehner and Sackmann, 1996). In the present work only the shape of the vesicle contour is relevant, while the absolute height is not. In this case it is sufficiently accurate to assume a zero aperture angle for calculating *h(x).* In this simplified approach, an inverse cosine transformation of the observed intensity distribution yields the vesicle contour *h(x)*:

$$h(x) = \frac{l}{4pn}\arccos(I(x) - I_{\max} - I_{\min}) \qquad (2)$$

From the equation (2), the vesicle contour between each two neighboring top and bottom points in Figure 4.5 (and thus the whole vesicle contour) can be totally reconstructed (*Figure 4.6*).

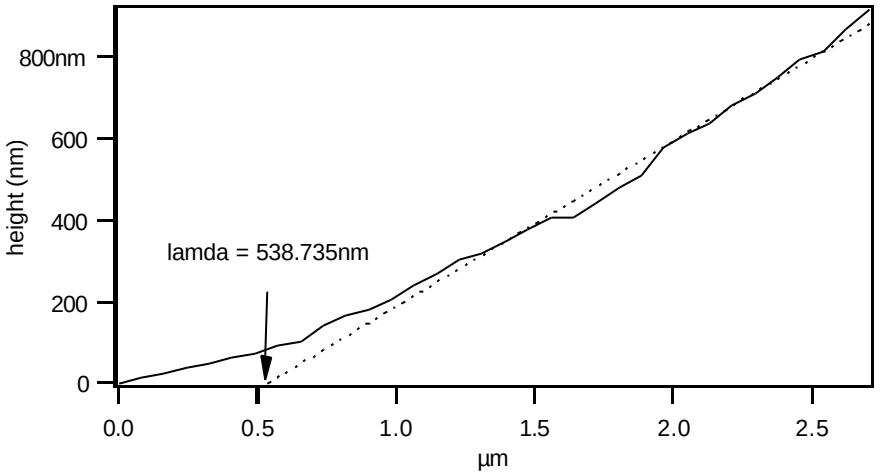

Figure 4.6: Cell contour near the contact area was constructed from Figure 4.5. The dashed line represents the linear fitting result, as described in Materials and Methods.

Elastic model of the vesicle contour near the substrate

The adhesion of soft and closed shells is not only determined by the adhesion energy W and the surface tension g, but also by the elasticity of the shell. For fluid lipid vesicles only bending elasticity is important, and a rigorous theory relating the shape of the adhering vesicle to the membrane tension, the osmotic pressure, and the adhesion energy is available (Seifert and Lipowsky, 1990). In this case, bending modulus, adhesion energy, and membrane tension can, in principle, be measured by analyzing the three-dimensional shape of the vesicle.

Recent studies of vesicle adhesion showed that the shape of adhering soft shells near the substrate is determined by the following two boundary conditions:

1) The balance of tensions that can be expressed in terms of Young´s law:

$$W = g(1 - \cos J_c) \qquad (3)$$

where J_c is the contact angle (*Figure 4.7*);

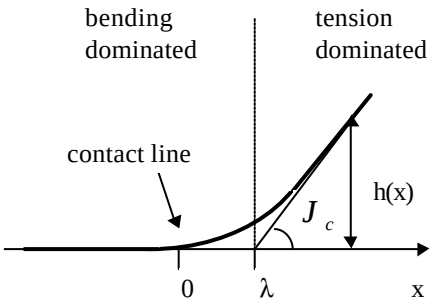

Figure 4.7: Schematic cell contour near the contact area, which is separated by the characteristic length λ into a bending dominated regime and a tension dominated regime, as described in Materials and Methods.

2) The equilibrium of bending moments relating the local radius of curvature R_c at the contact line to the bending modulus k and the adhesion energy W, according to

$$W = \frac{1}{2} k / R_c^2$$

The bending modulus k was determined by the method described in (Simson et al., 1998). For the vesicle system (50% DMPC / 50% cholesterol) used in the present work, k was determined as 100 k_BT.

A direct measurement of R_c is difficult and does not yield reliable results (Raedler et al., 1995). Following Bruinsma (1995), the difficulty can be overcome by calculating the approximate contour by minimizing the total free energy ΔG_r of the shell in the rim region around the contact line L, and the free energy ΔG of the contour per unit length is:

$$\Delta G = \int_0^\infty \left\{ \frac{k}{2} \left(\frac{\P^2 h(x)}{\P x^2} \right)^2 + \frac{g}{2} \left(\frac{\P h}{\P x} \right)^2 \right\} dx - \int_{-\infty}^0 W(x) dx$$

where u is the radius of the adhesion disk. Minimizing ΔG yields a fourth-order differential equation:

$$g \frac{\P^2 h}{\P x^2} - k \frac{\P^4 h}{\P x^4} = 0 \qquad (4)$$

The characteristic length scale

$$l = \sqrt{k / g} \qquad (5)$$

embedded in this differential equation separates regions of the vesicle contour dominated by lateral tension from regions near the contact line that are dominated by the bending modulus (Figure 4.7). Note that λ here is different from the above mentioned wave length λ.

A solution $h(x)$ of Equation (4) can be obtained by considering the following boundary conditions: $h(x) = 0$ within the contact area and $h(x) = J_c x$ for x large and positive, where J_c denotes the macroscopic contact angle (Bruinsma, 1996):

$$h(x) = \begin{cases} J_c (x - l) + J_c l e^{-x/l} & x \geq 0 \\ 0 & x \prec 0 \end{cases} \qquad (6)$$

J_c can be directly measured by a least-squares fit to the tension-dominated linear part of the reconstructed cell contour. The distance between the contact line and the intersection of the linear fit with the x axis defines the characteristic length l (Figure 4.6 and 4.7).
Now the adhesion energy W and the surface tension g can be obtained from the equations (3) and (5).

4.3 Results and discussion

4.3.1 Results

Lipopolymers in lipid membranes enable the design of artificial glycocalices to study the influence of steric repulsion on cell-substrate interactions or the accessibility of ligands to receptors and to minimize nonspecific binding effects (Sackmann, 1996). For reconstituted lipid vesicles containing membrane receptor proteins, a proper concentration of lipopolymers incorporated in the vesicle membranes can prevent nonspecific adhesion, while receptor proteins are still exposed enough to interact with related ligands. PEG 2000 PE was used in the present work. The average thickness of its headgroup in the mushroom configuration is ~3.5 nm (Albersdoerfer et al., 1997).

Giant RGD-lipid containing vesicles (the RGD vesicles) were composed of 1 – 2% of the RGD lipid, 1 – 5% of PEG 2000 PE, DMPC and cholesterol (molar ratio of the latter two lipids is 1:1). Cholesterol (about 50%) was included to make the vesicle membranes fluid at room temperature.

An osmotic gradient was established across the vesicle membrane - the sugar (sucrose) or salt (NaCl) concentration outside the vesicles was a little higher than inside. Thus, the vesicles deflated and obtained so called ´excess surface area´ which was necessary to form a flat adhesion area.

The diameters of the lipid vesicles produced by the eletroswelling method were 20 – 80 μm. The swelling solution was (170 mM sucrose, 1 mM NaN_3). For the experiments, 50 μl of the vesicles was mixed with 0.9 ml of (10 mM Hepes, pH 7.25, 100 mM NaCl, 1 mM $CaCl_2$, 1 mM NaN_3) (adhesion buffer), so that the osmotic pressure across the membranes was about 40 mOsm. Because of the presence of sucrose inside the vesicles, the specific gravity of the vesicles was larger than that of the surrounding solution. This made the vesicles sink to the bottom of the sample chamber, which was necessary for adhesion and simplified the observation.

For the observation of adhesion, 0.9 ml of $\alpha_{IIb}\beta_3$ was incubated in a sample cell for 1 hour at room temperature. The proteins which did not adhere to the glass surface were removed by rinsing the chamber several times with 0.9 ml of the adhesion buffer. Then the holes within the adhered $\alpha_{IIb}\beta_3$ layer on the surface were blocked with 0.9 ml of 3% BSA solution to avoid possible unspecific adhesion. The chamber was rinsed for another several times, and then 50 μl of the vesicles was mixed with 0.9 ml of the adhesion buffer in it for final observation.

Effect of Triton X-100 content in buffer upon RGD vesicle adhesion on the $\alpha_{IIb}\beta_3$ coated glass surfaces

It has been shown that at a normal concentration of detergents (e. g., larger than 0.1% for Triton X-100) $\alpha_{IIb}\beta_3$ was kept in a monomeric state in solution, and in the absence of detergents or at a very low detergent concentration, $\alpha_{IIb}\beta_3$ formed rosette like structure which resulted from the aggregation of the hydrophobic transmembrane fragments of both $\alpha_{IIb}\beta_3$ subunits (Carrell et al., 1985; Peter, 1999). Coating surfaces with $\alpha_{IIb}\beta_3$ rosettes, the structure might persist in the coat and a single layer of $\alpha_{IIb}\beta_3$ of high surface density would be formed (Tangemann and Engel, 1995).

To investigate the effect of Triton X-100 content in the coating solution on final adhesion, $\alpha_{IIb}\beta_3$ at the same concentration in buffer A containing high (0.1%) or low (0.01%) concentrations of Triton X-100 was used to coat glass and the related adhesions were observed respectively. *Figure 4.8* shows that strong adhesion only happened in the low detergent concentration. Presumably, this effect might come from increased active RGD

binding sites, because of a higher surface density of $\alpha_{IIb}\beta_3$ and/or a higher degree of freedom of the Triton-solubilized heterodimers for statistical binding.

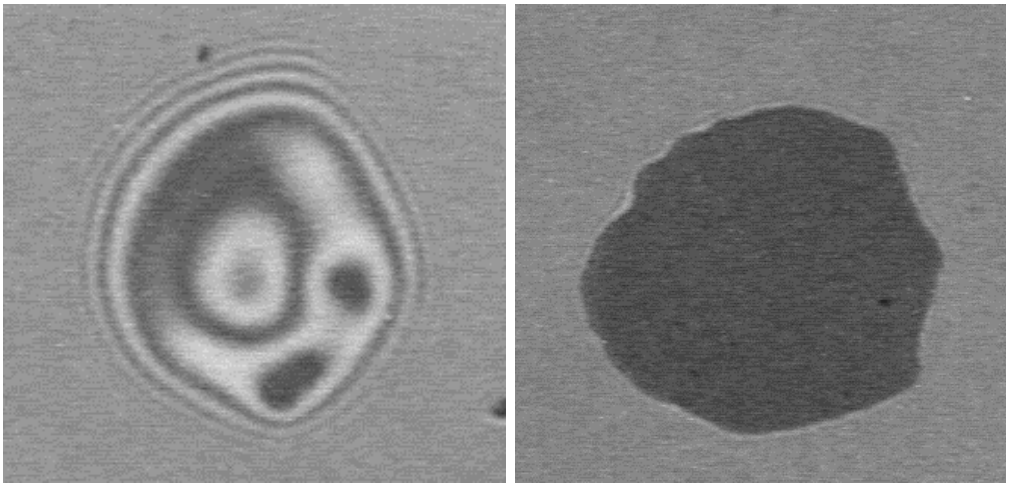

Figure 4.8: Effect of Triton X-100 content in the coating solution upon RGD vesicle adhesion on the $\alpha_{IIb}\beta_3$ coated surfaces. The coating solution contained 1 μg/ml of $\alpha_{IIb}\beta_3$ and 0.1% (**left**) or 0.01% (**right**) of Triton X-100. The RGD vesicles: 49.25% DMPC / 0.5% of the RGD lipid / 1% PEG 2000 PE / 49.25% cholesterol.

Observation of a typical adhesion procedure

A typical scenario of adhesion (246 seconds) is shown in *Figure 4.9*. The vesicle contained 0.5% of the RGD lipid and 1% PEG 2000 PE. 0.1 mg/ml of $\alpha_{IIb}\beta_3$ was used for coating the glass surface. Before tight adhesion the vesicle was attached to the surface only by gravity. This could be clearly seen by the strong flickering of the adhesion area. In the middle of the adhesion disk a ´blister´ was induced during the vesicle settlement on the surface. The tight adhesion started from a dark patch (arrow-pointed in Figure 4.9-2) where the vesicle membrane and the $\alpha_{IIb}\beta_3$ surface were in close contact, and the adhesion force was high enough to overcome the detachment forces such as thermal dynamic undulation of the vesicle membrane (flickering). Afterwards the adhesion patch expanded along the contact zone, and some new patches appeared at different time (arrow-pointed in Figure 4.9-6, Figure 4.9-7, and Figure 4.9-10). With the adhesion going on, all the adhesion areas that expanded from the separated adhesion patches merged into a single one. At last around the center of the adhesion disk, there´s still a relatively whiter area which represents the ´blister´ formed at the beginning of the adhesion process. In other cases, many adhesion disks appeared as completely black and round ones due to thorough adhesions and complete consumption of the excess surface area of the vesicles.

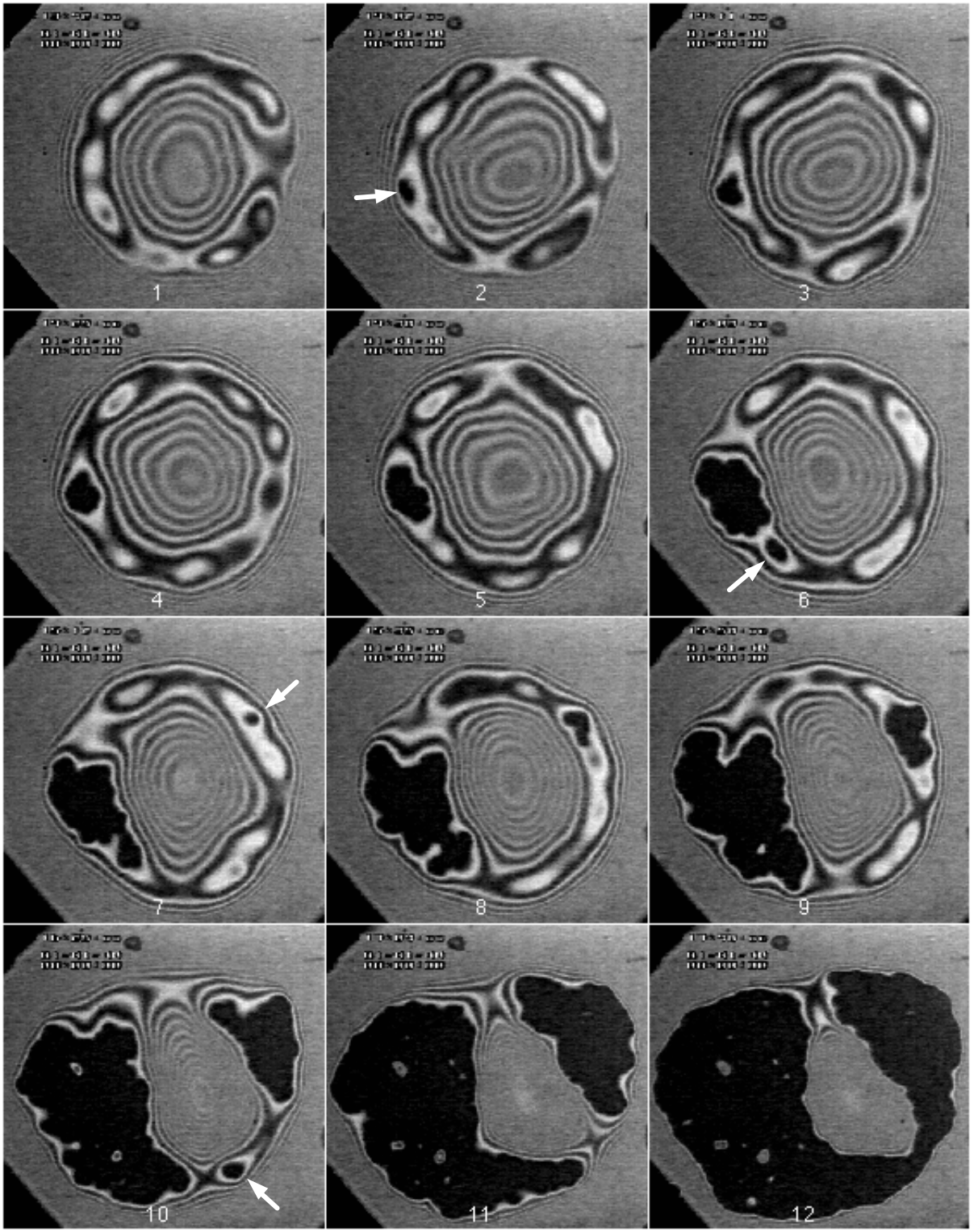

Figure 4.9: A typical adhesion process, which last 246 seconds. Lipid composition of the RGD vesicle: 0.5% of the RGD lipid / 1% PEG 2000 PE / 49.25% cholesterol / 49.25% DMPC. $\alpha_{IIb}\beta_3$ for coating the surface: 0.1 mg/ml in buffer A containing 0.01% instead of 0.1% of Triton X-100.

Evidences for specific adhesion

Control experiments were performed to confirm that the observed adhesion was specifically mediated by the lock-and-key interaction between $\alpha_{IIb}\beta_3$ and RGD. In *Figure 4.10a*, complete RGD vesicle adhesion took place on the surface which was coated with 0.1 mg/ml of $\alpha_{IIb}\beta_3$ and blocked with 3% BSA. In the presence of 3 mg/ml of the linear RGD peptide, Ac-GRGDFSK, adhesion disappeared because the linear peptide competitively bound to $\alpha_{IIb}\beta_3$ on the surface, thus blocked the binding sites for the RGD vesicles (*Figure 4.10b*). Similarly, when using the pure lipid vesicles instead of the RGD vesicles for the experiments (*Figure 4.10c*), or when the glass surface was coated with denatured (by heating) $\alpha_{IIb}\beta_3$ (*Figure 4.10d*), no adhesion was observed. If the glass surface was coated with BSA instead of $\alpha_{IIb}\beta_3$, the RGD vesicles only slightly adhered to the surface due to unspecific binding (*Figure 4.10e*).

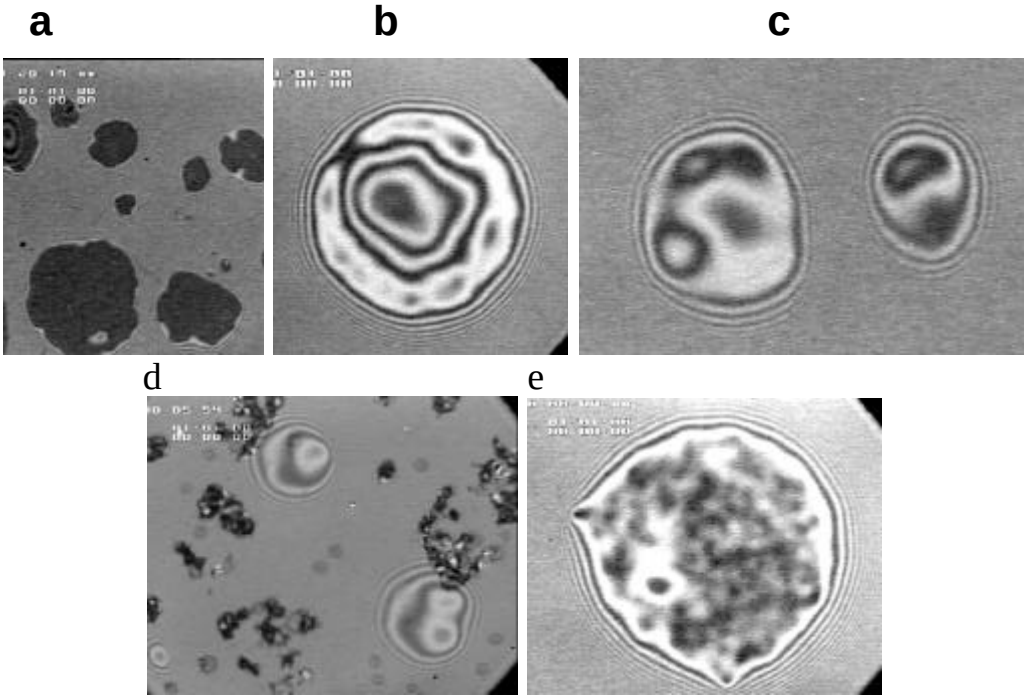

Figure 4.10: Specific and non-specific adhesions. **a**) Strong adhesion of the RGD vesicles (1.4% of the RGD lipid / 0.85% PEG 2000 PE / 48.88% cholesterol / 48.88% DMPC) on $\alpha_{IIb}\beta_3$ coated and BSA blocked surface. **b**) No adhesion of vesicles of the same composition as in (a) occurs on $\alpha_{IIb}\beta_3$ coated and BSA blocked surface, in the presence of 3 mg/ml of the linear RGD peptide Ac-GRGDFSK. **c**) No adhesion of the vesicles without the RGD lipid occurs on $\alpha_{IIb}\beta_3$ coated and BSA blocked surface. **d**) No adhesion of the same vesicles as in (a) occurs on $\alpha_{IIb}\beta_3$ coated and BSA blocked surface, which was heated up to 65°C for half an hour after BSA blocking. **e**) Much lower adhesion of the same vesicles as in (a) on BSA surface.

Effect of the content of $\alpha_{IIb}\beta_3$, PEG 2000 PE, and the RGD lipid

Specific adhesion mediated by the $\alpha_{IIb}\beta_3$ / RGD interaction was further confirmed by varying the amount of $\alpha_{IIb}\beta_3$ used for coating, or varying the proportion of PEG 2000 PE and the RGD lipid contained in the vesicle membranes. *Figure 4.11* shows an obvious tendency that with decrease of the concentration of $\alpha_{IIb}\beta_3$ (0.1 mg/ml – 0.01 μg/ml), the degree of adhesion of RGD vesicles also decreased.

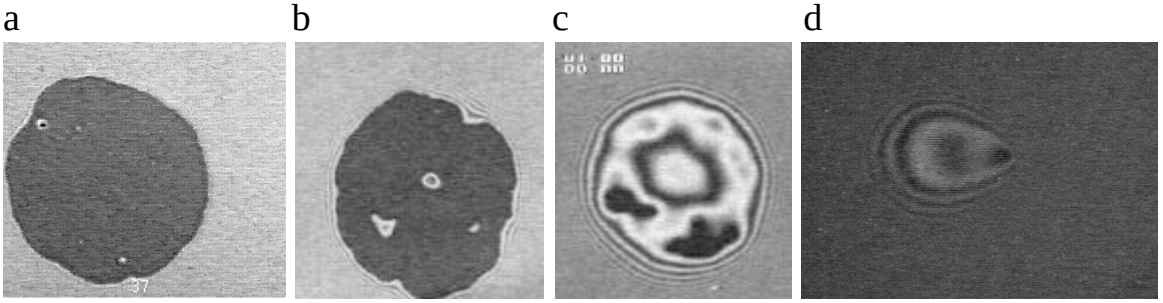

Figure 4.11: Adhesion is dependent on the $\alpha_{IIb}\beta_3$ concentration for coating the glass surface. Lipid composition of the RGD vesicles: 0.5% of the RGD lipid / 1% PEG 2000 PE / 49.25% cholesterol / 49.25% DMPC. $\alpha_{IIb}\beta_3$ concentration in buffer A containing 0.01% instead of 0.1% of Triton X-100: **a**) 100 μg/ml; **b**) 1μg /ml; **c**) 0.1 μg/ml; **d**) 0.01 μg/ml.

In the present work RICM and bright field microscopy share the same body microscope, so it×s possible to obtain both kinds of microscopic images of the same vesicle at the same time (*Figure 4.12a*). From the RICM images the adhesion disk areas can be easily figured out with NIH-image software. From the bright field microscopic images the total surface areas of the adhered vesicles can be calculated according to Zeno (Guttenberg, 2000). The ratio of adhesion disk area divided by the total vesicle surface area can be taken as a representative parameter of vesicle adhesion. The relationship between this surface ratio and the contents of RGD lipid / PEG 2000 PE in the vesicles is shown in *Figure 4.12b*. When the vesicles contained 1% PEG 2000 PE, significant adhesion happened if the RGD concentration was only a little higher than 0.05%. When the concentration of PEG 2000 PE was 3%, significant adhesion happened only after the RGD concentration was higher than 0.2%. At 5% PEG 2000 PE, the final adhesion efficiency was only 35% of the value for 1% PEG 2000 PE. The first two curves in Figure 12b all show an obvious jump at the above mentioned RGD concentration.

Cooperativity of adhesion

Figure 4.13 presents typical scenarios of adhesion kinetics of RGD vesicles which contained different RGD lipid and PEG 2000 PE concentrations. The complete adhesion of the 2% RGD lipid / 1% PEG 2000 PE vesicle was nearly attained within 42 seconds, while that of the 2% RGD lipid / 3% PEG 2000 PE vesicle took more than 390 seconds (more than 9 times longer). When the vesicle membrane contained 2% RGD lipid and 1% PEG 2000 PE, the adhesion kinetic curve appeared as a sigmoid curve, which indicates that the adhesion could be a cooperative process.

a

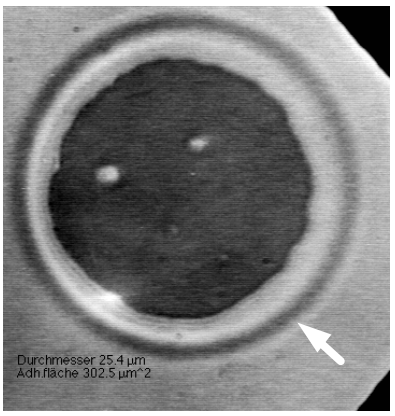

b

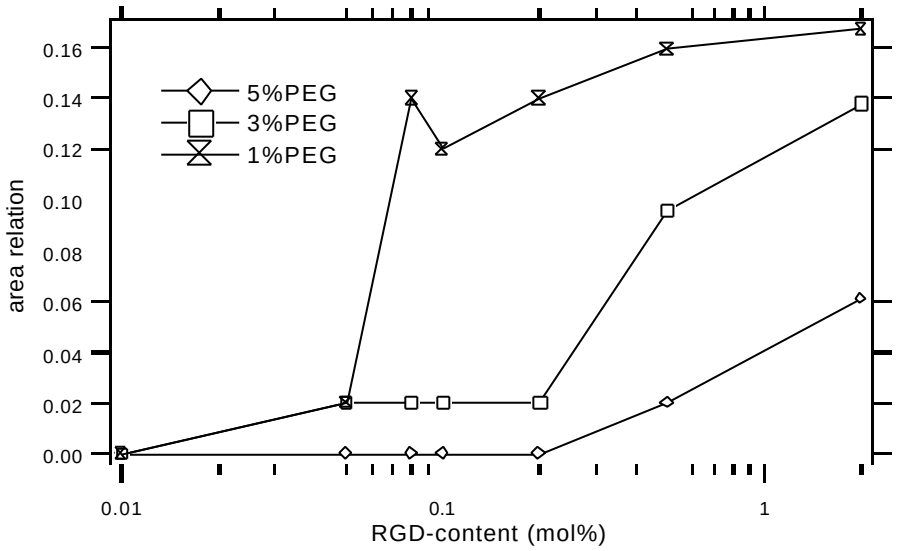

Figure 4.12: a) A vesicle could be visualized simultaneously by both RICM (showing the adhesion disc) and bright field microscopy (showing the arrow-pointed circumference of the vesicle). **b**) Adhesion is dependent on the RGD lipid and PEG 2000 PE contents in the RGD vesicles. Relative area values are obtained from adhesion disc area divided by total vesicle surface area. $\alpha_{IIb}\beta_3$ for coating the surface: 0.015 mg/ml in buffer A containing 0.01% instead of 0.1% of Triton X-100.

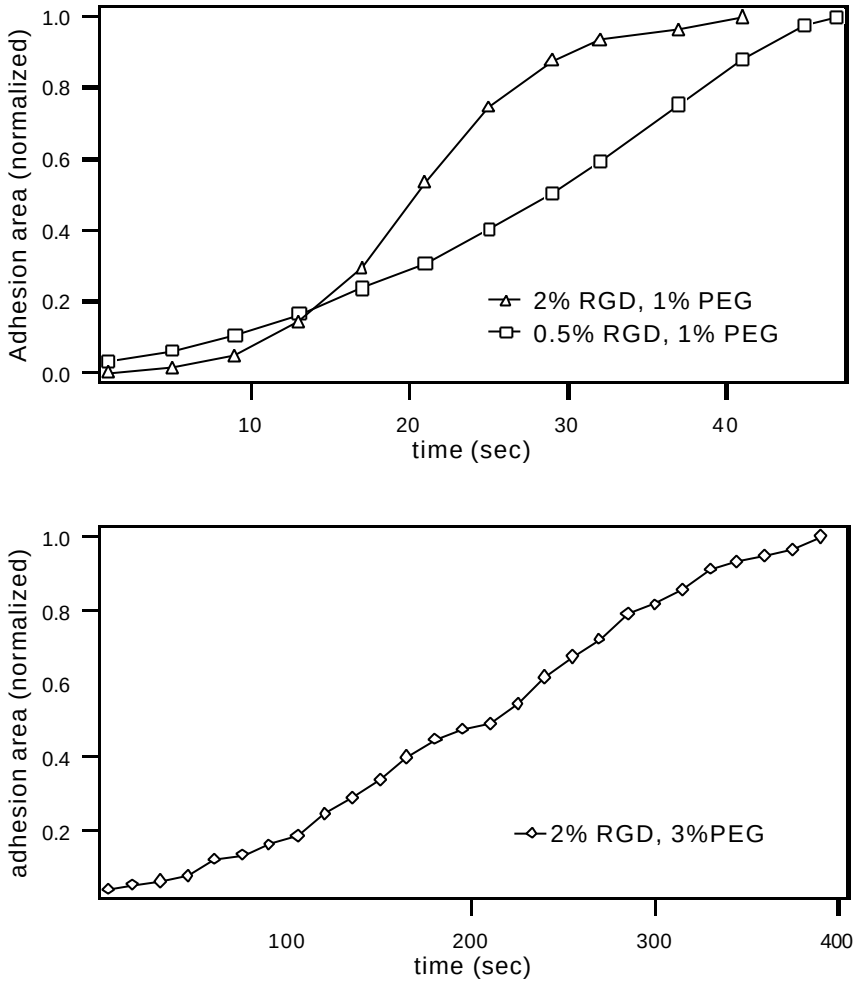

Figure 4.13: Adhesion kinetics. Normalized area values are obtained from adhesion areas at certain time divided by maximum adhesion areas. $\alpha_{IIb}\beta_3$ for coating the surface: 0.015 mg/ml in buffer A containing 0.01% instead of 0.1% of Triton X-100.

Calculation of adhesion energy

Three typical vesicles (containing 0.5% of the RGD lipid and 0.85% of PEG 2000 PE) of different adhesion stages were chosen for the adhesion energy calculation. For each vesicle, seven to eight lines were drawn accross the fringe pattern in the radial direction at random sites. From the light intensity distribution along these lines, the vesicle contours were determined. Analysis of the contours yielded adhesion energies, as explained in the methods section. The results are shown in *Figure 4.14* and *Table 4.1*. The values increased with the adhesion evolution, indicating increasing amount of involved receptor-ligand bonds per surface area. The values varied at different adhesion points within one vesicle (10^{-9}-10^{-7} J/m^2), and the variation between these values became relatively smaller at the end of adhesion procedure. This is reasonable since at the beginning, most parts except the regions nearby adhesion spots of the vesicles were in a state of relatively large thermal dynamic undulation, so that the reconstituted local contours (thus the adhesion energy) varied strongly. But at last, with the excess surface area being used up, the vesicle surface became much more strained and the adhsion disk became nearly a round one, as mentioned before, so that the shapes of

the reconstituted local vesicle contours (thus the values of the adhesion energy) were quite similar.

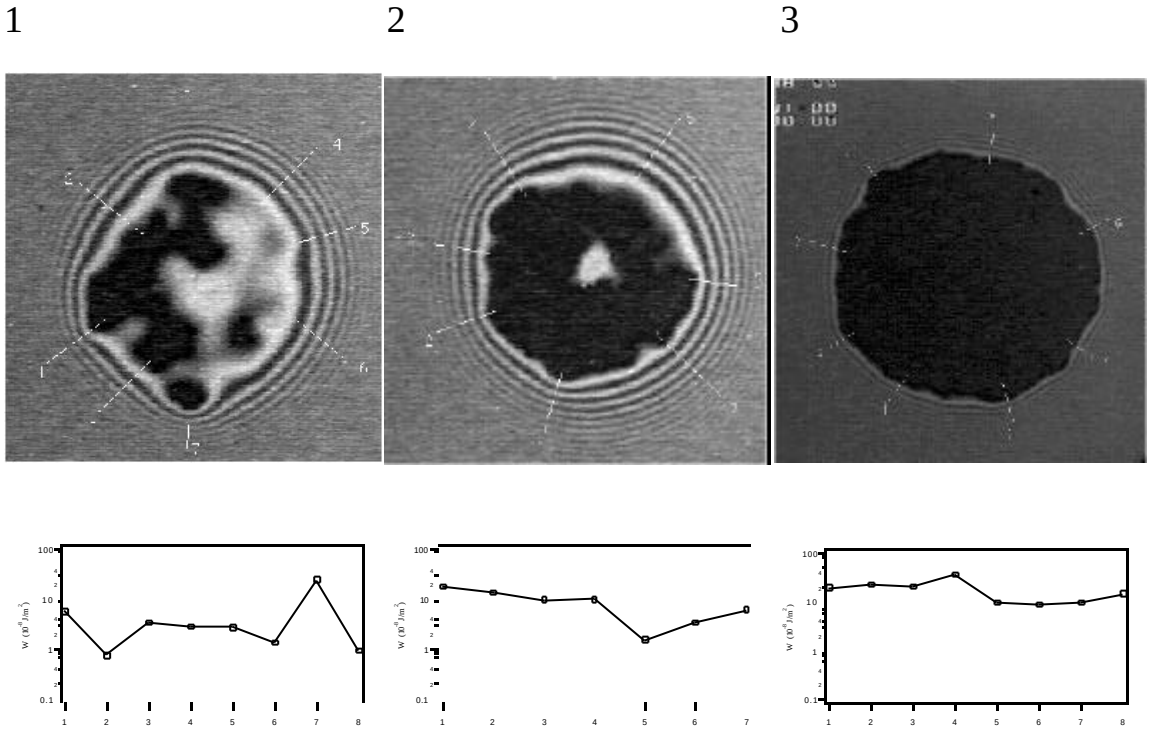

Figure 4.14: Calculation of adhesion energies. Lipid composition of the RGD vesicles: 0.5% of the RGD lipid / 0.85% PEG 2000 PE / 49.33% cholesterol / 49.33% DMPC. Coating $\alpha_{IIb}\beta_3$ concentration: 0.1 mg/ml in buffer A containing 0.01% instead of 0.1% of Triton X-100.

Table 4.1: Adhesion energies calculated from Figure 4.14

Lines	**Adhesion energy W (10^{-8} J/m^2)**		
	Vesicle 1	**Vesicle 2**	**Vesicle 3**
1	5.76	18.2	19.4
2	0.76	13.36	22.68
3	3.44	9.56	20.48
4	2.84	9.96	36.48
5	2.8	1.52	9.8
6	1.4	3.48	8.8
7	24.4	6.04	9.6
8	0.96	18.2	14.8

4.3.2 Discussion

The adhesion of cells is controlled by a complex interplay of specific lock-and-key forces and universal forces, as well as by the elasticity of the plasma membrane and the shape of the soft shell. The adhesion sites are believed to be formed by local aggregation of receptors, which is expected to be associated with the concomitant lateral displacement of carriers of the glycocalix. So the local repulsion between the opposing membranes is reduced, and this is required for the formation of tight adhesion plaques (Ammann and Lipowsky, 1996). Albersdoefer×s experiments (Albersdoerfer et al., 1997) showed that the formation of vesicle adhesion mediated by lock-and-key forces is a natural consequence of the competition between short-range attraction and long-range repulsion; the repulsion between vesicle and substrate is strongly determined by polymer-induced forces and undulation forces; the formation of tight contacts is also driven to some extent by local phase separation, resulting in the squeezing out of lipopolymers (repellers) from the adhesion domains.
In the present work, the main attractive force during the adhesion process was the interaction between $\alpha_{IIb}\beta_3$ and RGD. The main repulsive forces were generated by the lipopolymer PEG 2000 PE and vesicle membrane undulation. $\alpha_{IIb}\beta_3$ immobilized on glass could not move freely on the glass surface. At the same time, the vesicle membranes were in a fluid state at the room temperature, because of the high cholesterol content. This made it possible for the RGD lipid molecules to diffuse freely and concentrate around the adhesion patches or discs during the membrane stretching process. PEG 2000 PE could also be gradually squeezed out of the adhesion zone. As a result, in the local adhesion area the overall attractive forces were large enough to overcome the decoupling forces, so that adhesion could develop.
Adhesion started from the area where the vesicle surface containing ligands (RGD) and the supported surface containing receptors ($\alpha_{IIb}\beta_3$) were in close contact. Some patches formed and then stretched out and finally merged into one large adhesion disk. Adhesion was slowed down at a high PEG 2000 PE concentration. However, when vesicles contained proper concentrations of the RGD lipid (2%) and PEG 2000 PE (1%), a cooperative adhesion process appeared because of the interplay of the local forces: Once the balance between attractive forces and repulsive forces was broken because of involvement of more RGD ligands and less PEG 2000 PE through lateral movement within vesicle membranes (according to the results of Albersdoefer et al.), adhesion could develop relatively faster, until a new balance was reached when local RGD / $\alpha_{IIb}\beta_3$ interaction was saturated. The adhesion energies calculated from the last adhesion stage of the present experiments are of the order of 10^{-8} – 10^{-7} J/m^2 (Table 4.1), which is around 1 – 2 orders lower than what was measured from strong vesicle adhesion mediated by streptavidin-biotin interaction. This difference can be explained by the high binding energy of the streptavidin-biotin bond (~34 k_BT), and the high energy of the biotin-lipid binding in the membrane (~30 k_BT) (Albersdoerfer et al., 1997). In comparation with the adhesion of Dictyostelium Discoideum cells on BSA coated surfaces, the present adhesion energy values are even lower (2 – 3 oders of magnitude) (Simson et al., 1998), which may result from the complexity of the adhesion process of a real cell.
Real cell adhesion is much more complex than lipid vesicle adhesion which serves only as an artificial model system. As we have seen in the case of platelets, adhesion of cells is a much slower process (over 1 hour), and is accompanied with such phenomena as centralization of intracellular organells (on glass) and protrusion of pseudopodia. This is mainly a consequence of the involvement of cytoskeleton elements and many other adhesive factors (including different types of receptor-ligand reactions and intracellular signal transduction pathways).

4.3.3 Outlook

In the present work isolated $\alpha_{IIb}\beta_3$ was immobilized on glass without being incorporated into lipid bilayers. In order to simulate more closely natural cases where adhesive receptors can easily diffuse two dimensionally in cell membranes, integrin reconstitued in lipid vesicles can be used to coat glass and is possible to form lipid bilayers containing $\alpha_{IIb}\beta_3$ molecules by vesicle fusion method (Hillebrandt et al., 1999). Furthermore, shear fields in vivo (such as blood flow in the blood vessels) can be simulated and fine controlled by using lamellar flow chambers, to study their effects on adhesion. These experiments are still in progress in our laboratory.

5 Vesicle-vesicle adhesion in solution

5.1 Introduction

In this chapter, two kinds of vesicle-vesicle adhesion systems in solution were studied by means of fluorescence microscopy and cryoelectron microscopy (cryo EM), respectively (*Figure 5.1*).

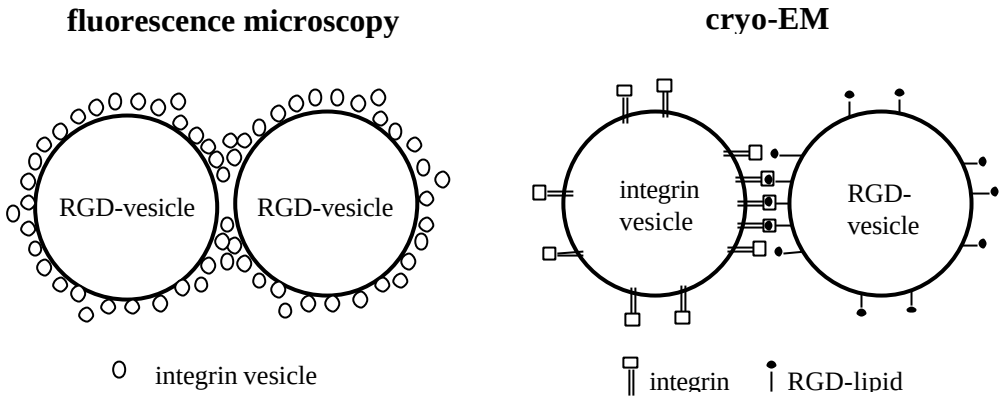

Figure 5.1: Vesicle-vesicle adhesion in solution.

Giant cRGD-lipid-containing vesicles can be easily produced by the electroswelling method (Section 4.2.2). The very large size of the vesicles (20 – 80 μm) makes it possible to observe their adhesion behaviors using light microscopy. Integrin $\alpha_{IIb}\beta_3$, on the other hand, can be reconstituted only into small lipid vesicles (Erb et al., 1997). Because each of the reconstituted vesicles contains much more than one $\alpha_{IIb}\beta_3$ molecule whose headgroup exposes outside the vesicle membrane, it is possible that the vesicles can act as multivalent ligands capable of mediating crosslinks between the RGD vesicles. In the present work, fluorescence-labeled $\alpha_{IIb}\beta_3$ was reconstituted into lipid vesicles. Adhesion between RGD vesicles mediated by the reconstituted $\alpha_{IIb}\beta_3$ vesicles was examined by epifluorescence and confocal fluorescence microscopy.
Cryo EM technique enables the imaging of biological structures in a close-to-native state with samples embedded in vitreous ice (Dubochet et al., 1988). Reconstituted $\alpha_{IIb}\beta_3$ vesicles have a diameter of 150 – 300 nm. RGD vesicles of similar sizes can be produced by the extruder method. Both kinds of vesicles are ideal candidates for cryo EM observations. In the work described in this chapter, fine structures of adhesion between $\alpha_{IIb}\beta_3$-containing and cRGD lipid-containing vesicles were observed by the cryo EM technique.

5.2 Materials and methods

5.2.1 Materials

DMPC, DMPG, cholesterol, and PEG 2000 PE were bought from Avanti Polar Lipids (Alabaster, AL, USA). Chloroform, methanol, and dimethylformamide (DMF) were bought from Fluka (Neu-Ulm, Germany) and were reagent p.a. grade. 5-(and-6)-carboxytetramethylrhodamine, succinimidyl ester (5(6)-TAMRA, SE) *mixed isomers* (Ex: 555nm, Em: 580nm) was bought from Molecular Probes, Inc. (Eugene, USA). Sepharose G-

25 PD-10 column (8.5 ml bed volume) was bought from Pharmacia (Freiburg, Germany). Bio-Beads SM2 (25 – 50 mesh) was bought from Bio-Rad laboratories Ltd. (Germany). All other chemicals were of the highest available purity and were purchased from Sigma (Deisenhofen, Germany) or Merck (Darmstadt, Germany).

5.2.2 Methods

Fluorescence labeling

$\alpha_{IIb}\beta_3$ (1 – 5 mg/ml) was dialyzed against labeling buffer (100 mM H_3BO_3-NaOH, pH 7.4, 1 mM $MgCl_2$, 1 mM $CaCl_2$, 0.02% NaN_3, 0.1% Triton X-100). 1 mg/ml of the fluorescent reagent (dissolved in DMF), 5-(and-6)-carboxytetramethylrhodamine, succinimidyl ester (5(6)-TAMRA, SE) *mixed isomers*, was slowly added to the dialyzed $\alpha_{IIb}\beta_3$. The final molar ratio of probe : protein was 60 : 1. The mixture was incubated at room temperature for 1 hour (rotating slowly) and then applied to a Sepharose G-25 PD-10 column. The column was first equilibrated with buffer A before use. $\alpha_{IIb}\beta_3$ was separated from the probe by washing the column with the same buffer. Usually 0.5 ml fractions were collected. $\alpha_{IIb}\beta_3$ appeared at around 2 – 2.5 ml. From the UV absorbance (ε = 80,000 $M^{-1}cm^{-1}$ in H_2O in presence of detergent) and the known protein concentration, a labeling efficiency of roughly 1:1 was derived.

Reconstitution of integrin $\alpha_{IIb}\beta_3$

$\alpha_{IIb}\beta_3$ was reconstituted into lipid vesicles according to Erb et al. (Erb et al., 1997). The quality of the reconstituted vesicle system was found to be highly reproducible if the lipid concentration suggested by Erb et al. (870 nM) was doubled.
The reconstitution buffer consists of 20 mM Tris-HCl, pH 7.4, 50 mM NaCl, 0.5 mM $CaCl_2$, and 3 mM (0.02%) NaN_3. $\alpha_{IIb}\beta_3$ was dialyzed against the reconstitution buffer containing 0.1% Triton X-100 before reconstitution.
The detailed procedure is described as following:

1) Lipids (DMPC, DMPG and PEG 2000 PE) with desired amounts were mixed and dried in a stream of nitrogen gas in a small glass container. The dialyzed $\alpha_{IIb}\beta_3$ was added to obtain a molar ratio of protein and lipids of 1 : 1000 – 1 : 2000. Fluorescence labeled $\alpha_{IIb}\beta_3$ was added up to 10% - 100% of the whole amount of $\alpha_{IIb}\beta_3$, if needed.
2) To swell the lipids in the solution, the protein-lipid mixture was stored at room temperature (rotating slowly) for 0.5 hour.
3) The mixture was incubated at 15 °C for 0.5 hour, and at 37 °C for 1.5 hours. Temperature was controlled with a water bath.
4) For 1ml of the protein-lipid mixture, 100 mg of washed Bio-Beads SM2 (25 – 50 mesh, see below for the washing procedure) was added, and the suspension was stored (rotating slowly) at room temperature for 3.5 hours.
5) The used beads were then replaced with 100 mg of washed ones (per 1ml of the above suspension), and the suspension was stored again at room temperature for 0.5 hour (rotating slowly).
6) Again the used beads were discarded, and thus obtained solution containing reconstituted vesicles was stored on ice for further use.
7) Discontinuous sucrose gradients were made in 6 plastic centrifugal tubes (Beckmann Ultra-Clear™, 11 × 60 mm, 4.4 ml, Beckmann Instruments, Inc., USA). From bottom to top of a tube, the sucrose concentrations of the four layers were 2.0 M, 1.2 M, 0.8 M, and

0.4 M, repectively. Each layer contained 0.8 ml of sucrose solution (with the reconstitution buffer).

8) 0.3 – 0.35 ml of reconsitituted vesicle suspension was placed carefully on top of each tube. The weight of the tubes was finally balanced with the reconstitution buffer.
9) The tubes were then put onto the Beckmann rotor SW60 (r_{av} = 91.7cm) and were centrifuged on a Beckmann L7-55 centrifuge for 20 – 24 hours, at 275,000 g (52,000 rpm) and 4 °C. The reconstituted protein containing liposomes were separated from the pure lipid vesicles and protein molecules in this step.
10) The condensed protein containing liposomes appeared as a thin white layer in a tube at the end of centrifugation. The layer was taken out of the tube carefully by a pipet.
11) The reconstituted vesicles were dialyzed against the required buffers and stored on ice for use within two days.

Cleaning procedure of Bio-Beads SM2 before use:

1) Washing with methanol.
2) Rinsing with Millipore water.
3) Rinsing with the reconstitution buffer.
4) Degassing (in the reconstitution buffer) in vacuum.

Preparation of the RGD vesicles

1) Giant unilamellar RGD vesicles were prepared by the electroswelling method described in Section 4.2.2.
2) Small unilamellar lipid vesicles were prepared by the extruder method: For electron microscopic studies, vacuum-dried lipid films were swollen in buffer A at 37 °C in a volume corresponding to a final lipid concentration of 1 mg/ml. Small unilamellar vesicles were then produced by 20 passages through polycarbonate filter membranes with controlled pore sizes (200 nm) by means of a LipoFast extruder (Milsch Equipment, Laudenbach, Germany). Vesicles were usually 50 – 150 nm in diameter.

Fluorescence microscopy

The epifluorescence microscopy (*Figure 5.2*) was performed on a Zeiss Axiovert 10 equipped with a Zeiss Plan-Apochromat 63×/1.40 oil objective (Zeiss, Oberkochen, Germany) and the filter set for rhodamine fluorescence. The pictures were taken with a SIT camera (Hamamatsu, Japan) and recorded on video tape by a ¼-inch S-VHS recorder (AG7350, Panasonic, Japan). The sample chamber was the same as used in the RICM experiments (described in Section 4.2.2).

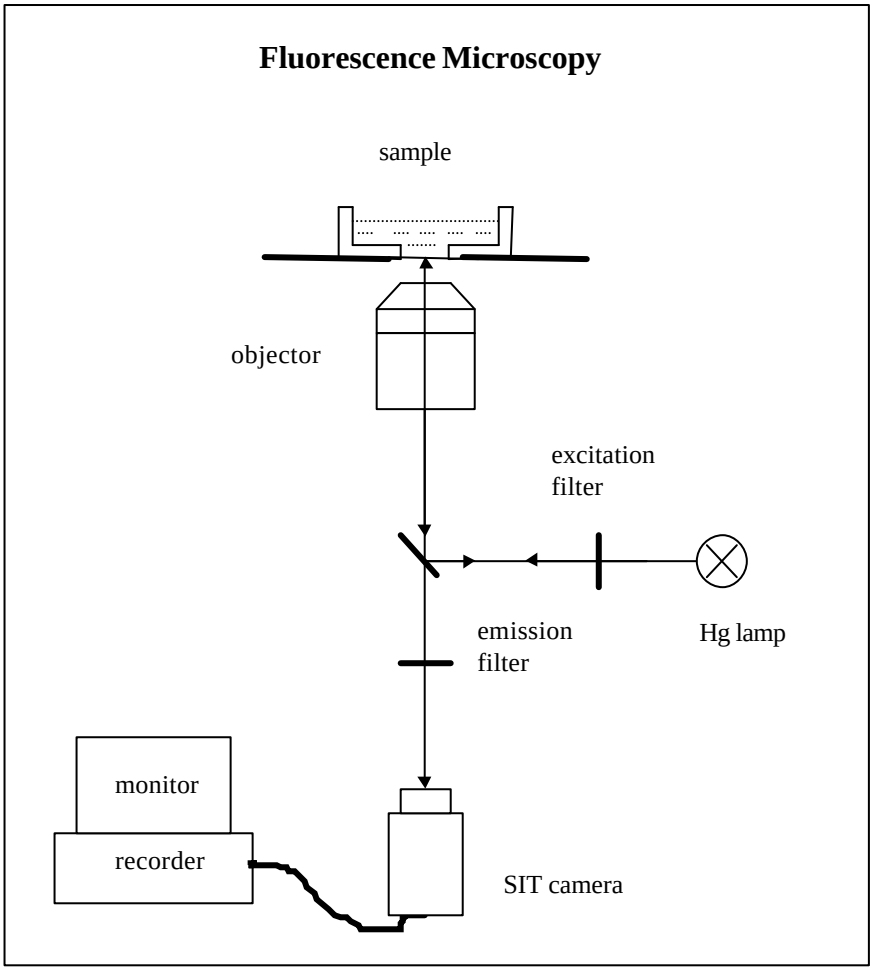

Figure 5.2: Schematic drawing of fluorescence microscopy.

Confocal laser scanning microscopy (CLSM)

3-dimensional images were taken by the confocal laser scanning microscopy with a Zeiss Axovert 100 microscope (Zeiss, Oberkochen, Germany), equipped with the Odyssey XL system from Noran Instruments (Middleton, WI, USA) system. A Plan Apochromat 63×/1.40 oil objective (Zeiss, Oberkochen, Germany) was used. Stacks of 36 slices were taken with 0.5 µm steps of the stepper motor and used for the calculation of 3-dimensional pictures with the NORAN Intervision™ software. The wave length of the laser beam was 568 nm and a pin hole size of 50 µm was used. In x and y directions, the image size was 620 × 479 pixels, with 0.13 × 0.13 µm/pixel. The sample chamber was the same as used in the RICM experiments (described in Section 4.2.2).

Phase contrast microscopy

The phase contrast microscope was built up together with RICM, with a 200W Halogen lamp used for illumination.

Image processing and calculation of adhesion energy

Contours of adhering vesicles were obtained from fluorescence micrographs by application of the software ´Pathfinder´ (self-made in Prof. Sackmann´s laboratory), and transfered to Igor Pro 3.11 (WaveMetrics, Inc., Oregon, USA) (*Figure 5.3a*). Through the same method as used in the RICM experiments (described in Section 4.2.2), adhesion energies could be obtained (*Figure 5.3b*).

a

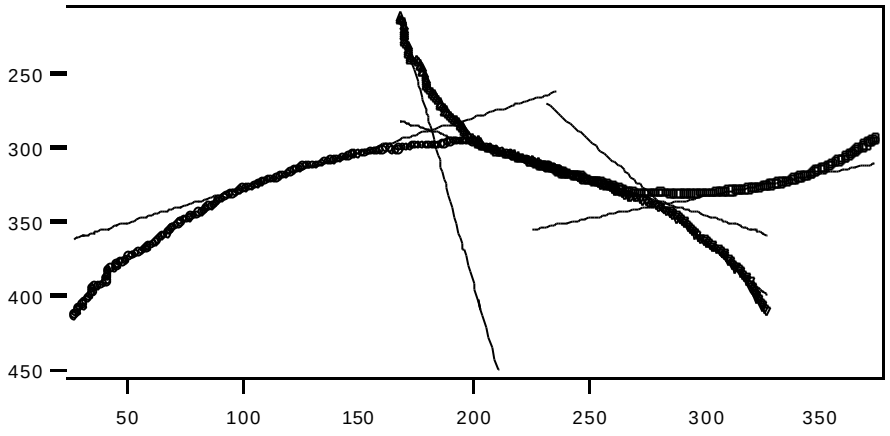

b

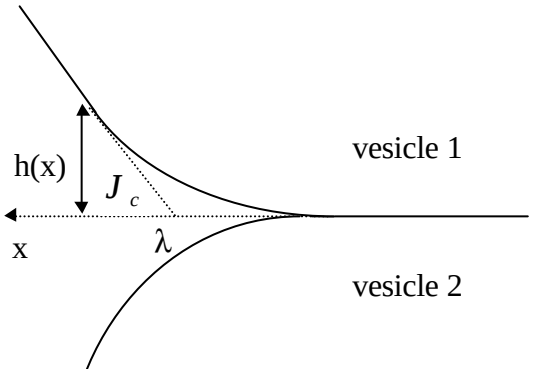

Figure 5.3: Vesicle-vesicle adhesion in solution. **a**) A sample of contours of two adhering vesicles obtained from a fluorescence micrograph by using ´Pathfinder´. **b**) Contour analysis for calculation of adhesion energy.

Cryo electron microscopy (cryo EM)

5 µl aliquots of samples (which had been incubated at 30 – 37 °C for 1 hour) were applied to holey carbon Quantifoil R2/2 EM-grids (Quantifoil Micro Tools GmbH, Jena, Germany). In some experiments 5 nm gold particles were included as an internal standard. Excessive liquid

was blotted with filter paper to a thickness less than 200 nm and the specimens were plunged into liquid ethane at -190 °C (Dubochet et al., 1988). The rapid-freezing technique (freezing rates $\approx 10^6$ K/s) not only guarantees preservation of the natural structure of the specimen, but also avoids the problems that arise in interpreting density patterns of negative staining electron micrographs resulting from poorly understood interactions between structure and stain typical for conventionally hydrated specimens. The grids were transferred to a Gatan 626 cryo-specimen holder (Gatan Inc., Pleasanton, CA, USA) and inserted into a Philips CM 120 Biofilter electron microscope (FEI Company, Hillsboro, OR, USA) under liquid nitrogen conditions. The post-column energy filter GIF 100 (Gatan Inc., Pleasanton, CA), attached to the microscope, enhances the contrast of the images, as inelastically scattered electrons are masked from the zero-loss electron beam (Grimm et. Al., 1998). The electrons are detected on a 1024 × 1024 CCD chip. The images were recorded by the Digital Micrograph 2.5 software (Gatan Inc., Pleasanton, USA) on a Mac 8500 computer, at a magnification of 14.500 × or 31.00 ×, corresponding to pixel sizes of 1.63 and 0.738 nm, respectively.

5.3 Results and discussion

5.3.1 Reconstitution of $\alpha_{IIb}\beta_3$ into the lipid vesicles

The success of a reconstitution could be easily judged from the position of the reconstituted vesicles in the sucrose gradient after centrifuging. The reconstituted $\alpha_{IIb}\beta_3$ vesicles had a higher relative gravity comparing to pure lipid vesicles, so they occupied a lower position in the gradient (*Figure 5.4*).

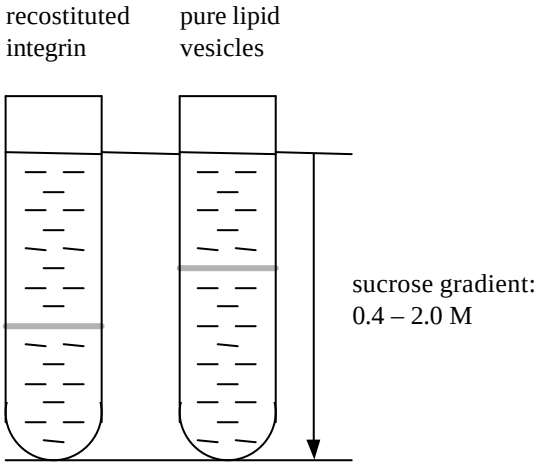

Figure 5.4: Schematic drawing of positions occupied by the reconstituted $\alpha_{IIb}\beta_3$ vesicles and pure lipid vesicles in the sucrose gradient after centrifuging. Pure lipid vesicles were prepared by the same reconstitution procedure, except that no integrin was included at the very beginning.

Reconstituted integrin vesicles were examined most closely by cryo electron microscopy (cryo EM). *Figure 5.5* presents some cryo EM images of tipical preparations of recontituted $\alpha_{IIb}\beta_3$ vesicles. The diameter of the vesicles was in the range of 150 – 300 nm, sometimes up to 450 nm, larger integrin-containing vesicles were not observed. The reconstituted $\alpha_{IIb}\beta_3$ molecules were clearly recognizable as small protrusions extending from both sides of the vesicle membrane (Figure 5.5b and 5.5c). These protrusions exhibited a rather regular size with a diameter of 8 – 10 nm and a length of 19 – 23 nm which was in good agreement with observations from other laboratories (Erb et al., 1997; Weisel, 1992). One striking feature of these integrin vesicles is that the protruding molecules were rather evenly distributed over the whole surface of the vesicles on both sides of the bilayer (Figure 5.5c). The distance between individual integrin heads on either side of the membrane was 5 – 10 nm. Assuming an average diameter of the heads of 10 nm, the side length of a square area occupied per integrin molecule in the local plane of the membrane was in the range of 15 – 20 nm which gives an area of 200 – 400 nm^2. Thus, if we assume that half of the molecules face to the inside and the other half to the outside, a vesicle of 300 nm in diameter contains 700 to 1250 integrin molecules. Calculating the ratio between integrin and lipid molecules, a value of 1 : 370 – 660 is obtained if a diameter of 2 nm is used for the integrin membrane spanning domain and an area of 0.6 nm^2 for the lipid heads.

a

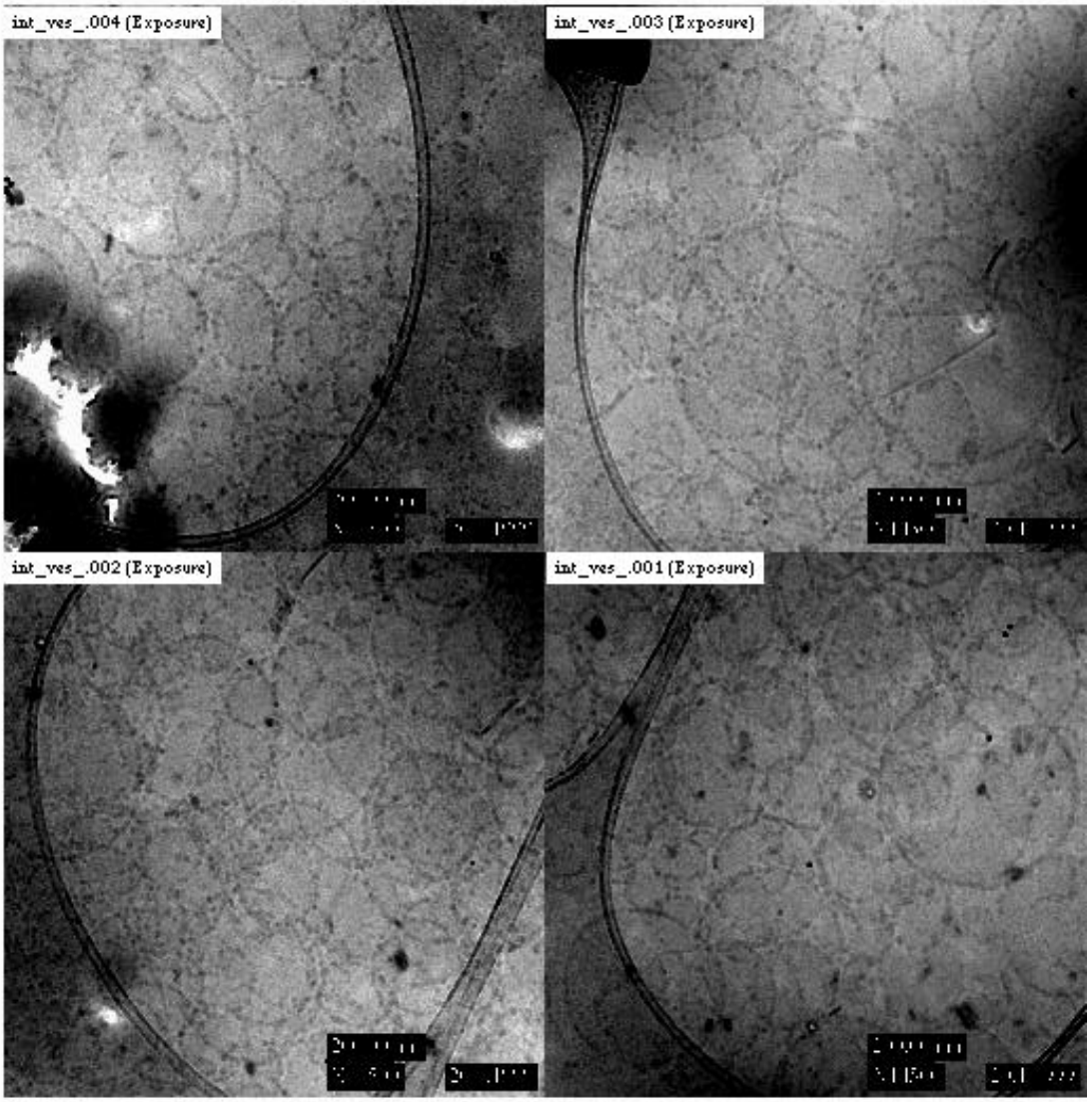
int_ves_.004 (Exposure)
int_ves_.003 (Exposure)
int_ves_.002 (Exposure)
int_ves_.001 (Exposure)
Int Ves 200199

b

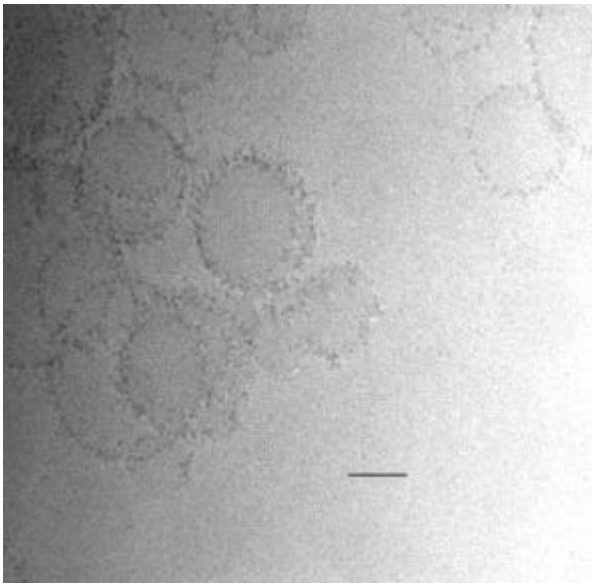

c

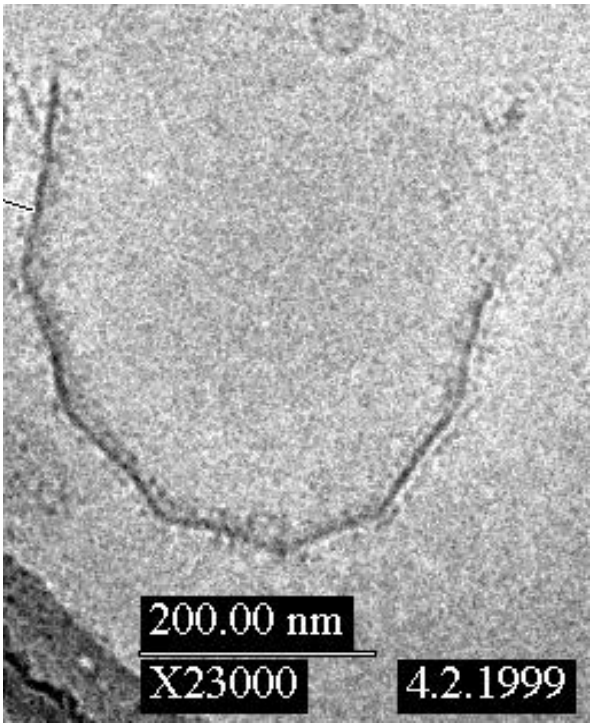

Figure 5.5: Cryo EM micrographs of the reconstituted $\alpha_{IIb}\beta_3$ vesicles. Lipid composition: 1% PEG 2000 PE / 49.5% DMPC / 49.5% DMPG. Bar in (b): 100 nm.

5.3.2 Adhesion between the recontituted $a_{IIb}b_3$ vesicles and the giant RGD vesicles: Fluorescence microscopic experiments

In the present work, 100% of fluorescence-labeled $\alpha_{IIb}\beta_3$ was used for the reconstitution. The binding of the reconstituted $\alpha_{IIb}\beta_3$ vesicles to the giant vesicles containing the RGD lipid was studied by microfluorescence. The lipid composition of the reconstituted $\alpha_{IIb}\beta_3$ vesicles was 49.5% DMPC / 49.5% DMPG / 1% PEG 2000 PE. The dialysis buffer after recontitution was the reconstitution buffer containing119 mM sucrose. The lipid compositon of the RGD vesicles was 48.5% DMPC / 48.5% cholesterol / 2% of the RGD lipid / 1% PEG 2000 PE.

0.95 ml of the reconstituted $\alpha_{IIb}\beta_3$ vesicles were mixed with 50 µl of the giant RGD vesicles in a sample chamber and then applied to the fluorescence microscope. Glass surface of the chamber bottom had been blocked with 3% BSA before use.
The giant RGD vesicles were not visible under the fluorescence microscope right after mixing, because in the vesicles no lipid was fluorescence-labeled. The reconstituted $\alpha_{IIb}\beta_3$ vesicles, on the other hand, appeared as small fluorescence spots because of their small size. About half an hour later, some large fluorescent circles appeared. And with increase of the light intensity of the circles over time, some of them began to adhere to each other. 2 – 3 hours later most of the circles were clustered (*Figure 5.6*).

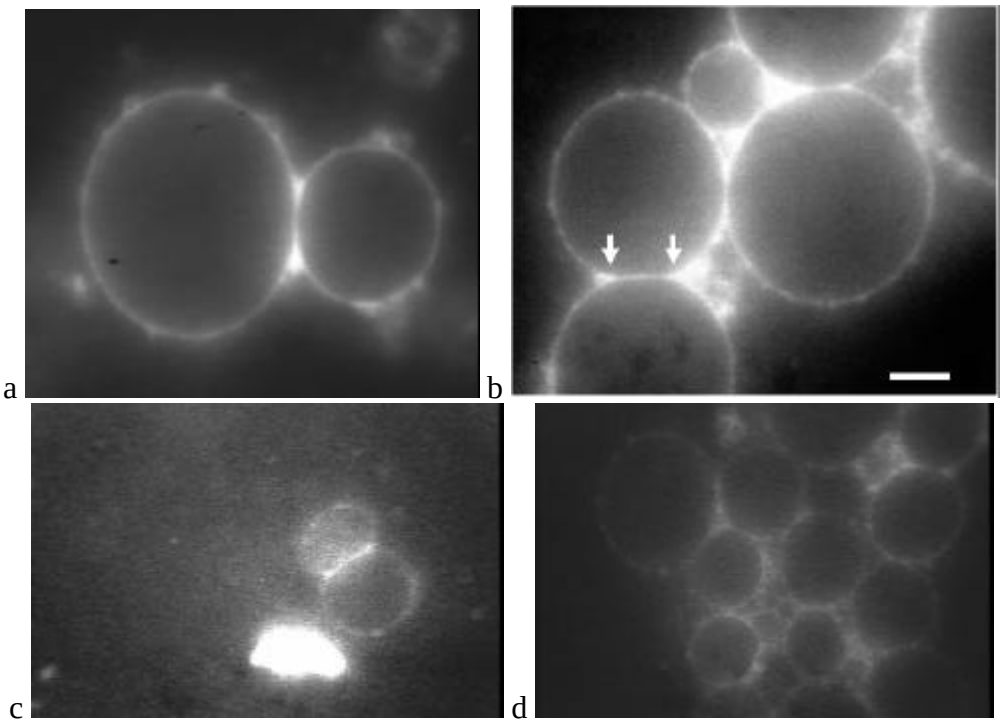

Figure 5.6: Fluorescence microscope images of the RGD vesicles cross-linked by the reconstituted $\alpha_{IIb}\beta_3$ vesicles, through binding of RGD to integrin. Bar in (b): 5 µm.

The fluorescent circles represented giant RGD vesicles decorated with the very small recontituted $\alpha_{IIb}\beta_3$ vesicles. Clustering of the circles suggested that the RGD vesicles were cross-linked by integrin/RGD interaction. To verify this conclusion, 100 µl of 1 mg/ml fibrinogen was added into the sample chamber in which the fluorescent circles were clustered. After half an hour, most fluorescence circles disappeared as expected (*Figure 5.7a*): The small $\alpha_{IIb}\beta_3$ vesicles were detached from the RGD vesicles because of the higher binding ability of fibrinogen to the reconstituted $\alpha_{IIb}\beta_3$. Under the phase contrast microscope, some RGD vesicles were still adhering to each other (*Figure 5.7b*) by the $\alpha_{IIb}\beta_3$ vesicles remaining in the adhesion area (Figure 7a).
In many cases, an enrichment of fluorescence at the rims of the adhesion areas between the giant vesicles was observed (arrows in Figure 5.6b). With the aid of confocal scanning microscopy we could reconstruct these vesicle complexes in three dimensions. *Figure 5.8* shows such a reconstruction of a pair of giant vesicles. The vesicles are viewed from a slightly oblique angle relative to their area of contact. It is evident that the fluorescence dots representing integrin-containing vesicles were concentrated in a ring-like structure along the

edge of the contact zone of the cross-linked giant vesicles. Such a process requires fluid membranes in which the molecules interacting between the two sorts of vesicles are free to move at least in the plane of the crosslinked membranes of the giant RGD vesicles.

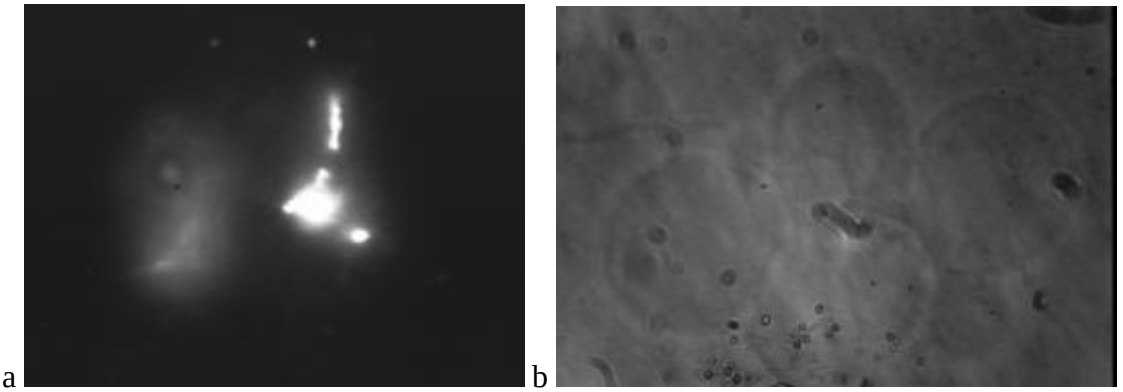

Figure 5.7: Effect of fibrinogen on the RGD vesicles cross-linked by the reconstituted $\alpha_{IIb}\beta_3$ vesicles. The two images were taken from the same observation area. Width of an image is 105.1 μm. **a**) Fluorescence microscopy. **b**) Phase contrast microscopy.

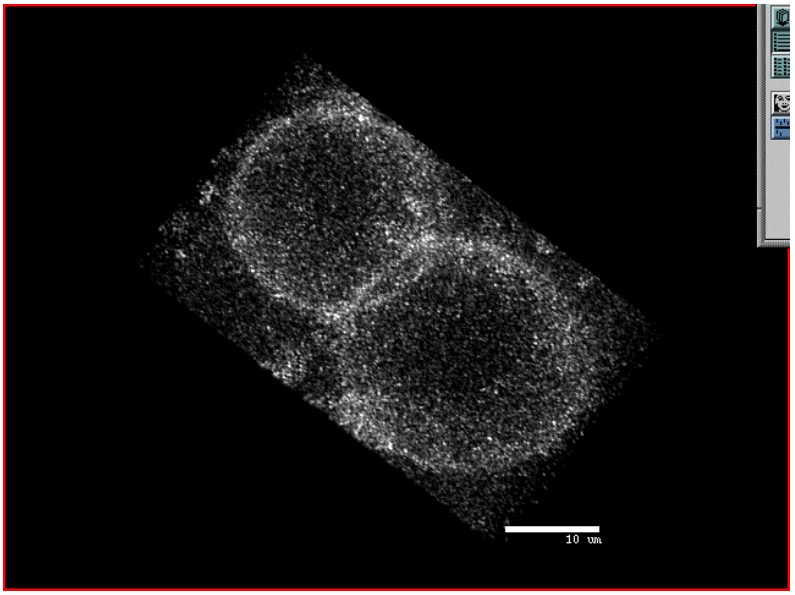

Figure 5.8: 3D image of the RGD vesicle cross-linking by the reconstituted $\alpha_{IIb}\beta_3$ vesicles obtained from the confocal fluorescence microscopy. Note the ring-like structure along the edge of the contact zone of the cross-linked vesicles.

Adhesion energies of the adhering RGD vesicles can also be calculated with the same method described in Section 4.2.2. Only the cases in which there were just two adhering giant RGD vesicles were chosen (as shown in Figure 5.6a and 5.6c). *Table 5.1* listed the adhesion energy values of five chosen reactions. Since many (if not most) of the small integrin vesicles were squeezed out of the contacting disc between two RGD vesicles during the adhesion process (as shown in Fiugre 5.8), the amount of integrin-RGD bond finally involved in the present adhesion reaction should be much smaller than in the adhesion process of the RGD vesicles on the integrin surface. So

the latter type of adhesion should be stronger and proceed more completely. This can explain why the values listed in Table 5.1 are lower than those obtained from the complete adhesion of the giant RGD vesicles on the $\alpha_{IIb}\beta_3$ coated surface (vesicle 3 in Figure 4.14 and Table 4.1).

Table 5.1.1: Adhesion energies calculated from five samples of the RGD vesicle adhesion mediated by the reconstituted $\alpha_{IIb}\beta_3$ vesicles.

Sample	Adheison Energy (10^{-8}J/m^2)
1	6.00
2	3.52
3	3.28
4	1.57
5	3.19

5.3.3 Adhesion between the recontituted $a_{IIb}b_3$ vesicles and the extruded RGD vesicles: Cryo electron microscopic experiments

Cryo electron microscopy was applied to study the crosslinks between $\alpha_{IIb}\beta_3$-containing and cRGD lipid-containing vesicles more closely.
Different from the procedure applied to produce giant vesicles for the light microscopic studies, the RGD vesicles used for electron microscopy were reduced in size by passing multilamellar lipid vesicle suspension 20 times through a polycarbonate membrane with a pore size of 200 nm. As shown in Figure 5.9a, the vesicles had a smooth surface and did not exhibit the grainy appearance characteristic for the membranes of integrin vesicles. Thus, when mixed with the $\alpha_{IIb}\beta_3$ vesicles they could be readily distinguished. The vesicles were composed of 5% of the RGD lipid and 95% DMPC. Because of the relatively high RGD lipid concentration, they were slightly polygonal, which was also different from pure lipid vesicles (50% DMPC / 50% DMPG) (Figure 5.9b).
$\alpha_{IIb}\beta_3$ was reconstituted into 50% DMPC / 50% DMPG vesicles (Figure 5.10). 0.9 ml of reconstituted $\alpha_{IIb}\beta_3$ was mixed with 0.1 ml of 5% RGD vesicles. The mixture was incubated at 30 – 37 °X for 1 hour and then applied to the microscope.
Figure $5.10A_1$ – $5.10A_4$ shows several snapshots. Most $\alpha_{IIb}\beta_3$ vesicles were associated with more than one RGD vesicle. In many cases, fine bridges (arrows) between the smaller RGD vesicles and the larger $\alpha_{IIb}\beta_3$ vesicles could be seen with a minimum distance of 9 – 12 nm. Not all bridges were seen equally clear since it depends on the focussing level whether the bridges exhibited optimal electron contrast. Within vesicle contacting areas, no local aggregation of $\alpha_{IIb}\beta_3$ molecules in the vesicle membranes was observed. This seems reasonable because in vivo aggregation of $\alpha_{IIb}\beta_3$ within focal adhesion plaques is based on the binding of both extracellular multivalent ligands (fibrinogen, for example) and intracellular cytoskeletons.
Chiruvolu´σ experiments (Chiruvolu et al., 1994) nicely showed by means of cryo electron microscopy the coupling between DPPE-biotin-containing vesicles mediated by streptavidin. The associated vesicles were still in their original, unstressed state, just as in the present case. But no bridges between the associated vesicles were seen, probably because of the relatively small molecular size of strpetavidin, comparing to the size of $\alpha_{IIb}\beta_3$.
In Figure 5.10B and 5.10C pure phospholipid vesicles were mixed either with $\alpha_{IIb}\beta_3$ vesicles or vesicles, respectively. In Figure 5.10B, no attachment between small vesicles (smooth surface) and larger vesicles (rough surface, integrin-containing) could be seen. In some cases

´βridge´ between integrin-containing vesicles with rough surfaces were observed (arrows in Figure 5.10B). They might be caused by unspecific interaction between integrin headgroups. In Figure 5.10B as well as in Figure 5.10C no regular association of the two populations of vesicles could be observed indicating that they did not exhibit non-specific interaction. Note that in order to present a better overview over the control preparations in Figure 5.10B and 5.10C, the magnification in these micrographs is lower than in Figure 5.10A (see scale bars).

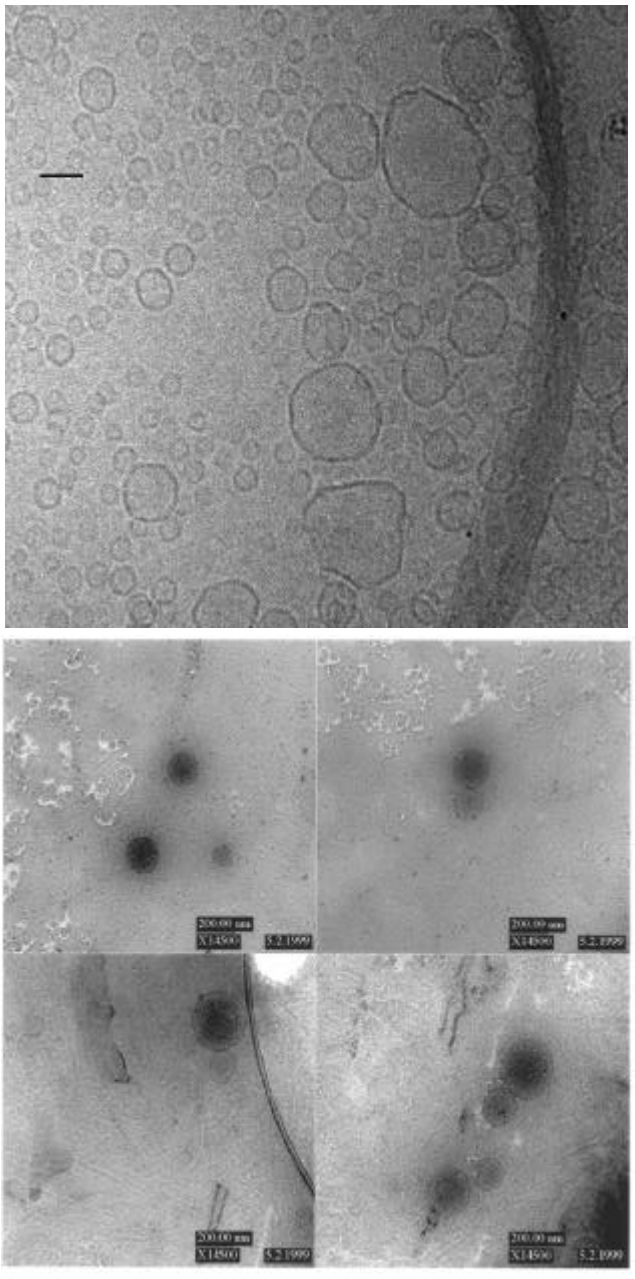

Figure 5.9: Cryo EM micrographs of: **a**) extruded 5% of the RGD lipid / 95% DMPC vesicles; **b**) extruded 50% DMPC / 50% DMPG vesicles. Bar in (a): 100 nm.

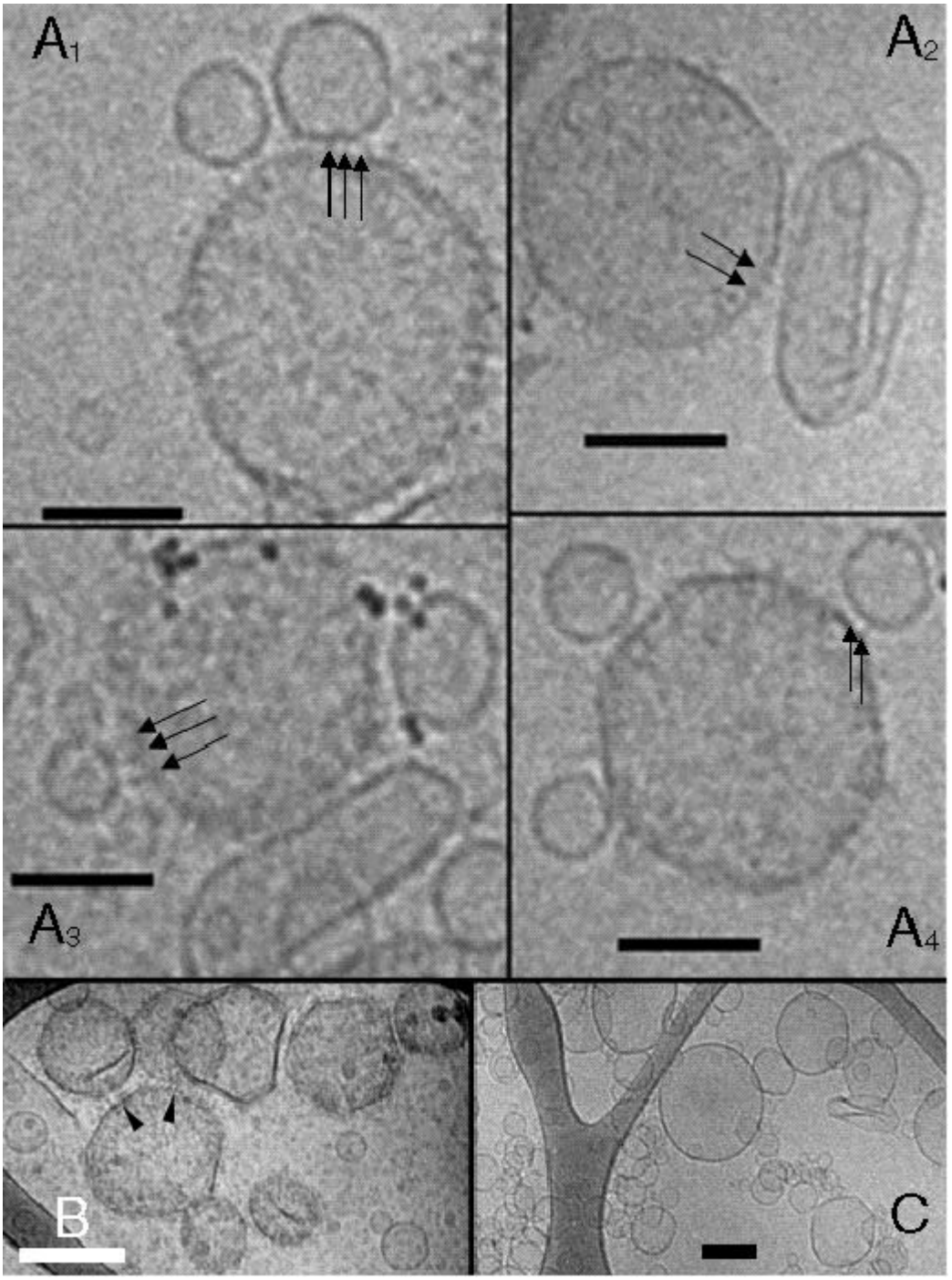

Figure 5.10: **A_1 – A_4**: a series of cryo EM snapshots of a mixture of integrin vesicles and cRGD vesicles. Arrows point to integrin/RGD bridges between vesicles. Dark spots in panel A_3: 5 nm gold particles. Magnification 31.000 ×; scale bars: 50 nm. **B**: a mixture of integrin vesicles with pure lipid vesicles (DMPC/DMPG = 1/1), scale bar: 200 nm. Arrowheads point to integrin/integrin attachments. **C**: a mixture of cRGD-vesicles with pure lipid vesicles as in B, scale bar: 200 nm. All but the integrin-containing vesicles were produced by extrusion. Note that, for a better overview, B and C are shown at lower magnification than A_1 – A_4. The irregular dark objects in the upper right corner of B are accidental artifacts of the preparation.

6 References

Adler, M., R. A. Lazarus, M. S. Dennis, and G. Wagner (1991). Solution structure of kistrin, a potent platelet aggregation inhibitor and GP IIb-IIIa antagonist. Science 253, 445-448.

Albersdoefer, A., T. Feder, and E. Sackmann (1997). Adhesion-induced domain formation by interplay of long-range repulsion and short-range attraction force: a model membrane study. Biophys. J. 73, 245-257.

Alberts, B., D. Bray, J. Lewis, R. Raff, K. Roberts, and J. D. Watson (1983). Molecular biology of the cell. Garland, New York.

Alberts, B., D. Bray, J. Lewis, M. Raff, K. Roberts, and J. D. Watson, Eds. (1994). Molecular Biology of the Cell, 3rd ed., Garland Publishing Inc., New York.

Ammann, A., and R. Lipowsky (1996). Discontinuous phase transitions of membranes: a Monte Carlo study. J. Phys. II France 6, 255-270.

Angelova, M. I. and D. S. Dimitrov (1986). Liposome electroformation. Farady Discuss. Chem. Soc. 81, 303-311.

Aumailley, M., M. Gurrath, G. Müller, J. Calvete, R. Timpl, and H. Kessler (1991). Arg-Gly-Asp constrained within cyclic pentapeptides. Strong and selective inhibitors of cell adhesion to vitronectin and laminin fragment P1. FEBS Lett. 291, 50-54.

Behrisch, A. (1998). Rezeptorvermittelte Wechselwirkung von Vesikeln und festkörpergestützten Membranen. Ein physikalisches Modell der Zelladhäsion. Ph. D thesis, Technical University of Munich.

Bell, G. I. (1978). Models for the specific adhesion of cells to cells. Science 200, 618-627.

Bruinsma, R. (1995). Adhesion and rolling of leukocytes: a physical model. Proc. NATO Adv. Inst. Phys. Biomater. NATO ASI Ser. 332, 61-75.

Calvete, J. J., M. V. Alvarez, G. Rivas, C.-L. Hew, A. Henschen, and J. Gonzalez-Rodriguez (1989). Interchain and intrachain disulphide bonds in human platelet glycoprotein Iib. Localization of the epitopes for several monoclonal antibodies. Biochem. J. 261, 551-560.

Calvete, J. J., A. Henschen, and J. Gonzalez-Rodriguez (1991). Assignment of disulphide bonds in human platelet GPIIIa. A disulphide pattern for the β-subunits of the integrin family. Biochem. J. 274, 63-71.

Calvete, J.J. (1993). Cell adhesion molecules (Hemler, M.E., and Mihich, E., Eds.). Plenum Press, New York.

Calvete, J. J. (1994). Clues for understanding the structure and function of a prototypic human integrin: the platelet glycoprotein IIb/IIIa complex. Thrombosis and Haemostasis 72(1), 1-15.

Carraway, K. L., C. A. C. Carraway, and K. L. Carraway III (1998). Signaling and the Cytoskeleton. Springer-Verlag and R. G. Landes Company.

Carrell, N. A., L. A. Fitzgerald, B. steiner, H. P. Erickson, and D. R. Phillips (1985). Structure of human platelet membrane glycoproteins IIb and IIIa as determined by electron microscopy. The Journal of Biological Chemistry 260, 1743-1749.

Cevc, G., Ed. (1993). Phospholipid Handbook. Marcel Dekker Inc., New York.

Charo, I. F., L. Nannizzi, D. R. Phillips, M. A. Hsu, and R. M. Scarborough (1991). Inhibition of fibrinogen binding to GP IIb-IIIa by a GP IIIa peptide. J. Biol. Chem. 266, 1415-1421.

Clark, E. A., and J. S. Brugge (1995). Integrins and signal transduction pathways: the road taken. Science 268, 233-239.

Coller, J.J. (1994). Coron. Artery Dis. 3, 1016–1029.

Dedhar, S., and G. E. Hannigan (1996). Integrin cytoplasmic interaction and biderectional transmembrane signaling. Curr. Opin. Cell Biol. 8, 657-669.

Dubochet, J., M. Adrian, J. Chang, J. C. Homo, J. Lepault, A. W. McDowall, and P. Schulz (1988). Cryo-electron microscopy of vitrified specimens. Quart. Rev. Biophys. 21, 129-228.

Erb, E.-M., K. Tangemann, B. Bohrmann, B. Müller, and J. Engel (1997). Integrin alphaIIb beta3 reconstituted into lipid bilayers is nonclustered in its activated state but clusters after fibrinogen binding. Biochemistry 36, 7295-7402.

Finsinger, D. (1997). Peptidische und peptidanaloge Antagonisten des Integrins $\alpha_v\beta_3$ – Beitraege zum Verstaendnis zellulaerer Adhaesion. Ph. D. thesis, Technical University of Munich.

Fitzgerald, L., Leung, B., and Phillips, D. R. (1985). A method for purifying the platelet membrane glycoprotein IIb-IIIa complex. Anal. Biochem. 151, 169-177.

Frojmovic, M. M., J. G. Milton (1982). Human platelet size, shape, and related functions in health and disease. Physiol. Rev. 62, 185-261.

Fujimura, K., and D. R. Phillips (1983). Calcium cation regulation of glycoprotein Iib-IIIa complex formation in platelet plasma membranes. J. Biol. Chem. 258, 10247-10252.

Galbraith, C. G., and M. P. Sheetz (1998). Forces on adhesive contacts affect cell function. Curr. Opin. Cell Biol. 10, 566-571.

Giancotti, F. G., and E. Ruoslahti (1999). Integrin signaling. Science 285, 1028-1032.

Gingell, D., and I. Todd (1979). Interference reflection microscopy. A quantitative theory for image interpretation and ist application to cell-substratum separation measurements. Biophys. J. 26, 507-526.

Gingell, D., I. Todd, and O. S. Heavens (1982). Quantitative interference microscopy: effect of microscope aperture. Opt. Acta (Lond.). 29, 901-908.

Ginsber, M. H., and E. F. Plow (1991). Arginyl-glycyl-aspartic acid (RGD): a cell adhesion motif. TIBS 16, 246-250.

Green, N. M. (1990). Avidin and streptavidin. Methods Enzymol. 184, 51-67.

Grimm, R., H. Singh, R. Rachel, D. Typke, W. Zillig, and W. Baumeister (1998). Electron tomography of ice-embedded prokaryotic cells. Biophys. J. 74, 1031-1042.

Gurrath, M., Müller, G., Kessler, H., Aumailley, M., and Timpl, R. (1992). Conformation/activity studies of rationally designed potent anti-adhesive RGD peptides. Eur. J. Biochem. 210, 911-921.

Guttenberg, Z. (2000). Zell adhäsion als Benetzungsübergang: Mikrooptische und Mikromechanische Untersuchung eines biomimetischen Modellsystems. Ph. D. thesis, Technical University of Munich.

Haubner, R., Finsinger, D. & Kessler, H. (1997). Angew. Chem . Int. Ed. 36, 1374-1389.

Heyn, S. P., R. W. Tillmann, M. Egger, and H. E. Gaub (1990). A miniaturized micro-fluorescence film balance for protein-containing lipid monolayers spread from a vesicle suspension. J Biochem Biophys Methods 22(2), 145-58.

Hillebrandt, H., G. Wiegand, M. Tanaka, and E. Sackmann (1999). High electric resistance polymer/lipid composite films on Indium-Tin-Oxide Electrodes. Langmuir 15, 8451-8459.

Howe, A., A. E. Aplin, S. K. Alahari, and R. L. Juliano (1998). Integrin signaling and cell growth control. Curr. Op. in Cell Biol. 10, 220-231.

Huber, W., J. Hurst, D. Schlatter, R. Barner, J. Hübscher, W. C. Kouns, and B. Steiner (1995). Determination of kinetic constants for the interaction between the platelet glycoprotein IIb-IIIa and fibrinogen by means of surface plasmon resonance. Eur. J. Biochem. 227, 647-656.

Hu, B., D. Finsinger, K. Peter, Z. Guttenberg, M. Baermann, H. Kessler, A. Escherich, L. Moroder, J. Boehm, W. Baumeister, S.-f. Sui, and E. Sackmann (2000). Inter-vesicle crosslinking with Integrin IIb/IIIa and cyclic-RGD-Lipopeptide: A model of cell-adhesion processes. Biochemsitry 39(40), 12284-12294.

Kantlehner, M., D. Finsinger, J. Meyer, P. Schaffner, A. Jonczyk, B. Diefenbach, B. Nies, and H. Kessler (1999). Angew. Chem. Int. Ed. Engl. 38, 560-562.

Kloczcwiak, M., S. Timmons, T. J. Lukas, and J. Hawiger (1984). Platelet recognition site on human fibrinogen: synthesis and structure-function relationship of peptides corresponding to the carboxyterminal segment of the γ chain. Biochemistry 23, 1767-1774.

Kouns, W.C., Roux, S., and Steiner, B. (1993). Curr. Op. Invest. Drug 2, 475–494.

Kuehner, M., R. Tampe, and E. Sackmann (1994). Lipid monolayer and bilayer supported on polymer films: composite polymer-lipid films on solid substrates. Biophys J. 67, 217-226.

Kuehner, M., and E. Sackmann (1996). Ultrathin hydrated dextran films grafted on glass: preparation and characterization of structural, viscous and elastic properties by quantitative microinterferometry. Langmuir 12, 4866-4876.

LaemmLi, U. K. (1970). Cleavage of structural proteins during the assembly of the head of bacteriophage T4. Nature (Lond) 227, 680-685.

Luna, E. J., A. Hitt (1992). Cytoskeleton-plasma membrane interactions. Science 258, 955-964.

Marbrey-Gaud, S. (1981). Liposomes: From Physical Structure to Therapeutic Application (Knight, Ed.), 105-138, Elsevier/North-Holland Biomedical Press, Amsterdam, NL.

Marcinkiewisz, C., S. Vijay-Kumar, M. A. McLane, and S. Niewwiarowski (1997). Significance of RGD loop and C-terminal domain of echistatin for recognition of alphaIIb beta3 and alpha(v) beta3 integrins and expression of ligand-induced binding site. Blood 90, 1565-1575.

Marguerie, G. A., T. S. Edgington, and E. F. Plow (1980). Interaction of fibrinogen with its platelet receptor as part of a multistep reaction in ADP-induced platelet aggregation. J Biol Chem. 255 (1), 154-61.

McElhaney, R.N. (1986). Differential scanning calorimetric studies of lipid-protein interactions in model membrane systems. Biochim Biophys Acta 864 (3-4), 361-421.

Mohwald, H. (1990). Phospholipid and phospholipid-protein monolayers at the air/water interface. Annu Rev Phys Chem. 41, 441-76.

Müller, B., H. G. Zerwes, K. Tangemann, J. Peters, and J. Engel (1993). Two-step binding mechanism of fibrinogen to alpha IIb beta 3 integrin reconstituted into planar lipid bilayers. J. Biol. Chem. 268, 6800-6808.

Naik, U. P., and L. V. Parise (1997). Structure and function of platelets $\alpha_{IIb}\beta_3$. Current Opinion in Hematology 4, 317-322.

Nardi, J. (1998). Non-equilibrium phenomena of free and bound vesicles: modelling cell adhesion and vesicle transport. Ph. D. thesis, Technical University of Munich.

Niija, K., E. Hodson, R. Bader, V. Byers-Ward, J. A. koziol, E. F. Plow, and Z. M. Ruggeri (1987). Increased surface expression of the membrane glycoprotein IIb/IIIa complex induced by platelet activation. Relationship to the binding of fibrinogen and platelet aggregation. Blood 70, 475-483.

Nissen, J., S. Gritsch, G. Wiegand, and J. O. Raedler (1999). Wetting of phospholipid membranes on hydrophilic surfaces – Concepts towards self-healing membranes. Eur. Phys. J. B 10, 335-344.

Pakalns, T., K. L. Haverstick, G. Fields, J. B. McCarthy, D. L. Mooradian, and M. Tirrell (1999). Cellular recognition of synthetic peptide amphiphiles in self-assembled monolayer films. Biomaterials 20, 2265-2279.

Peter, K. (1999). Isolation und Charakterisierung des Zellrezeptors Integrin $\alpha_{IIb}\beta_3$ – Studie zur Bindung an zytosolische Proteine und biokompatible Oberflaechen. Ph. D. thesis, 144-151.

Peterson, G.L. (1977). A simplification of the protein assay method of Lowry et al. which is more generally applicable. Anal.Biochem. 83, 346-356.

Pfaff, M., K. Tangemann, B. Müller, M. Gurrath, G. Müller, H. Kessler, R. Timpl, and J. Engel (1994). Selective recognition of cyclic RGD peptides of NMR defined conformation by alpha IIb beta 3, alpha V beta 3, and alpha 5 beta 1 integrins. J. Biol. Chem. 269, 20233-20238.

Phillips, D. R., and P. P. Agin (1977). Platelet plasma membrane glycoproteins. Evidence for the presence of nonequivalent disulfide bonds using nonreduced-reduced two-dimensional gel electrophoresis. J. Biol. Chem. 252, 2121-2126.

Phillips, D. R., and A. K. Baughan (1983). Fibrinogen binding to human platelet plasma membranes. Identification of two steps requiring divalent cations. J. Biol. Chem. 258, 10240-10246.

Phillips, D. R., I. F. Charo, L. V. Parise, and L. A. Fitzgerald (1988). The platelet membrane glycoprotein IIb-IIIa complex. Blood 71, 831-843.

Plow, E.F., S. E. D'Souza, and M. H. Ginsberg (1992). Ligand binding to GPIIb-IIIa: a status report. Sem. Thromb. Hemost. 18, 324-332.

Raedler, J., and E. Sackmann (1992). On the measurement of weak repulsive and frictional colloidal forces by reflection interference contrast microscopy. Langmuir 8, 848-853.

Raedler, J., T. J. Feder, H. H. Strey, and E. Sackmann (1995). Fluctuation analysis of tension-controlled undulation forces between giant vesicles and solid substrates. Phys. Rev. E. 51, 4526-4536.

Ruggeri, Z., M. (1997). Mechanisms initiating platelet thrombus formation. Thrombosis and Haemostasis 78 (1), 611-616.

Sackmann, E. (1996). Supported membranes: scientific and practical applications. Science 271, 43-48.

Samanen, J. M., J. Zdenka, D. Rieman, Tian-li Yue (1997). Curr. Pharmaceut. Design 3, 545-584.

Saudek, V., R. A. Atkinson, and J. T. Pelton (1991). Three-dimensional structure of echistatin, the smallest active RGD protein. Biochemistry 30, 7369-7372.

Seifert, U., and R. Lipowsky (1990). Adhesion of vesicles. Phys. Rev. A. 42, 4768-4771.

Shattil, S. J., M. H. Ginsberg, J. S. Brugge (1994). Adhesive signaling in platelets. Curr. Opin. Cell Biol. 6, 695-704.

Sims, J., S. Karp, and D. Ingber (1992). Altering the cellular mechanical force balance results in integrated changes in cell, cytoskeletal and nuclear shape. J. Cell Sci. 103, 1215-1222.

Simson, R., E. Wallraff, J. Faix, J. Niewoehner, G. Gerisch, and E. Sackmann (1998). Membrane bending modulus and adhesion energy of wild-type and mutant cells of Dictyostelium lacking Talin or Cortexillins. Biophysical Journal 74, 514-522.

Steiner, B., D. Cousot, A. Trzeciak, D. Gillessen, and P. Hadváry (1989). Ca2+-dependent binding of a synthetic Arg-Gly-Asp (RGD) peptide to a single site on the purified platelet glycoprotein IIb-IIIa complex. J. Biol. Chem. 264, 13102-13108.

Suehiro, K., J. W. Smith, and E. F. Plow (1996). The ligand recognition specificity of beta3 integrins. J. Biol. Chem. 271, 10365-10371.

Tangemann, K., and J. Engel (1995). Demonstration of non-linear detection in ELISA resulting in up to 1000-fold too high affinities of fibrinogen binding to integrin $\alpha_{IIb}\beta_3$. FEBS Letters 358, 179-181.

Weisel, J. W., C. Nagaswami, G. Vilaire, J. S. Bennett (1992). Examination of the platelet membrane glycoprotein IIb-IIIa complex and its interaction with fibrinogen and other ligands by electron microscopy. J Biol Chem. 267 (23), 16637-16643.

Williams, M. J., X. Du, J. C. Loftus, M. H. Ginsberg (1995). Platelet adhesion receptors. Sem. Cell Biol. 6, 305-314.

Wurzinger, L. J. (1990). Histophsiology of the circulating platelet. Advances in anatomy, embryology and cell biology, Vol. 120. Springer-Verlag Berlin Heidelberg.

Yamada, K. M., and S. Miyamoto (1995). Integrin transmembrane signaling and cytoskeletal control. Curr Opin Cell Biol 7, 681-689.

7 Abbreviations

BSA	bovine serum albumin
CLSM	confocal laser scanning microscopy
Cryo EM	cryo electron microscopy
Cyclic RGD-containing Hexapeptide	cyclo(-Arg-Gly-Asp-D-Phe-Lys-Gly-)
DMF	dimethylformamide
DMPC	1,2-dimyristoyl-*sn*-glycero-3-phosphocholine
DMPG	1,2-dimyristoyl-*sn*-glycero-3-phosphoglycerol
DPC-Cl	diphenylcarbamyl-Cl
DSC	differential scanning calorimetry
ELISA	enzyme-linked immunosorbant assay
FRAP	fluorescence recovery after photobleaching
ITO	indium-tin-oxide
PEG 2000 PE	1,2-Diacyl-*sn*-Glycero-3-Phosphoethanolamine-N-(Poly(ethylene glycol) 2000
PGE1	Prostagladin E1
PMSF	phenylmethylsulfonyl fluoride
RGD	Arg-Gly-Asp; Arginyl-glycyl-aspartic acid
RICM	reflection interference contrast microscopy
SPR	surface plasmon resonance